

Review

Electrode Materials, Structural Design, and Storage Mechanisms in Hybrid Supercapacitors

Xiaobing Du ¹, Zhuanglong Lin ¹, Xiaoxia Wang ^{1,*}, Kaiyou Zhang ², Hao Hu ³ and Shuge Dai ^{1,*} ¹ School of Physical and Engineering, Zhengzhou University, Zhengzhou 450052, China² Guangxi Key Laboratory of Optical and Electronic Materials and Devices, College of Materials Science and Engineering, Guilin University of Technology, Guilin 541004, China³ School of Material Science and Engineering, Henan University of Science and Technology, Luoyang 471023, China

* Correspondence: wangxiaoxia@zzu.edu.cn (X.W.); shugedai@zzu.edu.cn (S.D.)

Abstract: Currently, energy storage systems are of great importance in daily life due to our dependence on portable electronic devices and hybrid electric vehicles. Among these energy storage systems, hybrid supercapacitor devices, constructed from a battery-type positive electrode and a capacitor-type negative electrode, have attracted widespread interest due to their potential applications. In general, they have a high energy density, a long cycling life, high safety, and environmental friendliness. This review first addresses the recent developments in state-of-the-art electrode materials, the structural design of electrodes, and the optimization of electrode performance. Then we summarize the possible classification of hybrid supercapacitor devices, and their potential applications. Finally, the fundamental theoretical aspects, charge-storage mechanism, and future developing trends are discussed. This review is intended to provide future research directions for the next generation of high-performance energy storage devices.

Keywords: hybrid supercapacitors; electrode materials; design structure; energy storage mechanism



Citation: Du, X.; Lin, Z.; Wang, X.; Zhang, K.; Hu, H.; Dai, S. Electrode Materials, Structural Design, and Storage Mechanisms in Hybrid Supercapacitors. *Molecules* **2023**, *28*, 6432. <https://doi.org/10.3390/molecules28176432>

Academic Editor: Carlo Santoro

Received: 26 July 2023

Revised: 26 August 2023

Accepted: 28 August 2023

Published: 4 September 2023



Copyright: © 2023 by the authors. Licensee MDPI, Basel, Switzerland. This article is an open access article distributed under the terms and conditions of the Creative Commons Attribution (CC BY) license (<https://creativecommons.org/licenses/by/4.0/>).

1. Introduction

In recent years, the increasing environmental problems and energy challenges have stimulated urgent demand for developing green, efficient, and sustainable energy sources, as well as revolutionary technologies associated with energy conversion and storage systems [1,2]. Among the diverse energy storage devices, supercapacitors (SCs) have received extensive attention due to their high power density, fast charge and discharge rates, and long-term cycling stability [3–5]. Generally, SCs can be classified as electrical double-layer capacitors (EDLCs), pseudocapacitors (PCs), or hybrid supercapacitors (HSCs) depending on the energy storage mechanism [6–10]. EDLCs collect energy through the ion absorption/desorption on the electrode/electrolyte interface without the charge transfer reaction [7,8]. PCs harvest energy through fast redox reactions at or near the surface of the electrode material [3,9]. Different charge storage mechanisms occur in the electrode materials of HSCs. For example, the negative electrode utilizes the double-layer storage mechanism (activated carbon, graphene), whereas the others accumulate charge by using fast redox reactions (typically transition metal oxides and hydroxides) [11–14]. HSCs have attracted enormous attention as they can provide excellent performance with higher energy and power densities at high charge/discharge rates [12,13]. More importantly, HSCs provide an important future opportunity for energy storage devices to meet the demands of both higher energy and power densities for powering portable electronic devices, hybrid electric vehicles, and industrial equipment.

At present, nanostructured transition metal oxides, sulfides, and hydroxides [15–21] are being widely explored as positive electrodes for HSCs. Such materials display a very fast

charge/discharge rate to offer high power density. Unfortunately, many battery-type electrodes, such as $\text{Ni}(\text{OH})_2$ [22,23] or other materials, that exhibit faradaic behavior (even those that are electrochemically irreversible) have been considered as pseudocapacitive materials in many reports, which confuses the readers [24–26]. As suggested by Gogosti et al. [10], it is inappropriate to describe nickel-based oxides, sulfides, and hydroxides as pseudocapacitive electrode materials in alkaline aqueous electrolytes because they undergo faradaic reactions, where their electrochemical signature is analogous to that of a “battery” material. Therefore, the concept of “capacitance” (F) cannot be applied to purely faradaic behavior, and “capacity” (C or mAh) is the most appropriate and meaningful metric to represent the performance of such materials [26]. In addition, some researchers may mistakenly consider the HSCs as asymmetric supercapacitors (ASCs) that are based on two different supercapacitor-type electrodes (i.e., capacitive electrodes and/or pseudocapacitive electrodes), which also aggravates the confusion for readers [27]. The definition of an ASC device is very broad since it refers to every combination of positive and negative electrodes with the same nature regardless of the difference between the two electrodes (weight, thickness, material, etc.) [7]. However, an HSC device should be used when pairing two electrodes with different charge storage behaviors, such as one capacitive and the other faradaic, and the performance of such a device is in between a supercapacitor and a battery [27]. Some researchers have presented a well-rounded view in recent literature [27–29].

Herein, we will classify HSCs into several types based on the design and structure of the devices. It is well known that the performance of an energy storage device is determined mainly by the electrode materials. The design and development of nanomaterials and hybrid nanomaterials/nanostructures are considered as effective strategies to obtain advanced energy storage devices with high power, fast charging, and long cycle-life features [30,31]. More importantly, it enables us to develop a new generation of devices that approach the theoretical limit for electrochemical storage and deliver electrical energy rapidly and efficiently [30]. Although nanostructuring provides marvelous benefits, there are still some challenges in developing high-performance electrode nanomaterials for HSCs. For example, the electrode thickness of transition metal oxides and hydroxides ($\text{Ni}(\text{OH})_2$, NiS , NiO , etc.) is limited due to the low electrical and ionic conductivities of these materials, which retard the overall device kinetics. Both electronic and ionic conductivities are critical for increasing the rate performance of electrodes, especially when large and multivalent ions are used in electrolytes [32]. Therefore, it is necessary to improve electronic conduction by doping, partial reduction, and creating good electrical contact between nanomaterials and conductive additives [7]. Thus, some recent advances in electrode materials will be presented and discussed in this review article. Moreover, we will summarize the recent advances of HSCs, especially in the development of fundamental scientific principles and concepts. Then, we will provide a comprehensive summary of recent progress on electrode material design and burgeoning device constructions for high-performance HSCs. Finally, the future developing trends and perspectives, as well as the challenges, will also be discussed.

2. Recent Advances in Materials for Hybrid Supercapacitors

HSCs are generally composed of three components (Figure 1): electrodes, electrolytes, and separators. The performance of HSCs is mainly determined by the electrochemical activity and kinetic features of the electrodes. To improve the energy and power density of HSCs, it is crucial to enhance the kinetics of ion and electron transport in electrodes and at the electrode/electrolyte interface [33]. Therefore, electrode materials, as the essential soul of the devices, play a decisive role in the performance of HSCs.

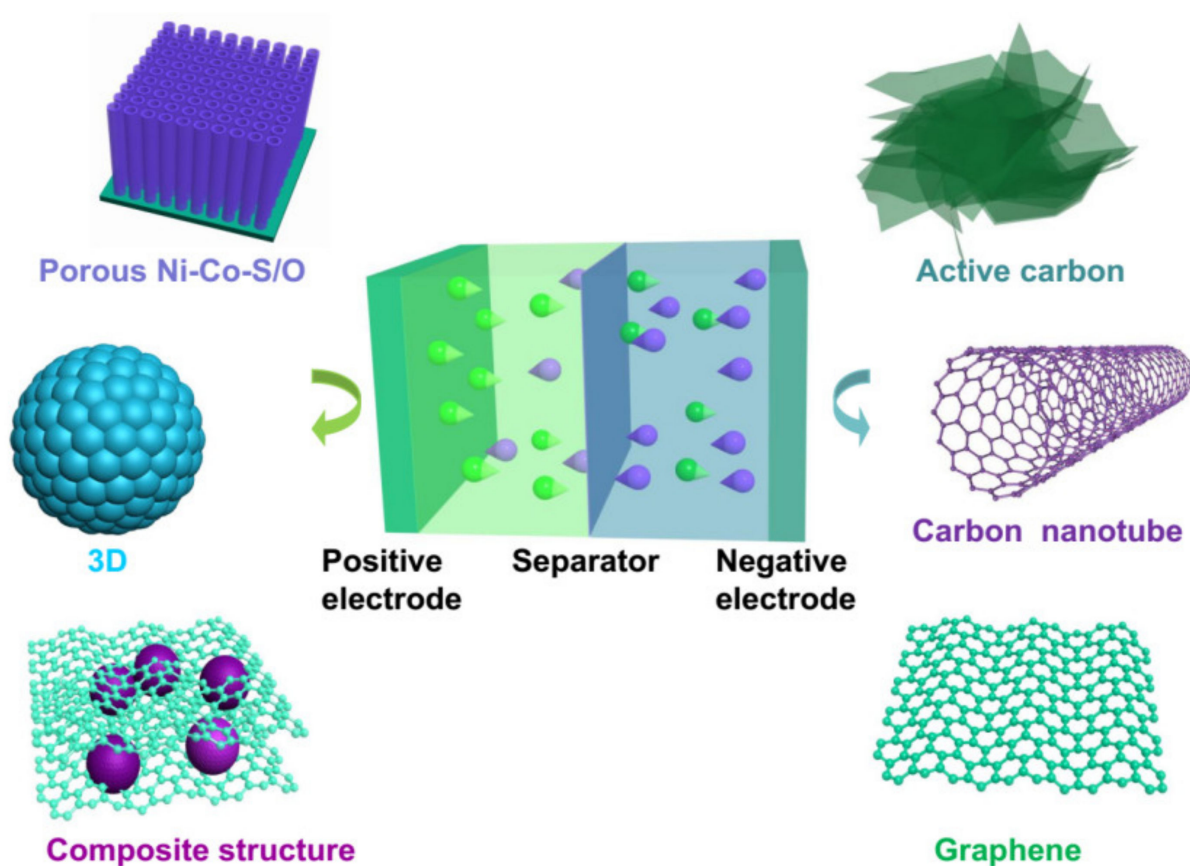


Figure 1. Illustration of a hybrid supercapacitor system.

2.1. Positive Electrode Materials

The performance of a HSC device is mainly determined by the positive electrode materials [10]. In recent years, transition metal oxides/sulfides/hydroxides [34] have been considered as promising electrode materials for HSCs since they can provide a variety of oxidation states for fast surface redox reactions.

2.1.1. Nickel Oxides/Hydroxides/Sulfides

Recently, Ni-based oxides/hydroxides, such as NiO [35–39] and Ni(OH)₂ [40–44], have been widely reported as electrode materials for HSCs due to their attractive theoretical specific capacity and potentially high-rate capability in alkaline aqueous solutions. NiO is a promising battery-type material due to its high theoretical specific capacity (1292 C g⁻¹ in a potential window of 0.5 V), well-defined redox behavior, and low cost [38]. For instance, Ren et al. [45] prepared honeycomb-like mesoporous NiO microspheres and revealed a high specific capacitance of 635 C g⁻¹ at 1 A g⁻¹. Even at 5 A g⁻¹, it also exhibited a high specific capacity of 472.5 C g⁻¹ with 88.4% retention after 3500 cycles, demonstrating its superior performance. Cai et al. [46] prepared NiO nanoparticles and found a high specific capacity of 693 C g⁻¹ at 1 A g⁻¹, but the rate of capability could only retain 62% (430 C g⁻¹) as the current density increased to 50 A g⁻¹. The poor rate performance is caused by its low electrical conductivity. Although many recent efforts have been carried out on NiO electrodes, the acquired specific capacity is usually lower than the theoretical capacity of NiO. The relatively poor conductivity of NiO limited its specific capacity, and hindered the fast electron transport required for high charge–discharge rates.

Compared to NiO materials, Ni(OH)₂ has been considered as a promising candidate for HSCs due to its high theoretical capacity (1041 C g⁻¹ in a potential window of 0.5 V), excellent redox behavior, ease of synthesis, abundant sources, low cost, and environmental friendliness [47]. Currently, many advances have been widely reported, as summarized

in Table 1. During the last decades, numerous efforts have been devoted to fabricating high-performance electrodes based on Ni(OH)₂ materials for energy storage devices, but there are still some challenging issues. Owing to its low conductivity, the Faradic redox reactions can only take place on its surface, and most of the reported Ni(OH)₂ materials are inaccessible to electrolyte ions and remain as dead volumes in HSCs [48,49]. In recent years, many strategies have been explored to address this issue, including the synthesis of nanoscale or porous structures (Figure 2a), atomic substitution or doping (Figure 2b), and forming a composite with carbon-based or other materials (Figure 2c) [50,51]. For instance, the as-prepared hybrid electrode (Ni(OH)₂/carbonnanotube/polymer) by Jiang et al. [49] delivered an ultrahigh specific capacity of 1631 C g⁻¹ at 5 mV s⁻¹, excellent rate capability (71.9% capacity retention at 100 mV s⁻¹), and long cycle life (85% capacitance retention after 20,000 cycles). In the hybrid, the conducting polymer coating contributes to stabilizing the whole electrode by reducing the dissolution of active materials, thus greatly improving the rate capability and cycling stability of the electrode. Fabricating a composite by incorporating highly conductive graphene nanosheets into Ni(OH)₂ materials is considered as the most effective strategy to enhance the intrinsic properties of Ni(OH)₂. Li et al. [52] reported a novel Ni(OH)₂/rGO hybrid material, which not only exhibited a high specific capacity (1007.5 C g⁻¹ at 0.5 A g⁻¹), but also showed good life cycle stability (108% capacitance retention after 8000 cycles), revealing its good performance by incorporating rGO. Guo et al. [53] prepared a Ni(OH)₂/rGO hybrid electrode and found a high specific capacity (1388 C g⁻¹ at 2 A g⁻¹) and remarkable rate capability (785 C g⁻¹ at 50 A g⁻¹). A Ni(OH)₂-porous nitrogen-doped graphene hybrid architecture was also synthesized by Aghazadeh et al. [54]. The composite exhibited a specific capacity of 701 C g⁻¹ and a capacity retention of 92.8% after 7000 cycles at 10 A g⁻¹. In addition, the electrochemical performances of Ni(OH)₂/rGO composites that have been reported thus far are compared in Table 2. It clearly reveals that, despite great achievement by hybridizing with rGO, Ni(OH)₂ still requires further improvements, particularly in high-rate performance as well as in long cycle life.

Table 1. Specific capacity of Ni(OH)₂ electrodes.

Electrode Materials	Electrolyte	Voltage (V)	Current Load or Scan Rate	Specific Capacity (C g ⁻¹)	Reference
3D nanoporous Ni(OH) ₂	6.0 M KOH	0–0.5	7 A g ⁻¹	759.5	[55]
Ni(OH) ₂ nanospheres	1.0 M KOH	0–0.5	20 A g ⁻¹	934	[56]
α-Ni(OH) ₂ nanobristles	1.0 M KOH	0–0.45	2 A g ⁻¹	940.5	[57]
Ni(OH) ₂ microspheres	2.0 M KOH	0–0.55	0.5 A g ⁻¹	704.5	[58]
Mesoporous α-Ni(OH) ₂	2.0 M KOH	0–0.55	0.5 A g ⁻¹	983.9	[59]
Ni(OH) ₂ nanoboxes	2.0 M KOH	0–0.5	1 A g ⁻¹	1247.5	[60]
α-Ni(OH) ₂ nanowires	2.0 M KOH	0–0.4	1 A g ⁻¹	889.2	[61]
Ni(OH) ₂ nanosheets	6.0 M KOH	0–0.5	2 A g ⁻¹	825.6	[62]
Ni(OH) ₂ nanoflakes	1.0 M KOH	0–0.4	1 A g ⁻¹	566.4	[63]
Ni(OH) ₂ nanocubes	3.0 M KOH	0–0.45	1 A g ⁻¹	828.9	[64]
Amorphous α-Ni(OH) ₂	2.0 M KOH	0–0.35	2 A g ⁻¹	818.3	[65]
Cabbage-like α-Ni(OH) ₂	1.0 M KOH	0.2–0.6	1 mA cm ⁻²	761.2	[66]
Ni(OH) ₂ nanosheets	2.0 M KOH	0–0.45	1 A g ⁻¹	1072.9	[67]
Ni(OH) ₂ platelets	2.0 M KOH	0–0.6	0.5 A g ⁻¹	1160.4	[68]
β-Ni(OH) ₂ nanosheets	6.0 M KOH	0–0.6	5 mV s ⁻¹	1041	[69]
α-Ni(OH) ₂	2.0 M KOH	0–0.5	2 mV s ⁻¹	267	[70]
α-Ni(OH) ₂ microspheres	6.0 M KOH	0–0.4	1 A g ⁻¹	992.3	[71]
β-Ni(OH) ₂ nanosheets	6.0 M KOH	0–0.4	5 mA cm ⁻²	790.3	[72]
β-Ni(OH) ₂	6.0 M KOH	–0.05–0.35	1 A g ⁻¹	712	[73]

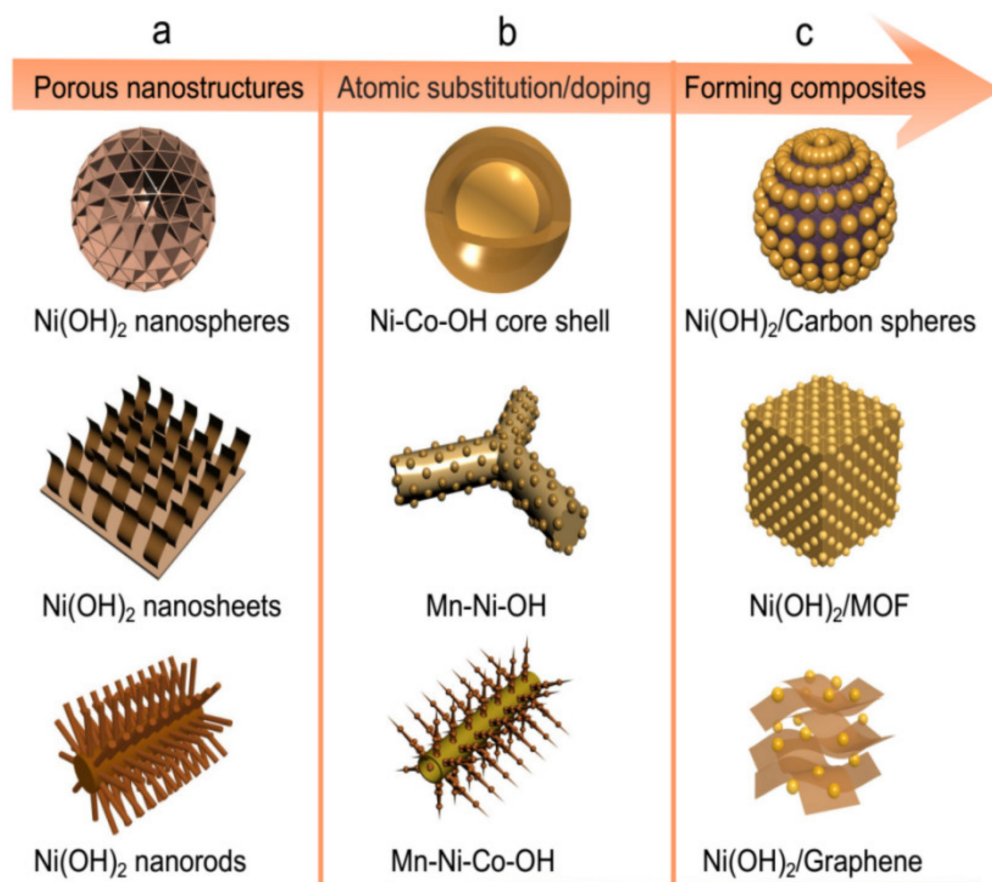


Figure 2. Illustration of nanoscale or porous structures of Ni(OH)₂ (a), atomic substitution or doping (b), and fabricating a composite with carbon-based or other materials (c).

Table 2. Summary of performances of Ni(OH)₂/rGO composites.

Electrode Materials	ΔE (V)	Maximum Capacity (C g ⁻¹)	Capacity Retention	Cycle Stability	Ref.
Ni(OH) ₂ nanoplatelets/rGO	0.45	955 C g ⁻¹ (1 A g ⁻¹)	58.6% (80 A g ⁻¹)	102% (5000 cycles)	[74]
3D Ni(OH) ₂ /rGO network	0.5	563 C g ⁻¹ (0.5 A g ⁻¹)	61.8% (10 A g ⁻¹)	87% (1000 cycles)	[75]
Ni(OH) ₂ /rGO	0.6	941 C g ⁻¹ (4 A g ⁻¹)	27% (11.2 A g ⁻¹)	75% (1000 cycles)	[76]
Ni(OH) ₂ /rGO aerogel	0.5	516 C g ⁻¹ (0.5 A g ⁻¹)	54.3% (2 A g ⁻¹)	95% (2000 cycles)	[77]
Ni(OH) ₂ /3D rGO	0.5	690 C g ⁻¹ (1 A g ⁻¹)	86.7% (60 A g ⁻¹)	78% (1000 cycles)	[78]
Ni(OH) ₂ nanoparticles/rGO	0.38	858 C g ⁻¹ (0.5 A g ⁻¹)	52.7% (10 A g ⁻¹)	89% (1000 cycles)	[79]
Ni(OH) ₂ nanosheets/rGO	0.45	838 C g ⁻¹ (0.8 A g ⁻¹)	62.3% (6.4 A g ⁻¹)	92% (2000 cycles)	[80]
Ni(OH) ₂ nanocrystals/rGO	0.5	951.5 C g ⁻¹ (1 A g ⁻¹)	60.9% (20 A g ⁻¹)	70% (1000 cycles)	[81]
Ni(OH) ₂ nanoplates/rGO	0.5	667 C g ⁻¹ (2.8 A g ⁻¹)	71% (45.7 A g ⁻¹)	100% (2000 cycles)	[82]
Ni(OH) ₂ /rGO	0.55	1206 C g ⁻¹ (2 mV s ⁻¹)	41% (20 mV s ⁻¹)	95% (2000 cycles)	[83]
Ni(OH) ₂ /rGO	0.55	954 C g ⁻¹ (1 mV s ⁻¹)	30% (50 mV s ⁻¹)	88% (1000 cycles)	[84]
β -Ni(OH) ₂ /rGO	0.5	971 C g ⁻¹ (1 A g ⁻¹)	67.9% (40 A g ⁻¹)	81% (2000 cycles)	[85]
Ni(OH) ₂ nanoflowers/rGO	0.55	598 C g ⁻¹ (1 A g ⁻¹)	58% (10 A g ⁻¹)	95% (1000 cycles)	[86]
Flower-like Ni(OH) ₂ /rGO	0.4	642 C g ⁻¹ (1 A g ⁻¹)	18.7% (30 A g ⁻¹)	86% (2200 cycles)	[87]
Ni(OH) ₂ /rGO	0.45	546 C g ⁻¹ (5 mV s ⁻¹)	35% (100 mV s ⁻¹)	88% (1000 cycles)	[88]

Compared with corresponding oxides/hydroxides, transition metal sulfides have higher conductivity, mechanical and thermal stability, and richer redox reactions [89]. Over the past few years, transition metal sulfides (NiS, Ni₃S₂, MoS₂, CoS, CuS, and FeS₂, etc.) with superior optical, electrical, magnetic, and catalytic properties have been extensively used in the field of lithium ion batteries, SCs, and hydrogen evolution reaction catalysts [90–93]. Among numerous transition metal sulfides, nickel sulfides have

been extensively investigated as positive electrode materials for HSCs due to their high electronic conductivity, low cost, and environmental sustainability [94–98]. For example, Zhang et al. [89] synthesized V-doped NiS₂ with a high specific capacity of 981 C g⁻¹ at 1 A g⁻¹, and a good electrochemical cycling stability (100% of the capacity is retained after 6000 cycles). The as-prepared nanocrystalline β-NiS by Kushwaha et al. [95] exhibited a high specific capacity of 710 C g⁻¹ at 1 A g⁻¹, and long cycle stability (86% of the capacity retention after 10,000 cycles). Although nickel sulfides have been reported as promising positive electrodes for HSCs, they still suffer from some drawbacks, such as poor kinetics, polarization, dissolution of polysulfides in the electrolyte, thus reducing its conductivity, electrode pulverization, and the capacity loss [96,97]. In order to overcome these shortcomings, many researchers have devoted themselves to exploring the composites of nickel sulfide with carbonaceous materials. For instance, the as-prepared graphene-wrapped NiS nanocomposite by Zhang et al. [98] showed high specific capacity (1078.9 C g⁻¹ at 2 A g⁻¹) and good rate capacity (580.3 C g⁻¹ at 15 A g⁻¹), revealing that graphene plays a critical role in improving the performance of nickel sulfide at high current densities. In our recent work [12], we also found that the incorporation of graphene with nickel sulfide could stabilize its electrochemical properties. When integrated with rGO, the Ni_xS_y/rGO (NiS-Ni₃S₂-Ni₃S₄/rGO) composite electrode demonstrated not only higher specific capacity (807 C g⁻¹ at 1 A g⁻¹) but also better rate capability (~72% capacity retention as the current density was increased from 1 to 20 A g⁻¹) [12]. Therefore, fabricating a composite with rGO is an effective strategy to enhance the specific capacity, rate capability, and cycling life of the whole electrode.

2.1.2. Cobalt Oxides/Hydroxides

Among various transition metal oxides, Co₃O₄ has attracted wide attention for its high energy storage capacity (3560 F g⁻¹), low cost, environmental friendliness, multiple valence sites, and high activity in water oxidation [99,100]. Electron and ion transport efficiency for charge storage in Co₃O₄-based pseudocapacitors mainly depends on electrode properties such as surface area, morphology, and alignment of nanocrystalline phases [101,102]. In the past decade, numerous Co₃O₄ nanostructures have been fabricated and tested for superior performance in the field of energy storage [103–110]. For example, Yang et al. [109] synthesized Pr-doped Co₃O₄ nanoflakes, which exhibited a high specific capacity of 640 C g⁻¹ at a current density of 2 A g⁻¹, and 64% of the capacity retention at a high current density of 10 A g⁻¹. Zhang et al. [110] fabricated the Cl-doped Co₃O₄ hierarchical nanospheres and observed significant performance with an ultrahigh specific capacity of 814 C g⁻¹ at a current density of 1 A g⁻¹, high-rate capability (63.2% capacity retention at 32 A g⁻¹) and good cycling stability. However, the observed specific capacity values for Co₃O₄ are much lower than their theoretical values, and the specific capacity usually severely decays at high charge/discharge currents. Therefore, it is an ongoing challenge to further improve its specific capacity and rate capability.

Cobalt hydroxide (Co(OH)₂) is another kind of cobalt compound that has been widely investigated for its rich redox reactions [111]. Compared with nickel oxide and hydroxide, cobalt hydroxide provides more electrons when a redox reaction is going on [112–114]. Furthermore, hydrotalcite-like cobalt hydroxide usually shows a positively charged Co(OH)_{2-x} layer and an interlayered gallery with negatively charged anions (e.g., Cl⁻, SO₄²⁻, NO₃³⁻) [115–118]. Recently, Xu et al. [117] reported the preparation of α-Co(OH)₂ nanoparticles by cobalt zeolitic-imidazolate frameworks (ZIF-67) hydrolyzation, and the as-prepared α-Co(OH)₂ nanoparticles presented superior specific capacity of 314 C g⁻¹ at a low current density of 1 A g⁻¹, high rate capability (77% of capacity retention at 20 A g⁻¹) and good cycling stability (100% of capacity retention after 20,000 cycles). In order to further improve the cycling stability, some researchers have tried to fabricate the hybrids. For instance, Gan et al. [119] recently reported the Co(OH)₂/CoS hybrid nanostructure, which displays high rate capability (75.8% capacity retention as the current density was increased from 0.5 to 10 A g⁻¹) and long cycling stability. Wang et al. [120]

synthesized a Co(OH)_2 /nitrogen-doped porous graphene composite and realized ultrahigh specific capacity (1144 C g^{-1} at 2 A g^{-1}), and long cycling stability (95.9% of capacity retention after 4000 cycles).

2.1.3. Multi-Metal Compounds

Owing to the multiple oxidation states and the synergistic effects between various metal ions, the multi-metal compounds show superior electrochemical performance for energy storage [12]. Generally, multi-metal compounds can be divided into multi-metal oxides, sulfides, and hydroxides. Multi-metal oxides, such as NiCo_2O_4 [121–123], ZnCo_2O_4 [124–127], MnMoO_4 [128–130], and CoMoO_4 [131–134], have been widely explored for energy conversion and storage. Among these multi-metal oxides, the NiCo_2O_4 nanomaterials have attracted increasing attention due to their merits of higher electrical conductivity, and higher electrochemical activity, which would offer richer redox reactions, including contributions from both $\text{Ni}^{2+}/\text{Ni}^{3+}$ and $\text{Co}^{3+}/\text{Co}^{4+}$ redox couples in the materials [121–123]. For example, Shen et al. [135] that reported the highly uniform NiCo_2O_4 hollow spheres exhibited a high specific capacity of 541 C g^{-1} at 1 A g^{-1} , and excellent rate performance (74.8% of capacity retention from 1 A g^{-1} to 15 A g^{-1}). In addition, it also demonstrated good cycling stability with 94.7% of capacity retention after 4000 cycles of continuous charge-discharge testing at the continuous charge-discharge testing at a current density of 5 A g^{-1} . All these superior performances are caused by the advantageous structural features of these NiCo_2O_4 hollow spheres [135]. Ji et al. [136] reported a NiCo_2O_4 positive electrode material with an urchin-like hollow hierarchical microsphere structure, which delivered a high capacity of 424 C g^{-1} at 0.5 A g^{-1} and satisfactory rate capability (62.6% capacity retention from 0.5 A g^{-1} to 10 A g^{-1}). To further enhance the electrochemical performance of NiCo_2O_4 , many researchers have tried to design 3D porous hybrid electrode architectures by incorporating carbon materials. This hybrid architecture could solve the intrinsic poor conductivity and inevitable agglomeration of NiCo_2O_4 electrode materials [137]. For example, Li et al. [137] prepared the layered NiCo_2O_4 /RGO nanocomposite and achieved an ultrahigh specific capacity of 694 C g^{-1} at 0.5 A g^{-1} and excellent cycle life with 90.2% capacity retention after 20,000 cycles at 5 A g^{-1} . Al-Rubaye et al. [138] recently reported the NiCo_2O_4 -rGO nanocomposite, which consists of NiCo_2O_4 hexagons wrapped in conducting rGO sheets, which exhibited a high specific capacity of 533 C g^{-1} at 2 A g^{-1} and excellent cycling stability with 98% capacity retention after 10,000 cycles. Sun et al. [139] reported the NiCo_2O_4 nanoparticle/three-dimensional porous graphene (NiCo_2O_4 /3D-G) composite by a facile hydrothermal method combined with subsequent annealing treatment. The obtained NiCo_2O_4 /3D-G hybrid electrode displayed a high specific capacity of 920 C g^{-1} at 1 A g^{-1} . When being used as a positive electrode for HSC, the NiCo_2O_4 /3D-G//rGO HSC device exhibited a high energy density of 73.8 W h kg^{-1} at a power density of 800 W kg^{-1} and long cycle stability with 94.3% capacity retention after 5000 cycles [139].

Compared to the multi-metal oxides, the multi-metal sulfides show better electrical conductivity, mechanical and thermal stability, and higher electrochemical activity [140–142]. Recently, many advances have been widely reported, including Ni-Co-S [143–148], KCu_7S_4 [149–152], CuCo_2S_4 [153–155], Zn-Co-S [156,157], Mn-Co-S [158–161], CuSbS_2 [162,163], SnCoS_2 [164–166]. Among these multi-metal sulfides, nickel-cobalt sulfides (NiCo_2S_4) have been reported with a much higher conductivity and richer redox reactions due to the electrochemical contributions from both nickel and cobalt ions, resulting in better electrochemical performance [167–169]. For example, Yu et al. [168] reported a facile self-sacrificial template method to synthesize uniform 3D NiCo_2S_4 hollow nanoprisms with controllable composition. SEM (Figure 3a) and TEM (Figure 3b,c) images display the rough surface and well-defined inner cavities of the NiCo_2S_4 hollow nanoprisms. When evaluated as an electrode for HSCs, the NiCo_2S_4 hollow nanoprisms show a high capacity (447.6 C g^{-1} at 1 A g^{-1}) and remarkable rate capability (65.4% retention of initial capacity from 1 to 20 A g^{-1}). Wang et al. [169] prepared NiCo_2S_4 nanosheets (Figure 3d,e) and realized an

ultrahigh specific capacity of 1384 C g^{-1} at 2 mA cm^{-2} . Guan et al. [170] reported an onion-like NiCo_2S_4 particle with unique hollow structured shells using onion-like metal oxide particles as the precursor, as illustrated in Figure 3f. As shown in the TEM images in Figure 3g–i, the onion-like NiCo_2S_4 particles are composed of several crumpled layers. Owing to its intriguing structural features, the obtained onion-like NiCo_2S_4 exhibited good electrochemical performance with a high specific capacity of 508 C g^{-1} and long cycling stability with 87% capacity retention after 10,000 cycles [170]. Typical CV curves of the NiCo_2S_4 electrode at different scanning rates are shown in Figure 3f. All these curves exhibit a typical battery-like feature. Figure 3g shows the galvanostatic charge-discharge curves of the electrode at various current densities in a potential window of 0–0.5 V. All these curves show a well-defined discharge voltage plateau at around 0.2–0.3 V, further demonstrating a good electrochemical battery-type characteristic and superior reversible redox reaction. Zhang et al. [146] reported a facile hydrothermal approach for the shape-controlled synthesis of NiCo_2S_4 architectures with four different morphologies of urchin (Figure 3j), tube (Figure 3k), flower (Figure 3l), and cubic-like (Figure 3m) microstructures. Among these architectures, the tube-like NiCo_2S_4 electrode exhibited the best specific capacity value of 419 C g^{-1} at a current density of 3 A g^{-1} [146]. Peng et al. [144] reported a facile two-step method to synthesize 3D core/shell-structured composites (CNTs@Ni-Co-S). Figure 3n,o exhibits the SEM images of the Ni@CNTs@Ni-Co-S composite, revealing the skeleton of CNTs to form a clear and with each other to form a highly open structure, providing abundant accessible typical core-shell hybrid structure. These nanosheets are interconnected pathways for electrolyte ions [144]. The TEM image (Figure 3p) presents the detailed information for the core/shell hierarchical nanostructures of CNTs@Ni-Co-S composites. At the interface between CNTs and Ni-Co-S nanosheets, Ni-Co-S nanosheets are found to adhere to the surface of CNTs robustly, which is favorable for electron transfer through CNTs to Ni-Co-S nanosheets [144]. The as-prepared composite electrode delivered a high specific capacity of 222 mA h g^{-1} at 4 A g^{-1} and excellent rate capability (193 mA h g^{-1} at 50 A g^{-1}) [144].

In recent years, multi-metal layered double hydroxides (LDH) have also attracted much more attention in the design of electrode materials for HSCs. Various successful achievements have been widely reported in the literature [171–176]. For example, Nagaraju et al. [173] reported a facile and cost-effective process to obtain well-assembled porous Ni-Co LDH nanosheets on conductive textile substrates (Ni-Co LDH NSs/CTs) using a two-electrode system-based electrochemical deposition method. SEM images indicate that the entire surface of the CTs has an average height of 1.2–1.3 μm (Figure 4a,b), and the surfaces of these nanosheets are smooth with a thickness of approximately 10–15 nm (Figure 4c) [173]. The as-prepared Ni-Co LDH NSs/CTs showed high specific capacity of (Figure 4d) and good cycling stability (Figure 4e). To further improve the performance, some researchers tried to incorporate foreign anions (e.g., nitrate, chloride, sulfate, acetate, etc.) into the interlayer region, or grow the active materials on nano-architected carbon-based materials (graphene, carbon nanotube, etc.) to form hybrids [174–176]. Figure 4f,g show the polyhedron morphology from typical SEM and TEM images of the NiCo-LDH/ Co_9S_8 sample, respectively. The as-prepared NiCo-LDH/ Co_9S_8 hybrid system collectively presents an ideal porous structure, rich redox chemistry, and high electrical conductivity matrix, which deliver a high specific capacity of 743.8 C g^{-1} (1653 F g^{-1}) at 4 A g^{-1} (Figure 4h) [174]. Moreover, a hybrid supercapacitor device based on NiCo-LDH/ Co_9S_8 polyhedrons and carbon nanotubes delivers a high specific capacitance of 194 F g^{-1} and superior rate capability of 77.8% (Figure 4i) [174]. Bai et al. [175] reported the synthesis and characterization of Ni-Co LDH hollow nanocages, which are deposited on commercial graphene nanosheets derived from ZIF-67/graphene pristine material via a structure-induced anisotropic chemical etching at elevated temperature (Figure 4j). Figure 4k,l show the SEM images of the Ni-Co LDH/graphene composite, indicating that the shell of the hollow structure is composed of interconnected nanosheets with ultrathin thickness. The unique nanocomposite electrode delivered a high specific capacity of 759 C g^{-1} (1265 F g^{-1}) at 1 A g^{-1} (Figure 4m). Recently, Liu et al. [176] synthesized the Ni-Co@Ni-Co LDH nanotube arrays

(NTAs) by using ZnO nanorod arrays (ZnO NRAs) grown on CFC as a template. SEM images show that the Ni-Co@Ni-Co LDH nanorod is a fungus composed of a big top and a small body (Figure 4n,o). The TEM image (Figure 4p) indicates that the top of the Ni-Co@Ni-Co LDH nanotube has a diameter of ~ 700 nm and consists of many nanosheets, whereas the body of the nanotube has a diameter of ~ 550 nm and consists of nanocrystals (20–30 nm in size) [176]. The SAED pattern (inset of Figure 4q) reveals that the body of the Ni-Co@Ni-Co LDH NTA consists of many nanocrystals, and the EDX mapping (Figure 4r) shows that Ni, Co, and O are well-dispersed and homogeneously mixed in the NTA. Owing to their intriguing structural features, the Ni-Co@Ni-Co LDH NTAs deliver excellent rate performance (82.1% capacity retention from 1 to 20 A g⁻¹) with an ultrahigh specific capacity of 1207 C g⁻¹ at 1 A g⁻¹ [176]. The Ni-Co@Ni-Co LDH NTAs are further paired with CNFs to fabricate HSCs, which delivered high specific capacitances of 280, 253, and 220 F g⁻¹ at discharge current densities of 5, 10, and 20 A g⁻¹, respectively. Most remarkably, the device exhibited an ultrahigh energy density of 100 Wh kg⁻¹ at a power density of 1500 W kg⁻¹ [176]. In addition to Ni and Co, some researchers also reported the effect of other transition metals (i.e., Zn, Mn, Al, and Fe) contents in Ni or Co electrode materials, as illustrated in Table 3.

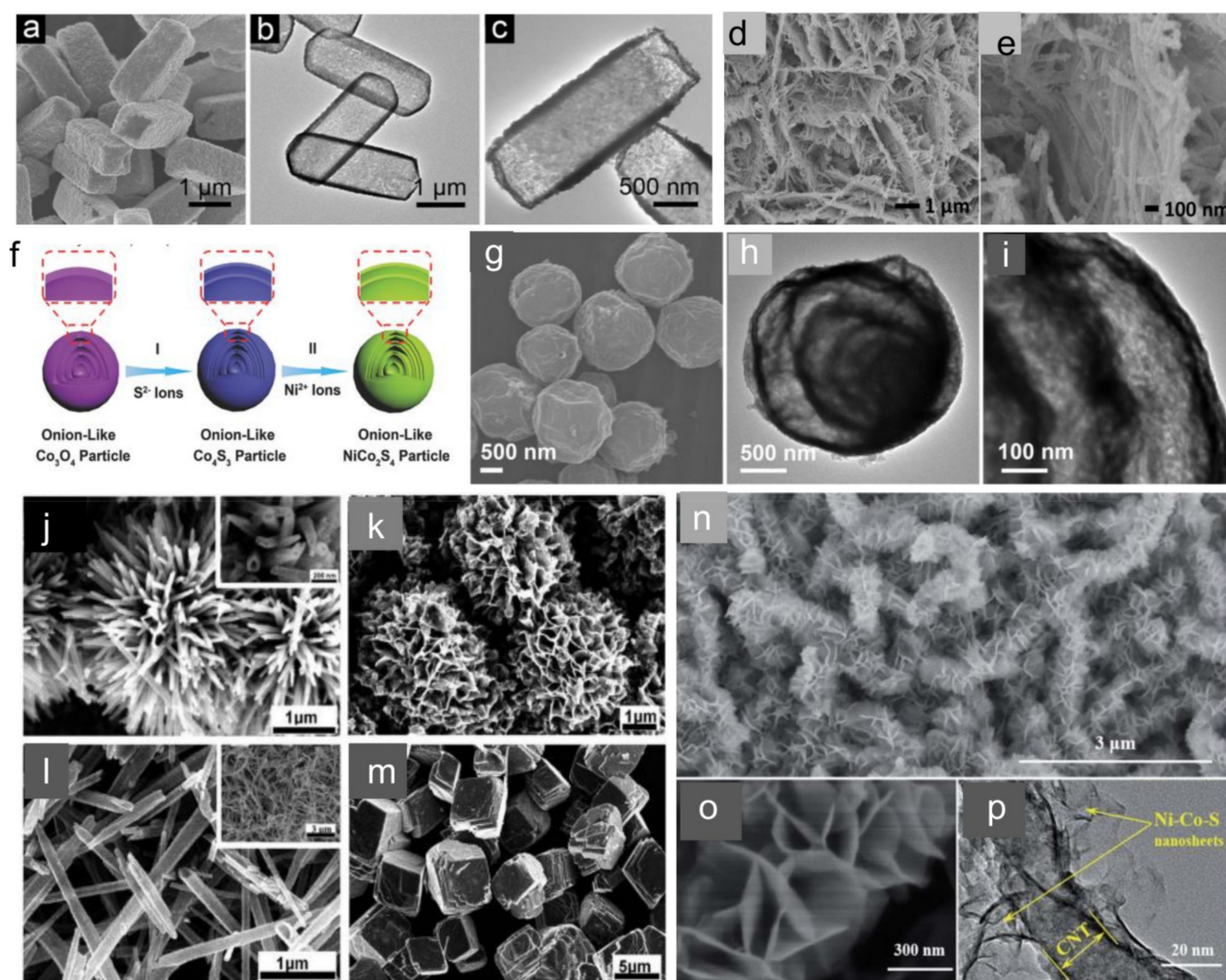


Figure 3. (a) SEM and (b,c) TEM images of NiCo₂S₄ hollow prisms [168] (Copyright 2014 WILEY-VCH Verlag GmbH & Co. KGaA, Weinheim). (d) SEM and (e) TEM images of NiCo₂S₄ nanosheet hetero-structured arrays [169] (Copyright 2015 Elsevier Ltd., all rights reserved). (f) Schematic illustration of the formation process; (g–i) TEM images of onion-like NiCo₂S₄ hollow

microspheres [170] (Copyright 2017 WILEY-VCH Verlag GmbH & Co. KGaA, Weinheim). (j–m) SEM images of NiCo₂S₄ with different morphologies: urchin (j), flower (k), tube (l), and cubic (m) [146] (Copyright 2014, The Royal Society of Chemistry). (n,o) SEM images of the core/shell-structured CNTs@Ni-Co-S hybrids. (p) TEM image for detailed core/shell structure information of the CNTs@Ni-Co-S hybrids [144] (Copyright 2016: The Royal Society of Chemistry).

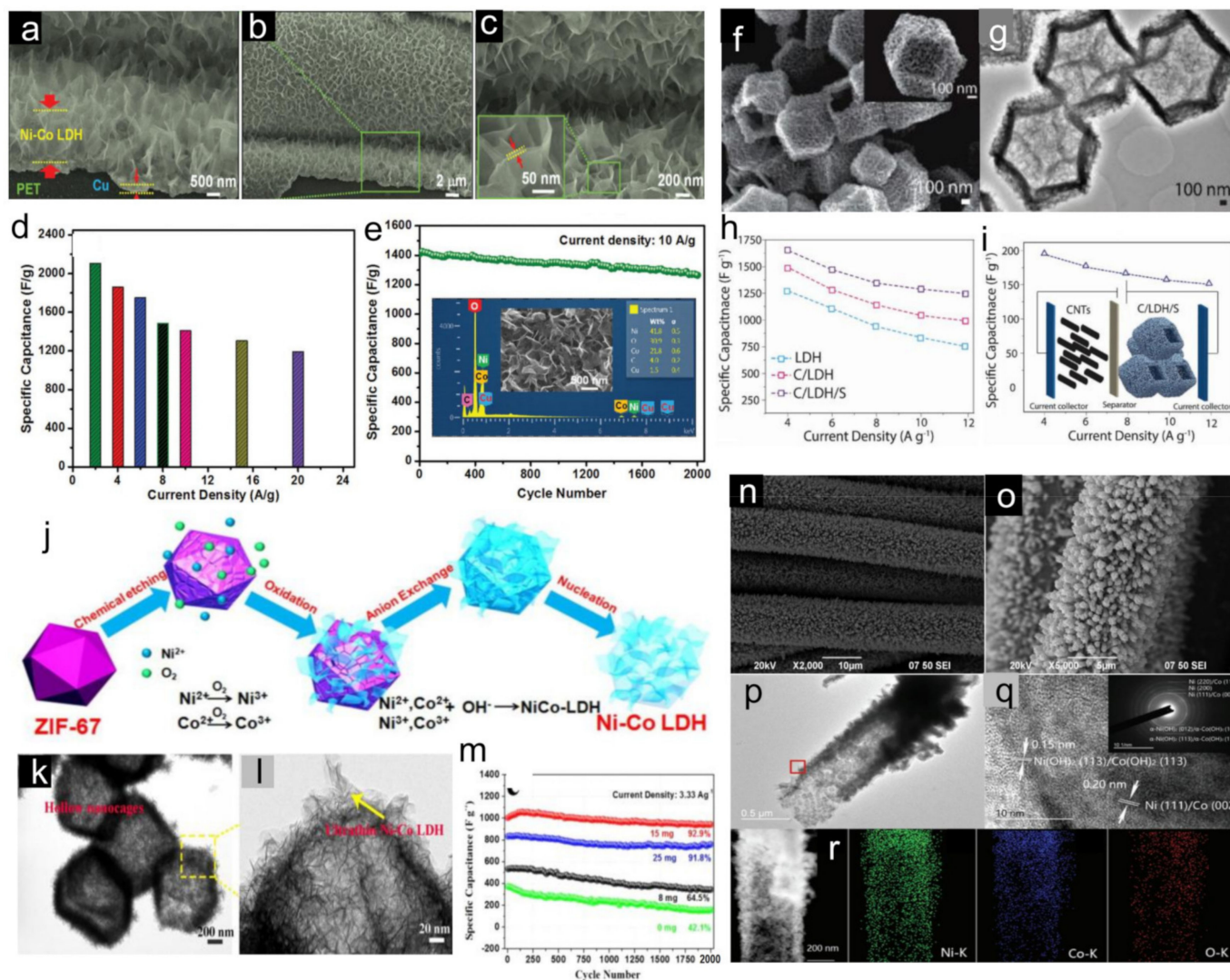


Figure 4. (a–c) FESEM images of the Ni-Co LDH NSs/CTs. (d) Specific capacitance values as a function of current density of Ni-Co LDH NSs/CTs. (e) Cycling performance of the sample at a current density of 10 A g^{−1} in 1 M KOH electrolyte solution. The inset of (e) shows the EDX spectrum and FE-SEM image of Ni-Co LDH NSs/CTs after the cycling process [173] (Copyright 2016: The Royal Society of Chemistry). SEM (f) and TEM (g) images of NiCo-LDH/Co₉S₈ polyhedrons. (h) Specific capacitances as a function of the current density. (i) Calculated specific capacitance values for NiCo-LDH/Co₉S₈//CNTs hybrid supercapacitor cells. Inset is a schematic illustration of the cells [174] (Copyright 2017 WILEY-VCH Verlag GmbH & Co. KGaA, Weinheim). (j) Schematic illustration of the possible mechanism of reaction involved in forming Ni-Co LDH. (k,l) TEM images of Ni-Co LDH hollow nanocages/graphene composites. (m) Cycling stability tests of the Ni-Co LDH/graphene composite with different graphene masses [175] (Copyright 2017 American Chemical Society). (n,o) SEM images of Ni-Co@Ni-Co LDH nanotube arrays. TEM (p) and HRTEM (q) images of Ni-Co@Ni-Co LDH NTAs. (r) TEM elemental mapping of Ni, Co, and O. (Ni:Co = 5:5) [176] (Copyright 2017 WILEY-VCH Verlag GmbH & Co. KGaA, Weinheim).

Table 3. Summary of performances of multi-metal LDH nanomaterials and their hybrids.

Electrode Materials	ΔE (V)	Maximum Capacity ($C g^{-1}$)	Capacity Retention	Cycle Stability	Ref.
NiCo-LDH/CC	0.5	908 $C g^{-1}$ (1 A g^{-1})	60% (100 A g^{-1})	88% (10000 cycles)	[177]
NiCo-LDH/CFC	0.45	1009 $C g^{-1}$ (1 A g^{-1})	61% (60 A g^{-1})	95% (2000 cycles)	[178]
NiCoAl-LDH	0.6	1237 $C g^{-1}$ (1 A g^{-1})	48.7% (10 A g^{-1})	93% (3000 cycles)	[179]
NiCoAl-LDH@BG-NF	0.5	999 $C g^{-1}$ (6 A g^{-1})	75.3% (20 A g^{-1})	91% (2000 cycles)	[180]
rGO/Ni _{0.75-x} Co _x Al _{0.25} -LDH	0.5	772 $C g^{-1}$ (1 A g^{-1})	70% (40 A g^{-1})	89% (2000 cycles)	[181]
MnCo-LDH@Ni(OH) ₂	0.4	928 $C g^{-1}$ (1 A g^{-1})	56.3% (30 A g^{-1})	91% (5000 cycles)	[182]
Ni _{0.76} Co _{0.24} -LDH	0.5	1279 $C g^{-1}$ (1 A g^{-1})	87.2% (30 A g^{-1})	70% (20000 cycles)	[183]
HCNs@NiCo-LDH	0.5	1095 $C g^{-1}$ (1 A g^{-1})	74.9% (20 A g^{-1})	—	[184]
NiCo-LDH/rGO	0.45	802 $C g^{-1}$ (1 A g^{-1})	76.9% (20 A g^{-1})	74% (1000 cycles)	[185]
NiCo-LDH@CNT/NF	0.4	818 $C g^{-1}$ (1 A g^{-1})	65.2% (20 A g^{-1})	—	[186]
rGO(25)@CoNiAl-LDH	0.45	839.7 $C g^{-1}$ (1 A g^{-1})	72.9% (10 A g^{-1})	100% (5000 cycles)	[187]
LEG/NiCo-LDH	0.45	1099 $C g^{-1}$ (1 A g^{-1})	83.5% (50 A g^{-1})	89% (5000 cycles)	[188]
NixCo _{2x} (OH) _{6x} @Ni	0.5	1146 $C g^{-1}$ (5 A g^{-1})	68% (100 A g^{-1})	90% (5000 cycles)	[189]
NiCo-LDHs	0.45	780 $C g^{-1}$ (6 A g^{-1})	66.1% (30 A g^{-1})	86% (1000 cycles)	[173]
Ni-Co LDH NSs/CTs	0.5	1052 $C g^{-1}$ (2 A g^{-1})	57% (20 A g^{-1})	90% (2000 cycles)	[190]
NiMn LDH/rGO	0.5	750 $C g^{-1}$ (1 A g^{-1})	45.3% (10 A g^{-1})	90% (5000 cycles)	[191]
CoMn-LDH	0.65	916 $C g^{-1}$ (1 A g^{-1})	71.1% (10 A g^{-1})	93% (3000 cycles)	[192]
10NiAl-LDH	0.4	849 $C g^{-1}$ (0.5 A g^{-1})	70.7% (20 A g^{-1})	92% (10,000 cycles)	[193]
NiCo ₂ O ₄ @NiCoAl-LDH	0.6	1088 $C g^{-1}$ (1 A g^{-1})	61% (20 A g^{-1})	93% (2000 cycles)	[175]
Ni-Co LDH/graphene	0.6	759 $C g^{-1}$ (1 A g^{-1})	50% (10 A g^{-1})	93% (2000 cycles)	[165]
NiAl-LDH	0.55	1023.8 $C g^{-1}$ (2 A g^{-1})	68.8% (50 A g^{-1})	86% (5000 cycles)	[194]
NiFe-LDH	0.4	1354 $C g^{-1}$ (5 A g^{-1})	53.7% (10 A g^{-1})	43% (500 cycles)	[195]
MnCo-LDH	0.45	230 $C g^{-1}$ (1 A g^{-1})	69.7% (20 A g^{-1})	92% (2000 cycles)	[196]
GO/NiAl-LDHs	0.4	384 $C g^{-1}$ (1 A g^{-1})	67% (10 A g^{-1})	70% (2000 cycles)	[197]
NiAl-LDHs	0.45	277.6 $C g^{-1}$ (1 A g^{-1})	73.6% (20 A g^{-1})	96% (2000 cycles)	[198]
Co-Al-LDH	0.45	377 $C g^{-1}$ (1 A g^{-1})	80.8% (100 A g^{-1})	95% (20,000 cycles)	[199]
A-NiCo-LDHs	0.5	1224 $C g^{-1}$ (1 A g^{-1})	67.1% (20 A g^{-1})	93% (10,000 cycles)	[176]
Ni-Co@Ni-Co LDH	0.5	1207 $C g^{-1}$ (1 A g^{-1})	82.1% (20 A g^{-1})	98% (5000 cycles)	[200]
Ni-Mn LDH/carbon	0.5	634 $C g^{-1}$ (1 A g^{-1})	78.4% (10 A g^{-1})	79% (5000 cycles)	[201]

2.2. Negative Electrode Materials

The negative electrode material is also crucial in developing high-performance HSCs with high energy density and excellent rate capability. Since the different mass ratios will affect the overall capacitance of the HSC device [202,203], to balance the charges stored on the two electrodes of HSCs, the matching ratio of positive and negative electrodes should be accurately calculated. Carbon materials, such as activated carbon (AC), carbon nanotubes (CNTs), and reduced graphene oxide (rGO), are widely utilized for electrode materials in SCs due to their easy accessibility, good processing ability, large surface area/porosity, low electrical resistivity, robust surface chemical environment, physicochemical stability, and low cost [33]. Currently, the most commonly used electro-active materials in HSC electrodes are AC, CNTs, and rGO materials.

2.2.1. Activated Carbon Materials

AC is the most commonly used negative electrode material in HSCs because of its low cost and large surface area. At present, the AC electrodes have been applied to commercial SCs with high power density. Many recent advances in AC-based HSCs have been widely reported, as summarized in Table 4. The capacitance of AC is not linearly related to its surface area and pores sizes, such that the specific capacitance of micropores is larger than that of mesopores [33,203]. Therefore, controlling the pore size distribution of AC electrodes is very important. Kierzek et al. [204] prepared microporous AC with a surface area in the 1900–3200 $m^2 g^{-1}$ range and a pore volume

of 1.05 to 1.61 cm³ g⁻¹. The capacitance values ranging from 200 to 320 F g⁻¹ were achieved compared with the 240 F g⁻¹ of the commercially available ACs [204,205]. AC with remarkable performance, similar to SC electrodes, has also been prepared using other methods. For instance, Zhang et al. [206] prepared AC by the ZnCl₂ activation method, and the material exhibited a high surface area of 1935 m² g⁻¹ and a total pore volume of 1.02 cm³ g⁻¹. Moreover, it showed a high specific capacitance of 374 F g⁻¹ (1 mol L⁻¹ H₂SO₄ electrolyte), excellent capacity retention, and long cycling stability. In brief, although AC has a long history of usage and production, its structural and chemical characteristics are experiencing continual evolution to meet the requirements of more demanding emergent applications [205].

Table 4. Summary of performances of HSCs based on AC as negative electrode.

Device	Voltage (V)	Energy Density (Wh kg ⁻¹)	Power Density (W kg ⁻¹)	Cycle Performance	Ref.
Zn-Ni-Al-Co oxide//AC	0–1.5	72.4	533	90% (10,000 cycles)	[207]
NiO/Ni ₃ S ₂ //AC	0–1.6	52.9	1600	92.9% (5000 cycles)	[208]
Ni(OH) ₂ //AC	0–1.3	35.7	490	81% (10,000 cycles)	[57]
Ni(OH) ₂ //AC	0–1.6	22	800	85.7% (4000 cycles)	[67]
Ni(OH) ₂ -AB//AC	0–1.4	18.7	1971	91% (5000 cycles)	[69]
β-Ni(OH) ₂ //AC	0–1.6	36.2	100.6	92% (1000 cycles)	[200]
rGONF/Ni(OH) ₂ //AC	0–1.7	44.1	467	77.4% (2000 cycles)	[209]
NiS//AC	0–1.8	31	900	100% (1000 cycles)	[210]
NiS//AC	0–1.6	33.4	800	87.3% (5000 cycles)	[211]
Ni/Co-LDHs//AC	0–1.6	165.5	1530	85% (500 cycles)	[212]
ZnCo ₂ O ₄ //AC	0–1.6	29.7	398.5	72.5% (1000 cycles)	[213]
ZnCo ₂ O ₄ //AC	0–1.6	33.98	800	93.3% (10,000 cycles)	[214]
NiCo ₂ O ₄ /rGO//AC	0–1.5	57	375	90.2% (20,000 cycles)	[137]
NiCo ₂ S ₄ /Co ₉ S ₈ //AC	0–1.5	33.5	150	65% (5000 cycles)	[144]
CuCo ₂ S ₄ -HNN//AC	0–1.6	44.1	800	94.1% (6000 cycles)	[215]
MCS/GNF//AC	0–1.6	54.26	1120	81.9% (4000 cycles)	[216]
NiCo ₂ S ₄ //AC	0–1.6	25.5	334	93.4% (1500 cycles)	[168]
NiCo ₂ S ₄ //AC	0–1.6	42.7	1583	92% (10,000 cycles)	[170]
NiCo ₂ S ₄ nanopetals//AC	0–1.6	35.6	819.5	94.3% (5000 cycles)	[217]
NiCo-LDH//AC	0–1.6	69.7	800	87% (20,000 cycles)	[177]
NiCo-LDH//AC	0–1.5	17.5	10500	91.2% (10,000 cycles)	[167]
MnCo-LDH@Ni(OH) ₂ //AC	0–1.5	47.9	750.7	90.9% (5000 cycles)	[182]
NiCo-LDH//AC	0–0.8	15.9	400	82.7% (20,000 cycles)	[183]
NiCo ₂ O ₄ @NiCoAl-LDH//AC	0–1.6	74.6	800	93% (2000 cycles)	[175]
NiCo-LDH/graphene//AC	0–1.7	68	594.9	94.2% (2500 cycles)	[165]
NiFe-LDH//AC	0–1.6	50.2	800	65% (2000 cycles)	[195]
NiMoO ₄ //AC	0–1.7	60.9	850	85.7% (10,000 cycles)	[218]
NiCo-10//AC	0–1.6	51.5	825	89.5% (6000 cycles)	[219]
NiSe ₂ //AC	0–1.6	44.8	969.7	87.4% (20,000 cycles)	[220]

2.2.2. Carbon Nanotube Materials

CNTs have been widely studied for SCs owing to their porous structure, high surface area, good electrical conductivity, and low density [221–223]. Owing to their unique tubular structures and the high density of mesopores, they exhibit much higher specific capacitance than ACs [224]. Compared to multiwalled CNTs, single-walled CNTs exhibit better electrochemical properties because of their large specific surface area (~1600 m² g⁻¹), high aspect ratio, fast charge transport, and large accessibility of electrolyte ions [225–227]. Recently, Wang et al. [227] reported hierarchically porous CNTs by a simple carbonization treatment, which displayed a high specific surface area of 1419 m² g⁻¹ and hierarchical micro-/meso-/macroporosity. This unique porous architecture delivered an ultrahigh specific capacitance of 286 F g⁻¹ at 0.1 A g⁻¹, and excellent rate capability (~71% capacity retention from 0.1 to 50 A g⁻¹) [227]. To increase the energy and power density of devices, other strategies have also been employed,

such as atomic doping and combining CNTs with other materials (e.g., metal oxides, ACs, and graphene) [228–231]. For example, Kim et al. [230] recently reported a polyimide/MWCNT composite electrode with a high specific capacitance of 333.4 F g^{-1} at 1 A g^{-1} . Jin et al. [231] reported a polyaniline/carbon nanotubes/graphene/polyester hybrid electrode with a high areal capacitance of 791 mF cm^{-2} at a current density of 1.5 mA cm^{-2} . Although various types of research have been carried out on CNTs for HSCs, most of the reported electrodes are often in powdered form or have a disordered texture with poor interconnectivity among micro-/mesoporous structures, which leads to a low specific capacitance and high internal resistance, thus resulting in a much lower energy and power density for devices [232–234]. Therefore, it is still a great challenge to further improve its performance.

2.2.3. Reduced Graphene Oxide Materials and Their Hybrids

Another promising negative electrode material for HSCs is graphene. Graphene, a two-dimensional carbon sheet with monoatomic layer thickness, has been widely explored as an ideal electrode material for SCs due to its unique properties, including its high theoretical surface area ($2630 \text{ m}^2 \text{ g}^{-1}$) and high in-plane electrical conductivity [235,236]. It has brought a sensational revolution in the field of energy storage and conversion. To date, various routes have been developed to fabricate graphene sheets, such as blade-coating, spray-coating, layer-by-layer assembly, interfacial self-assembly, and filtration assembly [237–242]. In principle, a supercapacitor based on graphene is capable of achieving a theoretical electrochemical double layer capacitance as high as 550 F g^{-1} [243,244]. However, the practical performance of graphene is far below the ideal one due to various reasons. One of the main reasons is that the 2D layered graphene sheets can easily restack to form dense lamellar microstructures, which greatly decreases the specific surface area of the original graphene sheets, causes inferior ion transport capabilities, and renders a substantial number of active sites inaccessible to reactants [245–248]. Therefore, a number of strategies have been developed to prevent aggregation of graphene sheets so as to increase surface area and promote the transport of electrolyte ions, including fabricating 3D porous nanostructures [249,250], nitrogen doping [251–253], and surface modification using molecular modifiers [254,255]. For example, Li et al. [249] fabricated electrochemically active graphene fiber fabrics (GFFs) with a hierarchical morphology by using a hydrothermal activation strategy (Figure 5a–e). In such a process, crumpling of the graphene sheets within graphene fibers made for efficient activation on GFFs with a largely increased specific surface area [249]. Recently, Liu et al. [250] reported a novel strategy for the synthesis of pseudocapacitive oxygen clusters in graphene frameworks with “paddy land” structures through low-temperature thermal annealing of graphene oxide (Figure 5f–h). The SEM image (Figure 5i) clearly shows the typical flakelike morphology, with the lateral size ranging from 500 nm to a few micrometers. Moreover, the TEM image (Figure 5j) indicates the smooth surface of the GO-160-8D with layer stacking structure. Moreover, a high-magnification TEM image clearly demonstrates that sp^3 carbon domains consisting of oxygen clusters are well distributed in the continuous sp^2 carbon network. The as-prepared functionalized graphene shows ultrahigh specific capacitance of 436 F g^{-1} at 0.5 A g^{-1} , excellent rate performance (261 F g^{-1} at 50 A g^{-1}) and long cycling stability (94% of capacitance retention after 10,000 cycles) [250]. Shao et al. [256] reported a 3D porous rGO film with a high conductivity (1905 S m^{-1}) and good tensile strength. The open surfaces of the 3D porous rGO films can be easily accessed by electrolyte ions without a diffusion limit, which guarantees a large capacitance at high current density/scan rate [256].

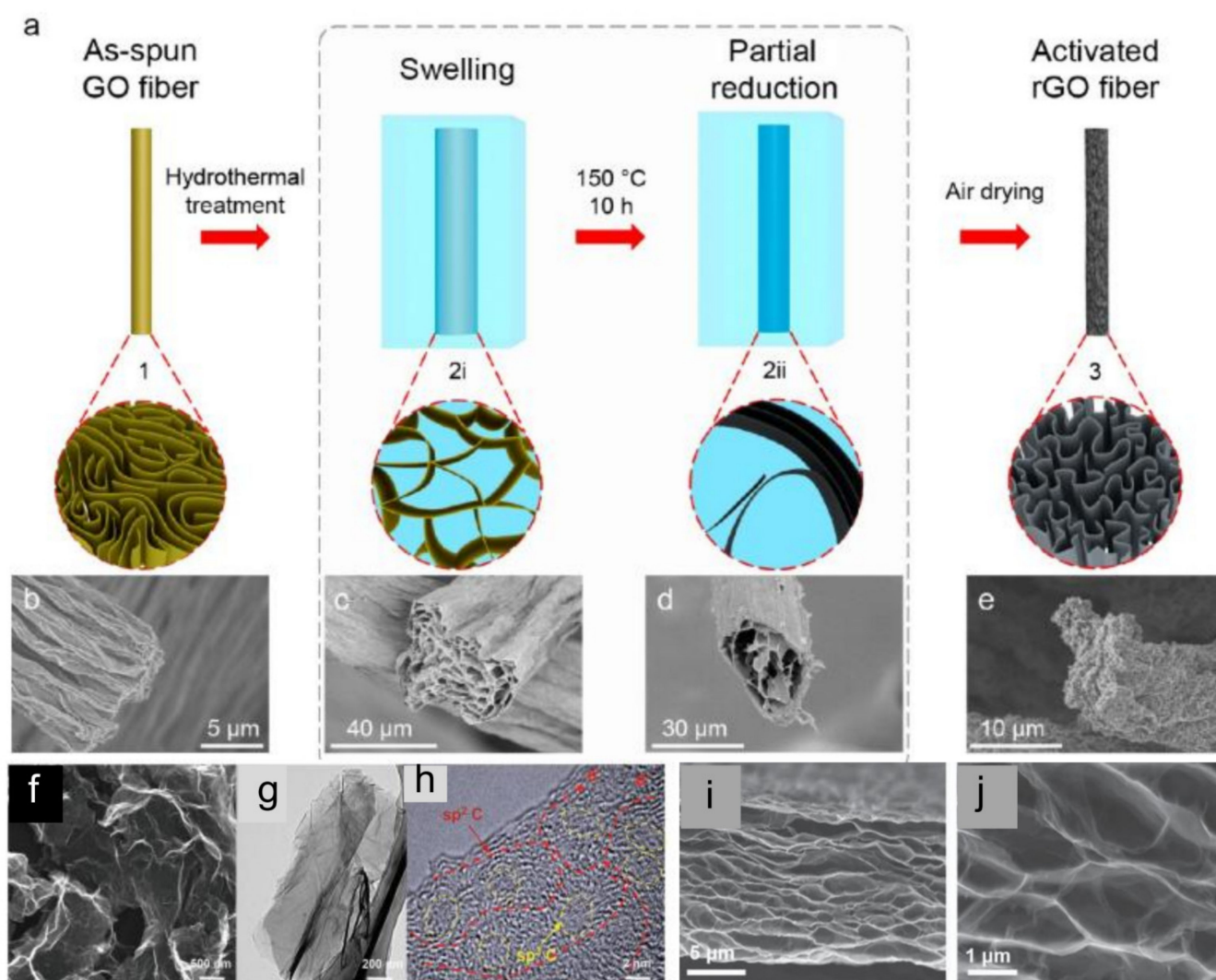


Figure 5. (a) Schematic diagram showing the structural evolution of graphene fibers during the hydrothermal activation process. Crosssectional SEM images of graphene fibers in the corresponding stages: (b) as-spun GO fiber, (c) swelled GO gel fiber at the beginning of hydrothermal treatment, (d) rGO gel fiber at the end of hydrothermal treatment, and (e) the resulted hierarchical rGO fiber after air-drying [249] (Copyright 2017 American Chemical Society). (f) SEM image of the GO-160-8D sample. (g) TEM image of the GO-160-8D sample. (h) high-magnification TEM image [250] (Copyright 2016 WILEY-VCH Verlag GmbH & Co. KGaA, Weinheim). (i,j) Specific capacitances of GO-160-8D under mass loadings of 2 and 10 mg cm⁻², and that of commercial activated carbon (YP-50) under a mass loading of 10 mg cm⁻² [256] (Copyright 2017 WILEY-VCH Verlag GmbH & Co. KGaA, Weinheim).

Nitrogen doping is considered as an effective strategy to enhance the electrochemical performance of graphene. Doping not only affects the electronic structure and properties of graphene, but it also reduces the degree of aggregation and results in a morphology that allows easy access to electrolyte ions [257]. Some researchers have demonstrated that N-doping could greatly improve the specific capacitance of graphene. In 2013, Lu et al. [258] developed a solvothermal method to prepare N-doped graphene and achieved a specific capacitance of 301 F g⁻¹. In 2015, Qin et al. [241] reported a thermal treatment method to prepare robust 3D N-doped graphene (R-3DNG) and achieved a specific capacitance of 509 F g⁻¹, which is approaching the theoretical capacitance of graphene (550 F g⁻¹). In 2016, Wang et al. [242] prepared N-doped graphene by treating polypyrrole-modified GO with plasmas, and observed a specific capacitance of 312 F g⁻¹. In 2017, Hang et al. [251] reported an N-superdoped 3D graphene network structure (3D GF-NG) by immersing

highly conductive GF with a 3D interconnected network structure into an aqueous solution of GO sheets (Figure 6a). The N-doped GO aerogels closely connected with the GF skeleton, forming an interconnected GF-NG network structure (Figure 6b,c), and demonstrating a large specific surface area of $583 \text{ m}^2 \text{ g}^{-1}$, through which electrolyte ions could easily access to the surface of graphene to form electric double layers [251]. The fabricated 3D N-doped rGO electrode delivered a high specific capacitance of 312 F g^{-1} at 5 mV s^{-1} [251]. In 2018, Zhang et al. [259] reported an advanced N-doped graphene electrode with an ultrahigh specific capacitance of 481 F g^{-1} at 1 A g^{-1} , and with superior cycling stability of 98.9% capacitance retention after 8000 cycles. Figure 6d shows the SEM image of the N-doped graphene nanosheets, revealing many densely stacked gibbous bubbles with one dimension of about 10 nm on the surface of undulated graphene nanosheets [259]. The TEM image of the N-doped graphene in Figure 6e illustrates its unique wrinkled structure. This unique structure improves the access of ions between the electrolyte and electrode surface and thereby enhances the transport rates toward the interface of the electrode [259]. The as-produced N-P-O co-doped 3D hierarchical porous graphene by Zhao et al. [260] exhibited many nanopores (Figure 6f), facilitating the high volumetric density of the product. As shown in Figure 6g, the density functional theory (DFT) calculations were performed to investigate the co-doping effect of N-P-O in the pristine graphene. All atoms in the models were free to fully relax [260]. The unique 3D hierarchical porous graphene electrode delivered an ultrahigh specific capacitance of 426 F g^{-1} .

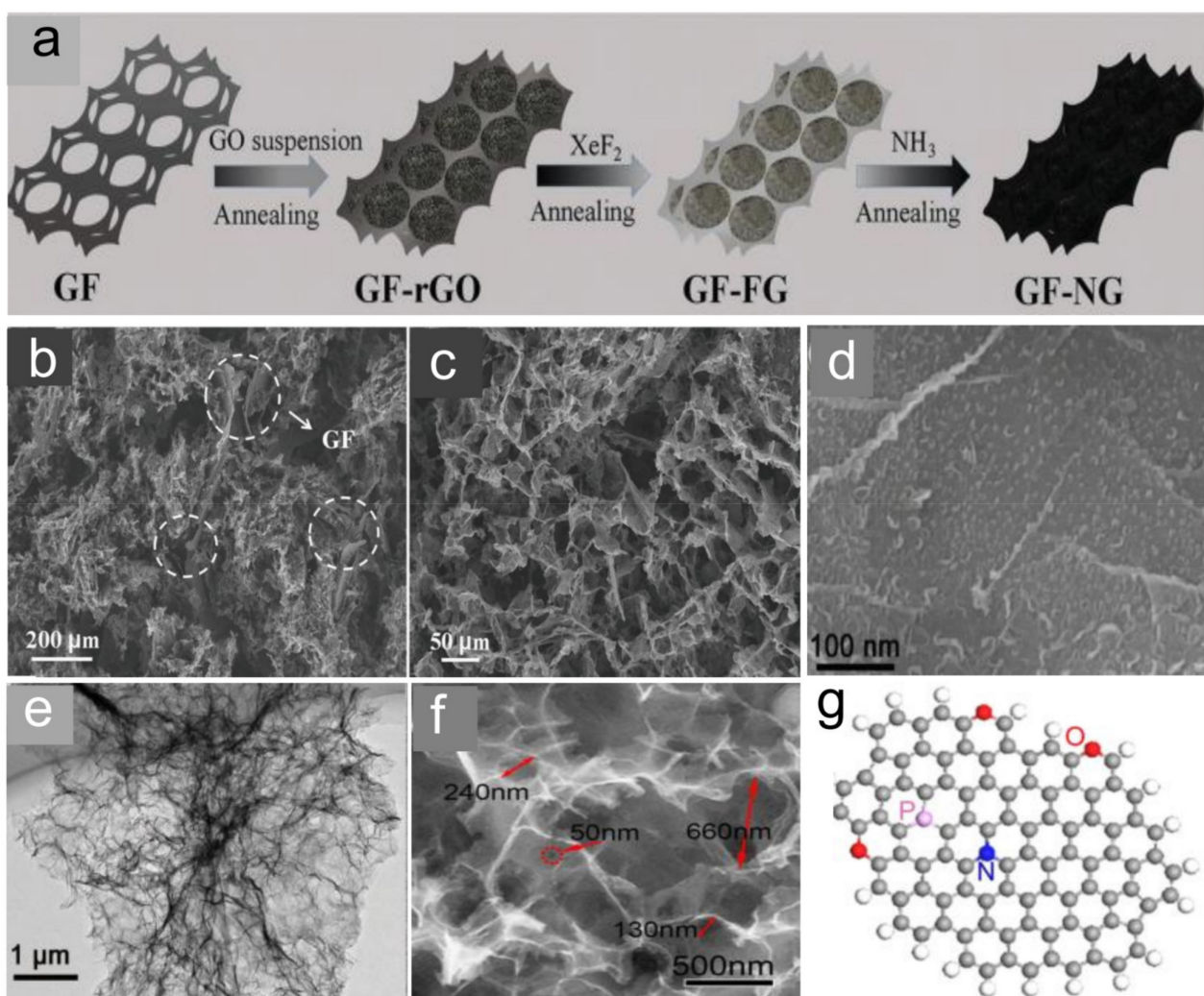


Figure 6. (a) Schematic drawing of the procedure for fabricating 3D GF-NG network macrostructure. (b) Low-magnification and (c) high-magnification cross-sectional FESEM images of GF-NG. The sections

marked by dots circles are the skeletons of GF [251] (Copyright 2017 WILEY-VCH Verlag GmbH & Co. KGaA, Weinheim). SEM (d) and TEM (e) images of N-doped graphene (Copyright 2017 WILEY-VCH Verlag GmbH & Co. KGaA, Weinheim) [259]. (f) SEM image of 3D hierarchical porous graphene. (g) Lowest Unoccupied Molecular Orbital of N-P-O co-doped graphene [260] (Copyright 2016 Elsevier Ltd., All rights reserved).

Modifying the surface structure of electrode materials could improve their compatibility with electrolytes, enrich redox sites, and enhance the surface conductivity, leading to good electrochemical performance [33]. Recently, oxygen- and nitrogen-containing groups have been well studied to modify the graphene surface. For example, Song et al. [254] recently reported different functionalized graphene networks by using amine molecules and a facile two-step hydrothermal method. The as-fabricated graphene composite exhibited an improved capacitance and fast ionic diffusion features in aqueous and organic electrolytes, with less than 10% capacitance decay during 10,000 charge/discharge cycles [254]. Li et al. [257] reported chemical compounds of GO and amine molecules as spacers by one-step hydrothermal reactions. The as-prepared graphene composite electrode exhibited excellent performance with a high specific capacitance of 597 F g^{-1} [255]. In conclusion, heteroatoms in doped graphene materials play a key role in electron transfer and energy conversion processes. The incorporation of nitrogen or molecular modifiers can provide the work electrodes with high-density active sites to enhance the capacitance performance. Moreover, it can also reduce the agglomeration level of graphene and create few-layer graphene sheets with interconnected open pores, which provide an effective pathway for charge transport.

3. Design Structures of Hybrid Supercapacitors

A HSC device usually contains positive and negative electrodes, an electrolyte, a separator (to prevent short circuits between electrodes), and current collectors. Besides the electrodes, electrolytes also play an important role in HSC performance. The electrolytes of HSCs could be organic (LiPF_6 , LiBF_4 , LiClO_4 , NaClO_4 , NaPF_6 , etc.), ionic liquid (BMIMBF_4), gel-polymer ($\text{PVA-H}_3\text{PO}_4$, PVA-LiCl , etc.), or aqueous of acidic (H_2SO_4 , $\text{CH}_3\text{SO}_3\text{H}$), alkaline (KOH , NaOH), and neutral (Na_2SO_4 , Li_2SO_4) [13]. Aqueous electrolytes usually have the advantages of high ionic conductivity, low cost, non-flammability, safety, and convenient assembly in air [261]. But its potential window is limited to 1.2 V, which is far lower than that of organic electrolytes (3.5–4 V). A high-potential window is a large merit for organic electrolytes, which could significantly contribute to high energy density. However, it is less conductive, expensive, usually flammable, and more toxic [13,261]. Ionic liquids as nonvolatile, highly stable electrolytes are considered as the most promising electrolytes compared to organic ones for HSC applications [13]. The gel-polymer electrolyte is usually used for designing and fabricating flexible/stretchable or even smart HSCs due to its merits of avoiding electrolyte leakage or without using an additional separator [262,263]. In this section, four main types of HSCs (Figure 7) are summarized and discussed in detail.

3.1. The Traditional Planar HSC Devices

The traditional HSC devices are constructed from two different types of planar electrodes, one membrane charge separator, and an electrolyte sandwiched together. They have demonstrated great potential in hybrid electric vehicles (electric buses and trains), the aerospace industry, and portable electronic devices [264,265]. To date, remarkable progress has been made in the development of high-performance HSCs. For example, Zhao et al. [50] reported a high-performance HSC device based on Ni-Co-Mn-OH/rGO as the positive electrode and PPD/rGO as the negative electrode (Figure 8a). The rate capability of the HSC device was evaluated by cyclic voltammetry at different scan rates. The shapes of CV curves were well maintained with the increase in scan rate from 5 to 100 mV s^{-1} , revealing the high-rate capability of the HSC device. Moreover, the as-fabricated device exhibited an energy density of 74.7 W h kg^{-1} at a power density of 1.68 kW kg^{-1} , while maintaining

a capacity retention of 91% after 10,000 cycles at a charge-discharge current density of 20 A g^{-1} . In addition, they also fabricated a high-performance HSC device based on $\text{Co}_x\text{Ni}_{1-x}(\text{OH})_2@\text{rGO}$ composite as a battery-type faradaic electrode and a p-p henylene-diamine (PPD)-modified rGO composite as a capacitive electrode (Figure 8b) [153]. The shapes of CV curves were well reserved as the scan rate was increased from 5 to 100 mV s^{-1} , indicating reasonably high-rate capability of the hybrid supercapacitor, as a result of the electrochemical properties of both the positive and negative electrodes [153]. Moreover, the as-fabricated HSC device also demonstrated a high energy density of 72 Wh kg^{-2} and excellent cycling life [153]. Recently, we also designed a HSC device, constructing it from $\text{NiS-Ni}_3\text{S}_2\text{-Ni}_3\text{S}_4/\text{rGO}$ ($\text{Ni}_x\text{S}_y/\text{rGO}$) as a battery-type faradaic electrode and graphene as a capacitive electrode (Figure 8c), which exhibited a similar electrochemical behavior in a voltage range of 0–1.6 V, a high energy density of 46 Wh kg^{-1} at a power density of 1.8 kW kg^{-1} , and good cycling stability [12]. Furthermore, we also fabricated a novel HSC device based on C@ZnNiCo-CHs as the positive electrode and N,S-codoped rGOs as the negative electrode (Figure 8d), which delivered an excellent electrochemical behavior in a voltage range of 0–1.6 V, a high energy density of 70.9 Wh kg^{-1} , and excellent cycling stability [266]. These findings not only provide a promising electrode material for high-performance HSCs, but also open a new avenue toward knowledge-based design of efficient electrode materials for other energy storage applications [50]. In brief, the traditional planar HSCs are beneficial for achieving a high ratio of energy delivery at high charge-discharge rates, but they are usually large in size, heavy in weight, and mechanically inflexible [7]. Therefore, an important goal for HSC is to develop the small-sized, portable, and flexible devices.

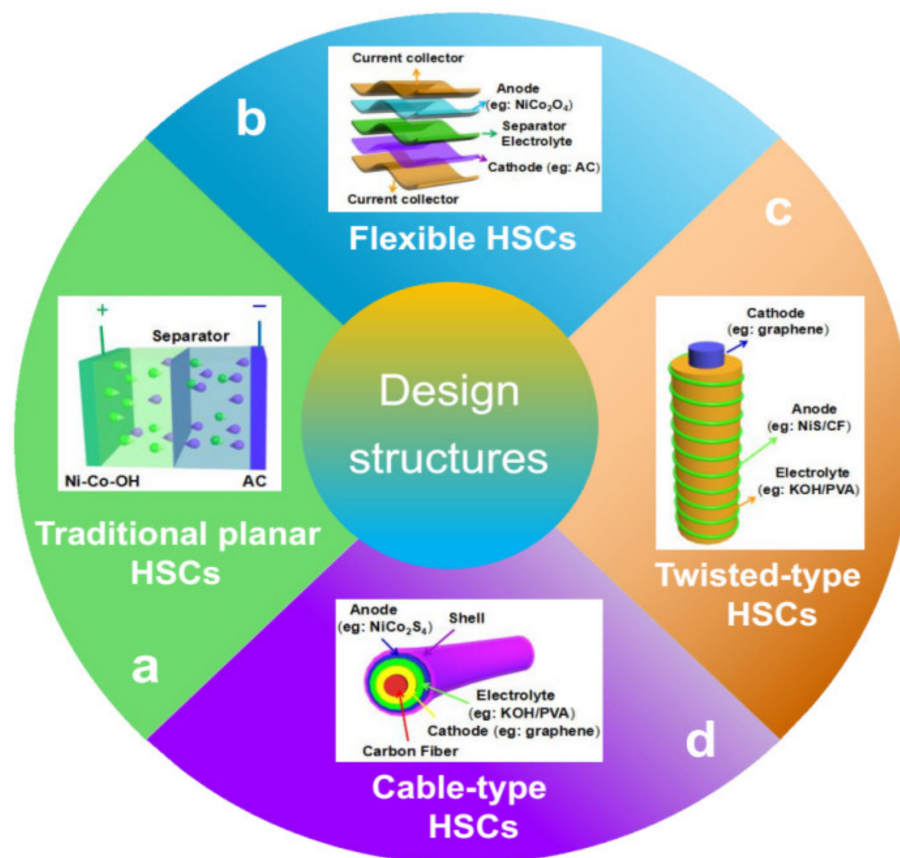


Figure 7. The hybrid supercapacitors with four representative structure types, namely, (a) traditional planar HSCs, (b) flexible HSCs, (c) twisted-type HSCs, and (d) cable-type HSCs.

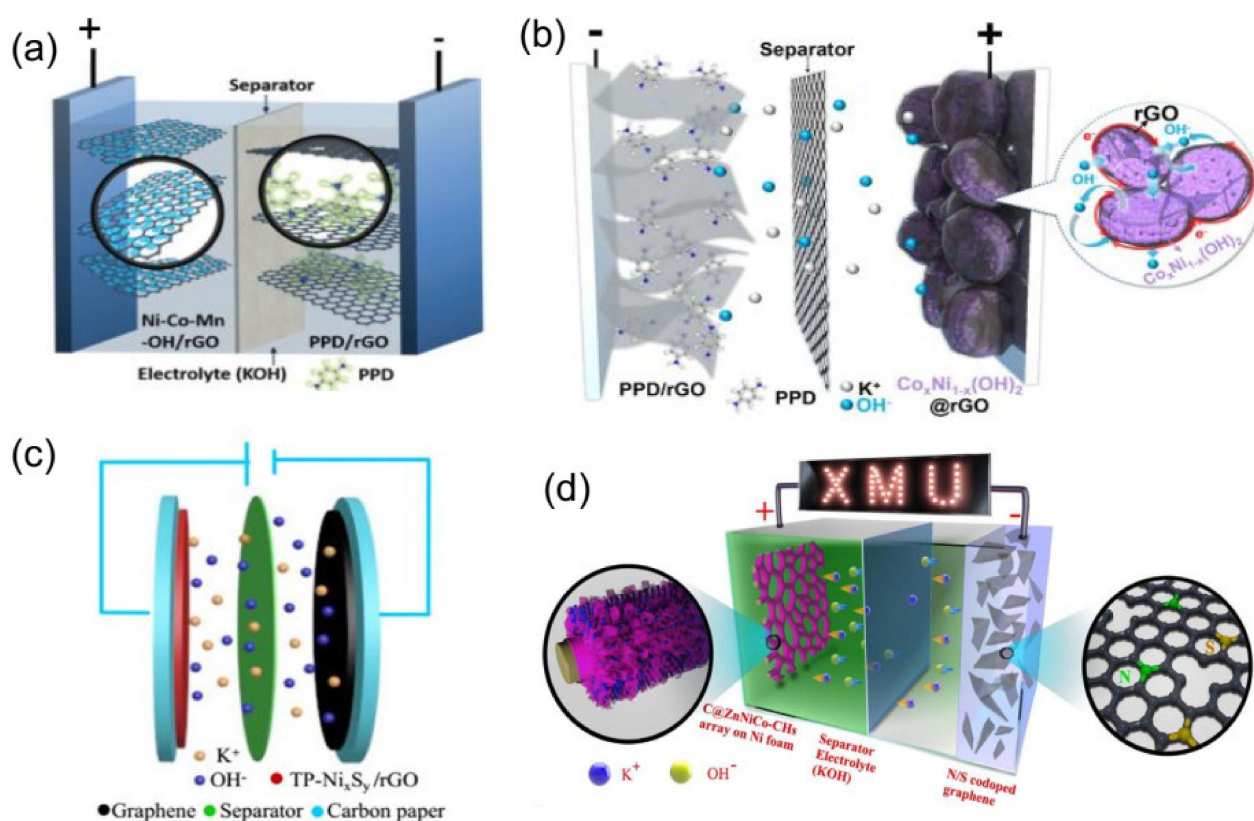


Figure 8. (a) Schematic illustration of the HSC device using Ni-Co-Mn-OH/rGO as positive electrode and PPD/rGO as negative electrode [50] (Copyright 2017 WILEY-VCH Verlag GmbH & Co. KGaA, Weinheim). (b) Schematic illustration of the hybrid supercapacitor device with a Co_xNi_{1-x}(OH)₂@rGO composite as a battery-type faradaic electrode and a p-phenylenediamine (PPD)-modified rGO composite as a capacitive electrode [153] (Copyright 2016 Elsevier B.V.). (c) Schematic illustration of the NiS-Ni₃S₂-Ni₃S₄/rGO//graphene hybrid supercapacitor device [12] (Copyright 2017 Elsevier Ltd., All rights reserved). (d) Schematic illustration of the C@ZnNiCo-CHs//N,S-codoped rGOs hybrid supercapacitor device [266] (Copyright 2018, published by Elsevier B.V.).

3.2. The Flexible HSC Devices

Owing to the rapid growth of portable and wearable consumer electronics, such as wearable displays, on-body sensors, artificial electronic skin, and distributed sensors, enormous effort has been devoted to flexible, wearable, and integratable electronics to meet the demands of modern society [267–269]. In recent years, some research has been done to fabricate stretchable HSC devices, mostly by using carbon fibers (CFs), nickel foam, or conductive polymers as substrates to achieve stretchability [270–274]. For example, Kim et al. [270] recently developed a flexible electrode based on binder-free nickel cobalt layered double hydroxide nanosheets adhered to nickel cobalt layered double hydroxide nanoflake arrays on nickel fabric (NC LDH NFAs@NSs/Ni fabric) using facile and eco-friendly synthesis methods (Figure 9a–d). The fabricated HSC device, constructed from the NC LDH NFAs@NSs/Ni fabric positive electrode and MnO₂/3D-Ni negative electrode, exhibited excellent electrochemical durability and flexibility. Zhang et al. [271] fabricated the HSC device based on the Ni-Co-S/graphene foam (GF) as the positive electrode and polypyrrole (PPy)/GF as the negative electrode (Figure 9e), which demonstrated robust flexibility under different bending angles. Recently, carbon-based fibers have also been widely used in flexible energy storage electrodes due to their unique features involving the high flexibility, good mechanical properties, and its unchanged sheet resistance even in a very high bending state [9]. For example, Huang et al. [272] designed and fabricated hierarchical core-branch Al-doped cobalt sulfide nanosheets anchored on Ni nanotube

arrays combined with carbon cloth (denoted as CC/H-Ni@Al-Co-S) (Figure 9f), which exhibited high specific capacity (1217 C g^{-1} at 1 A g^{-1}). Moreover, the as-fabricated CC/H-Ni@Al-Co-S//graphene/CNT HSC device not only demonstrated high flexibility, but also delivered a high energy density of 65.7 Wh kg^{-1} . Nagaraju et al. [275] reported the progress toward a high-performance HSC device based on a 3D Ni-electrode (Figure 9g), which delivered an excellent energy density of 75 Wh kg^{-1} and a high-power density of 5.3 kW kg^{-1} . Furthermore, the device also demonstrated excellent flexibility and a potential application for wearable energy management.

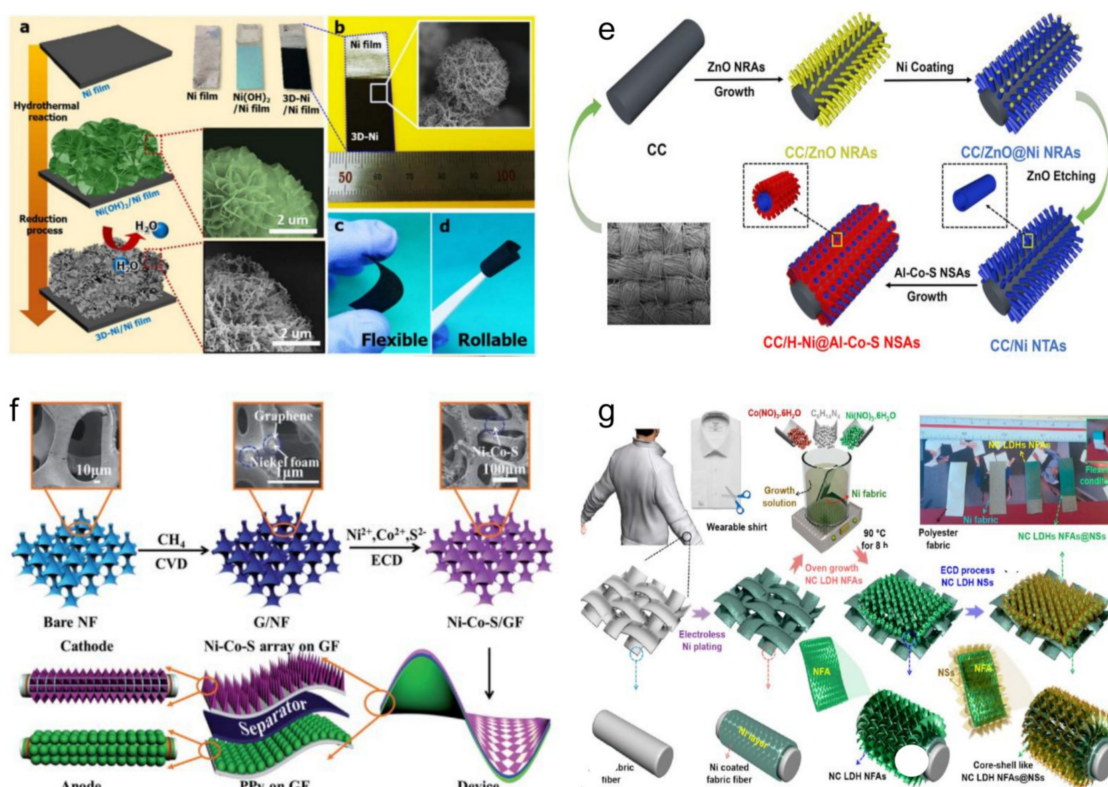


Figure 9. The fabrication and morphology of the mesoporous 3D-Ni current collector. (a) Schematic illustration of the fabrication procedure of the mesoporous 3D-Ni/Ni film (inset images are photographs and SEM images of the $\text{Ni}(\text{OH})_2/\text{Ni}$ film and the 3D-Ni/Ni film). (b) Photograph of the synthesized 3D-Ni/Ni film (the inset is a magnified SEM image). (c) Photograph of the 3D Ni/Ni film with flexible (d) and rollable properties [270] (Copyright 2017 Elsevier Ltd., All rights reserved). (e) Schematic illustration of the synthesis of the petal-like Ni-Co-S and the construction of HSC devices [271] (Copyright 2017 WILEY-VCH Verlag GmbH & Co. KGaA, Weinheim). (f) Schematic illustration of the fabrication of a hierarchical core-branch CC/H-Ni@Al-Co-S nanosheet electrode [272] (Copyright 2018 American Chemical Society). (g) Schematic illustration of the fabrication process of NC LDH NFAs@NSs/Ni fabric using a wearable polyester shirt [275] (Copyright 2017 American Chemical Society).

Up to date, various studies have been carried out on flexible planar HSC devices, but the cycling stability of HSCs still needs to be improved. The phase transformation, structural collapse, and volumetric expansion may be the most key factors that causing the reduction of capacity during long-term charging-discharging cycles [273]. The incorporation of metal cations into hybrid electrode materials can effectively prevent the phase transitions in active materials, which can improve their long-term cyclability [275]. Another effective method is to fabricate the nanostructured composites with graphene [275], which can effectively prevent the nanostructure from collapsing and avoid the corrosion of energy storage capacity.

3.3. The Twisted-Type HSC Devices

Unlike conventional rigid planar HSCs, the twisted-type HSCs can be directly used as flexible power sources in wearable, self-powered electronic devices [275]. They can be either co-woven/knitted into existing fabrics/textiles or they can be woven/knitted by themselves [276]. Recently, many advanced fiber-shaped HSC devices have been widely reported in the literature [276–280]. For instance, Sun et al. [280] reported a twisted-type HSC device assembled by twisting a molybdenum-nickel-cobalt ternary oxide/carbon nanotube fiber (MNCO/CNTF) positive electrode and thin carbon-coated vanadium nitride (VN) nanowire arrays on a CNTF negative electrode (Figure 10a), which delivered a high specific capacitance of 490.7 F cm^{-3} (1840 mF cm^{-2}) at a current density of 1 mA cm^{-2} and outstanding flexibility and stability with capacitance retention maintained at 90.2% after bending 3500 times. Jin et al. [281] reported a twisted-type HSC with PANI-coated carbon fiber thread as the positive electrode and functionalized carbon fiber thread as the negative electrode (Figure 10b), which also demonstrated high flexibility and stability. Liu et al. [282] recently reported a novel flexible twisted-type HSC with coaxial human hair/Ni/Graphene/MnO₂ fiber as the positive electrode and coaxial human hair/Ni/Graphene fiber as the negative electrode, which first reveals that human hair could also be used to fabricate flexible HSCs. The as-fabricated HSC exhibited excellent rate capability (up to 20 V s^{-1}), high volumetric energy density (1.81 mWh cm^{-3}), and excellent flexibility [282]. Senthilkumar et al. [283] fabricated the twisted-type HSC assembled by copper hexacyanoferrate coated carbon fibers (CuHCF@CFs) and porous carbon coated carbon fibers (PC@CFs) electrodes (Figure 10e), which also demonstrated outstanding flexibility (Figure 10f) and a high energy density of 10.6 Wh kg^{-1} . In general, the flexible twisted-type HSCs are attractive as power sources for miniaturized electronic devices, because they have small volumes and could be easily integrated into variously shaped structures [284]. However, these HSCs still suffer from relatively low capacitance and a high production cost, which cannot meet the ever-increasing demand for flexible devices. In addition, some technical challenges still limit the development of strong, flexible, and wearable HSC devices with high performance. Therefore, more efforts are needed in searching for new structured active materials with high electron conductivity, high electrochemical sites, and novel fiber current collectors with strong mechanical stability and ultra-high flexibility to develop fiber-shaped flexible HSC devices with high performances.

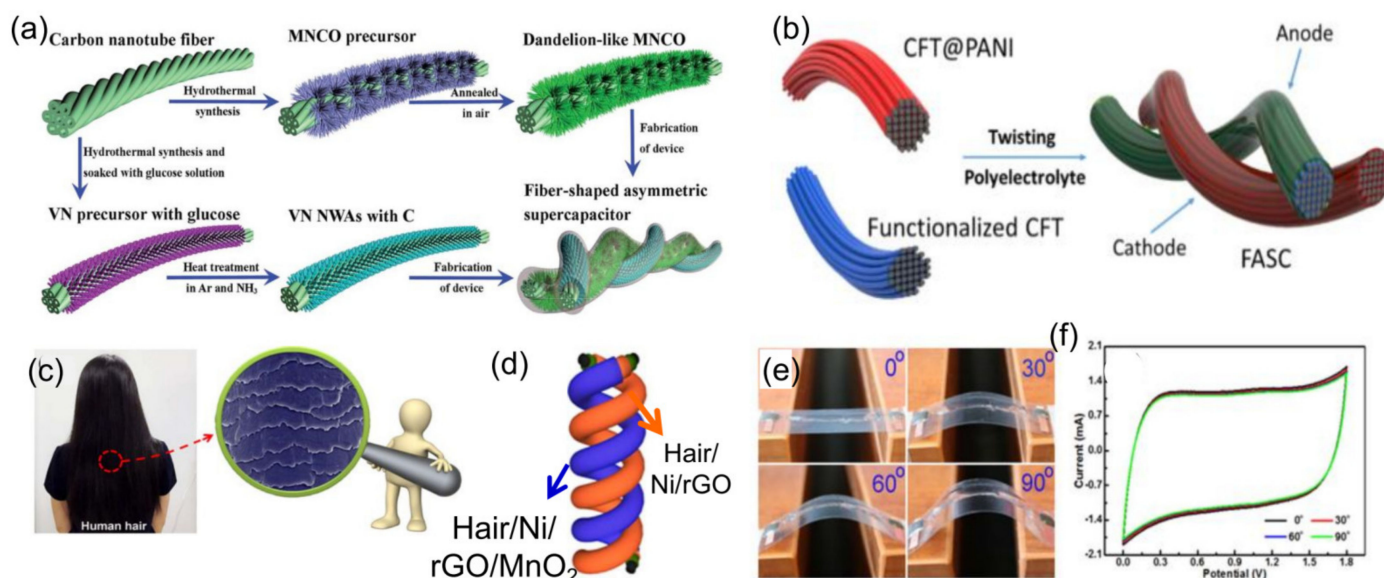


Figure 10. (a) Detailed schematic illustration of the fabrication process for the twisted-type HSC device [280] (Copyright 2017: The Royal Society of Chemistry). (b) Schematic illustration of the fabrication of the twisted-type HSC device [281] (Copyright 2015 Elsevier Ltd. All rights reserved).

(c) Photograph of human hair, and (d) schematic diagram of the HSC devices constructed by twisting the human hair/Ni/rGO/MnO₂ fiber and human hair/Ni/rGO fiber together [282] (Copyright 2017 Elsevier Ltd. All rights reserved). (e) Schematic illustration of the fabrication of twisted-type HSC device. (f) CV curves (at 15 mV s⁻¹) under different bending conditions [283] (Copyright 2016 The Royal Society of Chemistry).

3.4. The Cable-Type HSC Devices

Among various flexible energy storage devices, the cable-type HSCs have attracted increasing attention due to their merits of low weight, tiny volume, high flexibility, and wearability [285,286]. So far, many advanced cable-type SC devices have been widely reported in the literature [287–290]. For instance, Zhang et al. [287] recently reported a facile and cost-effective method to directly grow three-dimensionally well-aligned zinc-nickel-cobalt oxide (ZnCO)@Ni(OH)₂ nanowire arrays on a carbon nanotube fiber (Figure 11a) with an ultra-high specific capacitance of 2847.5 F cm⁻³ (10.678 F cm⁻²) at a current density of 1 mA cm⁻². Moreover, they also fabricated a novel cable-type HSC device based on ZnCO@Ni(OH)₂ NWAs/CNTF as the positive electrode and a thin layer of carbon-coated vanadium nitride nanowire arrays on a carbon nanotube strip as the negative electrode, which demonstrated excellent flexibility and stability. Li et al. [288] developed a novel flexible cable-type HSC device based on Cu//CuO@LDH as the positive electrode and Cu//AC as the negative electrode (Figure 11b), which also presented great flexibility and excellent cycling stability. Nagaraju et al. [289] recently also fabricated a cable-type HSC device based on nickel oxide nanosheet grafted carbon nanotube coupled copper oxide nanowire arrays (NiO NSs@CNTs@CuO NWAs/Cu fibers) as the positive electrode and AC as the negative electrode (Figure 11c), which demonstrated excellent flexibility and stability. Gao et al. [290] reported a flexible cable-type HSC (Figure 11d) based on the Ni-Co DHs and pen ink electrodes on metallized CF. Moreover, the as-fabricated device also delivered good cycling stability and high energy [290]. This low-cost and high-performance flexible cable-type HSC provides an alternative strategy toward efficient flexible energy storage devices and wearable energy equipment.

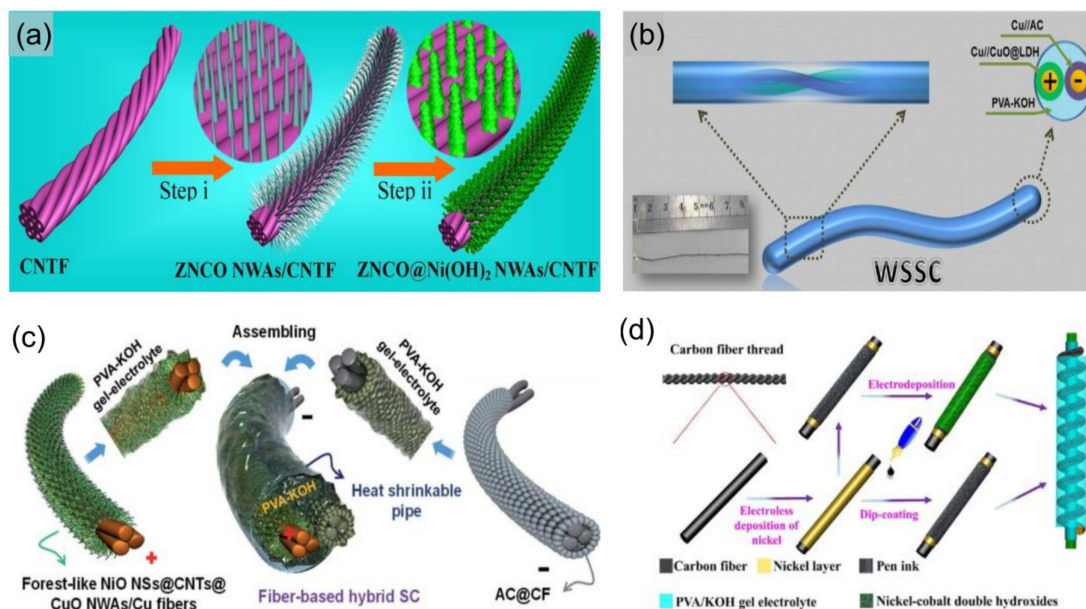


Figure 11. (a) Schematic fabrication process of the ZnCO@Ni(OH)₂ NWAs on a carbon nanotube fiber [287] (Copyright 2017 American Chemical Society). (b) Schematic representation of the flexible cable-type HSC device based on CuO@CoFeLDH and active carbon electrodes [288] (Copyright 2016 Elsevier Ltd., all rights reserved). (c) Schematic diagram showing the fabrication process of the HSC device [289] (Copyright 2018 WILEY-VCH Verlag GmbH & Co. KGaA, Weinheim). (d) Schematic diagram of the fabrication procedure of the HSC device [290] (Copyright 2017 American Chemical Society).

4. The Charge-Storage Mechanism of Hybrid Supercapacitors

For a better understanding of the operative mechanisms of the combination of Faradaic and capacitive electrodes in hybrid supercapacitors, some basic theoretical aspects will be discussed in this section. Moreover, how to distinguish between a capacitor-like and a battery-like electrode materials will also be presented in the next paragraphs. Figure 12 depicts the characteristic behavior of these conventional energy storage materials. The capacity of the batteries relies predominantly on the Faradaic reaction that is made possible by the intercalation/de-intercalation of charge-compensating ions (H^+ , Li^+ , or Na^+) within the crystalline structure of electrode materials [27]. However, the capacitance of the supercapacitors mainly depends on the electrochemical adsorption/desorption of cations and anions at the electrode/electrolyte interface (double-layer capacitive) or surface faradaic redox reactions (pseudocapacitive) at the surface of electrode materials [7,27]. Some researchers may ask how to determine whether a new material that it should be classified as a battery-type or a capacitor-type material. As we all know, the electrochemical behaviors of the batteries and supercapacitors are both characterized by the cyclic voltammetry (CV) and galvanostatic charge/discharge (GCD) tests. A related analysis of the energy storage mechanisms can be performed from the CV curves. The kinetic information obtained from the peak current (i) response can be summarized using the following equation [4,27]:

$$i = av^b \quad (1)$$

where the measured current i at a fixed potential obeys a power law relationship with the potential sweep rate v [27]. The b -value is determined by the slope of the $\log(v)$ – $\log(i)$ plots. In general, the b value of 0.5 represents a semi-infinite diffusion behavior, whereas 1.0 indicates a capacitive process [50,267]. The peak current (i) response of battery-type materials exhibits classic semi-infinite diffusion because of phase transformations, thus resulting in low Coulombic efficiency and poor rate performance. The CV curves of the corresponding electrodes show prominent and widely separated peaks associated with the reduction and oxidation, and the discharge curves exhibit obvious plateaus (Figure 12a) [7]. However, the current (i) response of capacitor-type materials is not controlled by the diffusion process, and it exhibits a linear current response dependency on the scan rate [7]. The CV curves of the corresponding electrodes show a rectangular or approximate rectangular shape, and the discharge curves exhibit a linear voltage response during constant current charge-discharge (Figure 12b). Hence, the capacitor-type electrode materials exhibit high power density but poor energy density, whereas the battery-type materials show high energy density but poor power density.

As a patent for an energy-storage device that combined a double-layer capacitor electrode with a positive nickel battery was reported by Varakin et al. in the mid-1990s [291]. In during the past few years, similar energy-storage devices have been widely reported in numerous publications. Unfortunately, the concept of such energy storage devices is very confusing in many publications. As suggested by Brousse et al. [7], the term of hybrid supercapacitors should be used when pairing two electrodes with various charge storage behaviors (i.e., one faradaic and one capacitive). The concept of an asymmetric supercapacitor covers a wider range of electrode combinations because it can be used for supercapacitors using two electrodes of the same nature but with various mass loadings, or two electrodes using various materials [7]. It should be emphasized that a relatively complex charge-storage mechanism occurs in the hybrid supercapacitor devices and some hybrid nanocomposite electrodes, and the corresponding electrochemical characteristics are neither purely capacitor-type nor purely battery-type. As a new type of hybrid charge storage mechanism, the current (i) response to the sweep rate (v) will depend on the electrochemical reaction associated with diffusion-controlled and surface-controlled (capacitive) reaction. Therefore, the current response (i) at a fixed sweep rate (v) can be summarized according to the following equation [50,267]:

$$i(v) = k_1v^{1/2} + k_2v \quad (2)$$

By determining both k_1 and k_2 , we can distinguish the fraction of the current arising from cation intercalation ($k_1v^{1/2}$) and that from capacitive (k_2v) processes at each potential [267]. The total energy stored in the hybrid supercapacitors is the sum of the energy stored in the battery-type electrode and that of the capacitor-type electrode (Figure 12c). The battery-type electrode is used to improve the energy densities compared to those of typical double-layer capacitors and pseudocapacitors. On the other hand, the capacitor-type electrode is used to improve the power densities of the cells compared to the typical batteries. The main reason is that the capacitor component can improve the electron transfer to the battery component in the hybrid system, causing a better charge transfer reaction at high rates. Hence, the hybrid supercapacitors can usually exhibit high power densities.

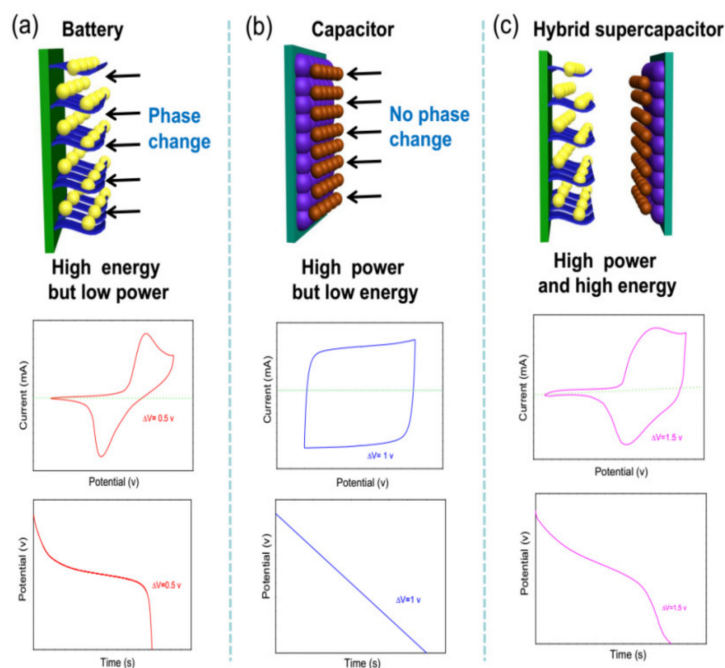


Figure 12. Schematic of charge storage mechanisms, cyclic voltammograms, and corresponding galvanostatic discharge curves for batteries (a), capacitors (b), hybrid supercapacitors (c).

Obviously, the total energy storage capacity and rate capability of the hybrid supercapacitors can be optimized by expanding the operating potential window and designing porous hybrid nanostructured composite materials. The operating potential window of the hybrid supercapacitors can be extended to $\sim 1.5\text{ V}$ or even higher (Figure 12). The hybrid nanostructured electrodes, which combine battery components (transition metal oxides/sulfides) with capacitor components (carbon-based), usually exhibit higher electrochemical performance, especially high-rate performance and cycle life. The charge storage of this hybrid electrode will be due to both battery and capacitor components: firstly, the capacitor component is charged via electrostatic forces until the electrode potential reaches the redox reaction potential of the battery component [292]. Then, the battery component is charged through the Faradaic reaction until the faradaic component reaches its full-charge state [293]. It should be emphasized that calculating the capacitance of such electrodes by using the equation derived for capacitors will lead to greatly overestimated capacitance values that can be found in many publications. As suggested by Brousse et al. [7], the specific capacity (C) instead of the capacitance of such electrodes should be calculated according to the following equations:

$$Q = i_m \Delta t \quad (3)$$

where $i_m = I/m$ ($A\ g^{-1}$) is the current density, m is the mass of the active electrode material, I is the current, and Δt is the discharge time [12,50]. Regarding the detailed information, Brousse et al. have given an excellent comment in their publication [7].

With the development of renewable energy and electrified transportation, it can be expected that the energy conversion and energy storage devices will become more and more important in our daily lives. In the future, energy storage systems will mainly focus on hybrid devices combining the best features of battery-type Faradaic electrodes and capacitive electrodes. Understanding of the synergistic effect among different active components on the electron transportation and surface reactions is very challenging and significant. For the negative electrode, the challenge is still increasing the capacitance, which is critical for charge/weight/volume balance with the positive electrode to maximize the energy density of the device. Non-planar hybrid electrode architectures will play an important role in future energy storage systems. Conventional electrodes cannot satisfy the development of flexible and lightweight devices in modern electronics; it is still a challenge to develop a highly flexible and portable integrated energy package. The integration of HSCs with other multifunctions such as electrochromism, shape memory, photo self-charging, thermal self-protective, and self-healing will be significant and require further study.

5. Conclusions

In this review, we summarized the development of recent advances in HSCs, including the electrode materials, such as transition metal oxides/sulfides/hydroxides and carbon-based materials (activated carbon and graphene), the working principles/mechanisms, and purposeful design/optimization. In general, the HSCs have been developed as attractive high-energy storage devices combining a typical battery-type electrode with a large positive cutoff potential and a capacitive electrode with a high overpotential in the negative potential range, rendering a significant increase in the overall cell operating voltage.

The traditional planar architectures are very limited in the thickness of the Faradaic electrode due to the low electrical and ionic conductivities, which retard the overall device kinetics. Nanostructuring, especially 3D hybrid architectures, reducing the mass-transfer resistances and ion diffusion pathways, and increasing the electrical conductivity and stability, are good strategies to solve this issue. In addition, it can also promote rapid electron and ion accessibility to electrochemically active sites and ease the electron hopping between neighboring nanoparticles. Nanostructured composite materials are considered as the most promising candidates for fabricating high-performance HSC devices. However, complex preparation methods and fabrication processes hinder their wider practical application. The challenge is to explore novel electrode materials or architectures to fabricate high-performance HSCs using a cost-effective technology.

Recently, enormous efforts have been devoted to the significant advancement in flexible electrode design and device construction for high-performance HSCs. The development of flexible, portable, and wearable energy storage devices has paved the way for the further applications of renewable energy to power electric cars and enable the internet of things. However, there are still some challenging issues for promoting the practical commercial application of HSCs. For example, the morphology and structure of nanomaterials are sometimes difficult to maintain during the long cycles because of their poor mechanical and chemical properties. In addition, the structural evolution and degradation information of electrode materials is difficult to uncover during the long cycling process, and advanced tools are to be developed to reveal the mechanisms of some complex phenomena. Therefore, future efforts should be focused on providing comprehensive insight into the fundamental understanding of the relationship between the electrochemical properties and the structure.

Funding: This work was supported by the National Natural Science Foundation of China (Grant No. 21805247) and the China Postdoctoral Science Foundation (Grant No. 2018M630831).

Institutional Review Board Statement: Not applicable.

Informed Consent Statement: Not applicable.

Data Availability Statement: Not applicable.

Conflicts of Interest: The authors declare no conflict of interest.

References

1. Zhu, Y.C.; Deng, J.; Olivier, F. Breaking the strength barrier. *Nat. Energy* **2023**, *23*, 1264. [[CrossRef](#)]
2. Wang, F.; Lee, J.Y.; Chen, L.; Zhang, G.Y.; He, S.J.; Han, J.Q.; Ahn, J.; Cheong, J.Y.; Jiang, S.H.; Kim, I.D. Inspired by Wood: Thick Electrodes for Supercapacitors. *ACS Nano* **2023**, *17*, 8866–8898. [[CrossRef](#)] [[PubMed](#)]
3. Feng, D.W.; Lei, T.; Lukatskaya, M.R.; Park, J.; Huang, Z.H.; Lee, M.; Shaw, L.; Chen, S.C.; Yakovenko, A.A.; Kulkarni, A.; et al. Robust and conductive two-dimensional metal-organic frameworks with exceptionally high volumetric and areal capacitance. *Nat. Energy* **2018**, *3*, 30–36. [[CrossRef](#)]
4. Li, K.D.; Zhao, T.; Wang, H.F.; Zhang, S.; Deng, C. From 1D nanotube arrays to 2D nanosheet networks on silver-coated textiles: New insights into the factors determining the performance of a core-shell hierarchical structure for wearable supercapacitors. *J. Mater. Chem. A* **2018**, *6*, 1561–1573. [[CrossRef](#)]
5. Li, X.M.; Zheng, Q.W.; Li, C.M.; Liu, G.Q.; Yang, Q.Z.; Wang, Y.C.; Sun, P.C.; Tian, H.M.; Wang, C.H.; Chen, X.L.; et al. Bubble Up Induced Graphene Microspheres for Engineering Capacitive Energy Storage. *Adv. Energy Mater.* **2023**, *13*, 2203761. [[CrossRef](#)]
6. Ma, H.Y.; Liang, J.; Qiu, J.; Li, J.; Ma, L.X.; Sheng, H.W.; Shao, M.J.; Wang, Q.; Li, F.F.; Fu, Y.J.; et al. A Biocompatible Supercapacitor Diode with Enhanced Rectification Capability toward Ion/Electron-Coupling Logic Operations. *Adv. Mater.* **2023**, *35*, 2301218. [[CrossRef](#)]
7. Brousse, T.; Belanger, D.; Long, J.W. To Be or Not to Be Pseudocapacitive? *J. Electrochem. Soc.* **2015**, *162*, A5185–A5189. [[CrossRef](#)]
8. Conway, B.E. Transition from supercapacitor to battery behavior in electrochemical energy storage. *J. Electrochem. Soc.* **1991**, *138*, 1539–1548. [[CrossRef](#)]
9. Luo, X.Y.; Zheng, H.; Lai, W.D.; Yuan, P.; Li, S.W.; Li, D.; Chen, Y. Defect Engineering of Carbons for Energy Conversion and Storage Applications. *Energy Environ. Mater.* **2023**, *6*, e12402. [[CrossRef](#)]
10. Lukatskaya, M.R.; Dunn, B.; Gogotsi, Y. Multidimensional materials and device architectures for future hybrid energy storage. *Nat. Commun.* **2016**, *7*, 12647. [[CrossRef](#)]
11. Dai, S.G.; Bai, Y.C.; Shen, W.X.; Zhang, S.; Hu, H.; Fu, J.W.; Wang, X.C.; Hu, C.G.; Liu, M.L. Core-shell structured Fe₂O₃@Fe₃C@C nanochains and Ni-Co carbonate hydroxide hybridized microspheres for high-performance battery-type supercapacitor. *J. Power Sources* **2021**, *482*, 228915. [[CrossRef](#)]
12. Dai, S.G.; Zhao, B.; Qu, C.; Chen, D.C.; Dang, D.; Song, B.; deGleea, B.M.; Fu, J.W.; Hu, C.G.; Wong, C.P.; et al. Controlled synthesis of three-phase Ni_xS_y/rGO nanoflake electrodes for hybrid supercapacitors with high energy and power density. *Nano Energy* **2017**, *33*, 522–531. [[CrossRef](#)]
13. Zuo, W.H.; Li, R.Z.; Zhou, C.; Li, Y.Y.; Xia, J.L.; Liu, J.P. Battery-supercapacitor hybrid devices: Recent progress and future prospects. *Adv. Sci.* **2017**, *4*, 1600539. [[CrossRef](#)] [[PubMed](#)]
14. Dai, S.G.; Zhang, Z.F.; Xu, J.M.; Shen, W.X.; Zhang, Q.B.; Yang, X.G.; Xu, T.T.; Dang, D.; Hu, H.; Zhao, B.T.; et al. In situ Raman study of nickel bicarbonate for high-performance energy storage device. *Nano Energy* **2019**, *64*, 103919. [[CrossRef](#)]
15. Huang, N.B.; Sun, Y.; Liu, S.; Wang, X.Y.; Zhang, J.J.; Guo, L.K.; Bi, J.P.; Sun, X.N. Microwave-Assisted Rational Designed CNT-Mn₃O₄/CoWO₄ Hybrid Nanocomposites for High Performance Battery-Supercapacitor Hybrid Device. *Small* **2023**, e2300696. [[CrossRef](#)]
16. Soserov, L.; Marinova, D.; Koleva, V.; Stoyanova, A.; Stoyanova, R. Comparison of the Properties of Ni–Mn Hydroxides/Oxides with Ni–Mn Phosphates for the Purpose of Hybrid Supercapacitors. *Batteries* **2022**, *10*, 3390. [[CrossRef](#)]
17. Shen, W.X.; Zang, J.H.; Hu, H.; Xu, J.M.; Zhang, Z.F.; Yan, R.Q.; Dai, S.G. Controlled synthesis of KCu₇S₄/rGO nanocomposites for electrochemical energy storage. *Mater. Des.* **2020**, *195*, 108992. [[CrossRef](#)]
18. Chen, K.; Li, X.; Zang, J.; Zhang, Z.; Wang, Y.; Lou, Q.; Bai, Y.; Fu, J.; Zhuang, C.; Zhang, Y.; et al. Robust VS₄@rGO nanocomposite as a high-capacity and long-life cathode material for aqueous zinc-ion batteries. *Nanoscale* **2021**, *13*, 12370–12378. [[CrossRef](#)]
19. Meng, H.Y.; Wang, S.L.; Ma, X.Y.; Zhang, D.H.; Zhang, L.L.; Liu, X.Y.; Zhang, L. Matching CP@NCOH/NF Cathode and GH/FNP/NF Anode for High-Performance Asymmetric Supercapacitor. *Small* **2023**, *19*, 2207496. [[CrossRef](#)]
20. Wang, C.X.; Liu, Y.W.; Sun, Y.S.; Cui, L.; Liu, J.Q. 3D nanoflower-like and core-shell structured MCo₂O₄@MCo₂S₄@polypyrrole (M = Cu, Mn) composites as supercapacitor electrode materials with ultrahigh specific capacitances. *J. Mater. Chem. A* **2023**, *11*, 7639–7651. [[CrossRef](#)]
21. Abbas, Z.; Hussain, N.; Ahmed, I.; Mobin, S.M. Cu-Metal Organic Framework Derived Multilevel Hierarchy (Cu/Cu_xO@NC) as a Bifunctional Electrode for High-Performance Supercapacitors and Oxygen Evolution Reaction. *Inorg. Chem.* **2023**, *62*, 8835–8845. [[CrossRef](#)] [[PubMed](#)]
22. Hu, G.; Tang, C.; Li, C.; Li, H.; Wang, Y.; Gong, H. The sol-gel-derived nickel-cobalt oxides with high supercapacitor performances. *J. Electrochem. Soc.* **2011**, *158*, A695–A699. [[CrossRef](#)]
23. Chen, X.Y.; Wang, S.C.; Qiao, G.Q.; Lu, G.X.; Cui, H.Z.; Wang, X.Z. Fabrication of Three-Dimensional Porous NiO/Amorphous Ni(OH)₂ Composites for Supercapacitors. *Energy Fuels* **2020**, *34*, 16783–16790. [[CrossRef](#)]
24. Xin, Y.F.; Dai, X.; Lv, G.J.; Wei, X.D.; Li, S.; Li, Z.Q.; Xue, T.; Shi, M.; Zou, K.Y.; Chen, Y.Z.; et al. Stability-Enhanced α-Ni(OH)₂ Pillared by Metaborate Anions for Pseudocapacitors. *ACS Appl. Mater. Interfaces* **2021**, *13*, 28118–28128. [[CrossRef](#)] [[PubMed](#)]

25. Bhagwan, J.; Han, J.I. Promotive Effect of MWCNTs on α -NiS Microstructure and Their Application in Aqueous Asymmetric Supercapacitor. *Energy Fuels* **2022**, *36*, 15210–15220. [[CrossRef](#)]
26. Wang, Y.Z.; Liu, Y.X.; Wang, H.Q.; Liu, W.; Li, Y.; Zhang, J.F.; Hou, H.; Yang, J.L. Ultrathin NiCo-MOF Nanosheets for High-Performance Supercapacitor Electrodes. *ACS Appl. Energy Mater.* **2019**, *2*, 2063–2071. [[CrossRef](#)]
27. Wang, Y.G.; Song, Y.F.; Xia, Y.Y. Electrochemical capacitors: Mechanism, materials, systems, characterization and applications. *Chem. Soc. Rev.* **2016**, *45*, 5925–5950. [[CrossRef](#)] [[PubMed](#)]
28. Cericola, D.; Kotz, R. Hybridization of rechargeable batteries and electrochemical capacitors: Principles and limits. *Electrochim. Acta* **2012**, *782*, 1–17. [[CrossRef](#)]
29. Thounthong, P.; Raël, S.; Davat, B. Energy management of fuel cell/battery/supercapacitor hybrid power source for vehicle applications. *J. Power Sources* **2009**, *193*, 376–385. [[CrossRef](#)]
30. Gogosti, Y. What nano can do for energy storage. *ACS Nano* **2014**, *8*, 5369–5371.
31. Wang, K.B.; Chen, C.Y.; Li, Y.H.; Hong, Y.; Wu, H.; Zhang, C.; Zhang, Q.C. Insight into Electrochemical Performance of Nitrogen Doped Carbon/NiCo-Alloy Active Nanocomposites. *Small* **2023**, *19*, 2300054. [[CrossRef](#)] [[PubMed](#)]
32. Lee, S.; Cho, J. Critical requirements for rapid charging of rechargeable Al-and Li-ion batteries. *Angew. Chem. Int. Ed.* **2015**, *54*, 9452–9455. [[CrossRef](#)] [[PubMed](#)]
33. Liu, C.; Li, F.; Ma, L.P.; Cheng, H.M. Advanced materials for energy storage. *Adv Mater.* **2010**, *22*, E28–E62. [[CrossRef](#)]
34. Marinova, D.; Kalapsazova, M.; Zlatanova, Z.; Mereacre, L.; Zhecheva, E.; Stoyanova, R. Lithium Manganese Sulfates as a New Class of Supercapattery Materials at Elevated Temperatures. *Materials* **2023**, *16*, 4798. [[CrossRef](#)] [[PubMed](#)]
35. Kang, M.; Zhou, H.; Qin, B.; Zhao, N.; Lv, B.L. Ultrathin Nanosheet-Assembled, Phosphate Ion-Functionalized NiO Microspheres as Efficient Supercapacitor Materials. *ACS Appl. Energy Mater.* **2020**, *3*, 9980–9988. [[CrossRef](#)]
36. Zhao, J.; Wang, S.M.; Gao, L.J.; Zhang, D.; Guo, Y.Y.; Xu, R.Q. NiO Nanoparticles Anchored on N-Doped Laser-Induced Graphene for Flexible Planar Micro-Supercapacitors. *ACS Appl. Nano Mater.* **2022**, *5*, 11314–11323. [[CrossRef](#)]
37. Wang, G.S.; Yan, Z.X.; Wang, N.H.; Xiang, M.; Xu, Z.H. NiO/Ni Metal-Organic Framework Nanostructures for Asymmetric Supercapacitors. *ACS Appl. Nano Mater.* **2021**, *4*, 9034–9043. [[CrossRef](#)]
38. Meng, G.; Yang, Q.; Wu, X.C.; Wan, P.B.; Li, Y.P.; Lei, X.D.; Sun, X.M.; Liu, J.F. Hierarchical mesoporous NiO nanoarrays with ultrahigh capacitance for aqueous hybrid supercapacitor. *Nano Energy* **2016**, *30*, 831–839. [[CrossRef](#)]
39. Gao, D.Y.; Liu, R.N.; Han, D.D.; Xu, P.C.; Wang, P.; Wei, Y. Constructing Ni-Co PBA derived 3D/1D/2D NiO/NiCo₂O₄/NiMn-LDH hierarchical heterostructures for ultrahigh rate capability in hybrid supercapacitors. *J. Mater. Chem. A* **2023**, *11*, 9546–9554. [[CrossRef](#)]
40. Wu, X.L.; Zeng, F.; Song, X.Y.; Sha, X.F.; Zhou, H.T.; Zhang, X.G.; Liu, Z.; Yu, M.H.; Jiang, C.Z. In-situ growth of Ni(OH)₂ nanoplates on highly oxidized graphene for all-solid-state flexible supercapacitors. *Chem. Eng. J.* **2023**, *456*, 140947. [[CrossRef](#)]
41. Lu, Y.; Qin, Y.H.; Chen, M.Y.; Liu, G.F.; Qi, P.C.; Wu, H.; Tang, Y.W. Multi-dimensional Ni(OH)₂/(Ni(OH)₂(NiOOH)_{1.67})₈₅₇@Ni₃S₂ hierarchical structure for high-performance asymmetric supercapacitor. *Appl. Surf. Sci.* **2023**, *6*, 155625. [[CrossRef](#)]
42. Wang, K.; Zhang, X.L.; Zhang, X.Q.; Chen, D.Y.; Lin, Q.L. A novel Ni(OH)₂/graphene nanosheets electrode with high capacitance and excellent cycling stability for pseudocapacitors. *J. Power Sources* **2016**, *9*, 153. [[CrossRef](#)]
43. Han, C.; Si, H.Z.; Sang, S.B.; Liu, K.Y.; Liu, H.T.; Wu, Q.M. Carbon Dots Doped with Ni(OH)₂ as Thin-Film Electrodes for Supercapacitors. *ACS Appl. Nano Mater.* **2020**, *3*, 12106–12114. [[CrossRef](#)]
44. Jiang, Z.M.; Xu, T.T.; Dai, S.G.; Yan, C.C.; Ma, C.Y.; Wang, X.C.; Xu, J.M.; Zhang, S.; Wang, Y. 3D mesoporous Ni(OH)₂/WS₂ nanofibers with highly enhanced performance for energy storage devices. *Energy Technol.* **2019**, *7*, 1800476. [[CrossRef](#)]
45. Ren, X.C.; Guo, C.L.; Xu, L.Q.; Li, T.T.; Hou, L.F.; We, Y.H. Facile synthesis of hierarchical mesoporous honeycomb-like NiO for aqueous asymmetric supercapacitors. *ACS Appl. Mater. Interfaces* **2015**, *7*, 19930–19940. [[CrossRef](#)] [[PubMed](#)]
46. Cai, G.F.; Wang, X.; Cui, M.Q.; Darmawan, P.; Wang, J.X.; Eh, A.L.; Lee, P.S. Electrochromo-supercapacitor based on direct growth of NiO nanoparticles. *Nano Energy* **2015**, *12*, 258–267. [[CrossRef](#)]
47. Krishna, P.G.; Debendra, A.; Indu, B.; Vivek, S.; Maya, D.; Shova, N.; Jyotendra, K.; Kisan, C.; Amar, P.Y. Nickel Oxide-Incorporated Polyaniline Nanocomposites as an Efficient Electrode Material for Supercapacitor Application. *Inorganics* **2022**, *10*, 86.
48. Hong, Y.W.; Yang, J.X.; Choi, W.M.; Wang, J.J.; Xu, J.L. B-Doped g-C₃N₄ Quantum Dots-Modified Ni(OH)₂ Nanoflowers as an Efficient and Stable Electrode for Supercapacitors. *ACS Appl. Energy Mater.* **2021**, *4*, 1496–1504. [[CrossRef](#)]
49. Jiang, W.C.; Yu, D.S.; Zhang, Q.; Goh, K.L.; Wei, L.; Yong, Y.L.; Jiang, R.G.; Wei, J.; Chen, Y. Ternary hybrids of amorphous nickel hydroxide-carbon nanotube-conducting polymer for supercapacitors with high energy density, excellent rate capability, and long cycle life. *Adv. Funct. Mater.* **2015**, *25*, 1063–1073. [[CrossRef](#)]
50. Zhao, B.; Zhang, L.; Zhang, Q.B.; Chen, D.C.; Cheng, Y.; Deng, X.; Chen, Y.; Murphy, R.; Xiong, X.H.; Song, B.; et al. Rational Design of Nickel Hydroxide-Based Nanocrystals on Graphene for Ultrafast Energy Storage. *Adv. Energy Mater.* **2017**, *8*, 1702247. [[CrossRef](#)]
51. Wan, N.W.K.; Lim, H.N.; Ibrahim, I.; Huang, N.M.; Foo, C.Y.; Jiang, Z.T. Electrochemical performance of aqueous hybrid supercapacitor based on LiFePO₄/Si/graphene composite. *Chem. Eng. J.* **2023**, *456*, 141132. [[CrossRef](#)]
52. Li, Z.Y.; Ma, Q.; Zhang, H.B.; Zhang, Q.H.; Zhang, K.L.; Mei, H.; Xu, B.; Sun, D.F. Self-Assembly of Metal-Organic Frameworks on Graphene Oxide Nanosheets and In Situ Conversion into a Nickel Hydroxide/Graphene Oxide Battery-Type Electrode. *Inorg. Chem.* **2022**, *61*, 12129–12137. [[CrossRef](#)] [[PubMed](#)]

53. Guo, B.L.; Gao, Y.H.; Li, Y.Y.; Sun, X.; Chen, S.L.; Li, M.C. Ni(OH)₂ Nanosheets Grown on Reduced Graphene Oxide for Supercapacitor Electrodes. *ACS Appl. Nano Mater.* **2022**, *5*, 7471–7480. [[CrossRef](#)]
54. Aghazadeh, M.; Rad, H.F. In situ growth of Ni(OH)₂-porous nitrogen-doped graphene composite onto Ni foam support as advanced electrochemical supercapacitors materials. *J. Mater. Sci. Mater. Electron.* **2022**, *33*, 11038–11054. [[CrossRef](#)]
55. Girish, S.G.; Deepak, P.D.; Sujata, S.S.; Chandrakant, D.L. One step hydrothermal synthesis of micro-belts like β-Ni(OH)₂ thin films for supercapacitors. *Ceram. Int.* **2013**, *1*, 91.
56. Ji, J.Y.; Zhang, L.L.; Ji, H.X.; Li, Y.; Zhao, X.; Bai, X.; Fan, X.B.; Zhang, F.B.; Ruoff, R.S. Nanoporous Ni(OH)₂ thin film on 3D ultrathin-graphite foam for asymmetric supercapacitor. *ACS Nano* **2013**, *7*, 6237–6243. [[CrossRef](#)]
57. Li, H.B.; Yu, M.H.; Wang, F.X.; Liu, P.; Liang, Y.; Xiao, J.; Wang, C.X.; Tong, Y.X.; Yang, G.W. Amorphous nickel hydroxide nanospheres with ultrahigh capacitance and energy density as electrochemical pseudocapacitor materials. *Nat. Commun.* **2013**, *4*, 1894. [[CrossRef](#)] [[PubMed](#)]
58. Meng, X.H.; Deng, D. Bio-inspired synthesis of α-Ni(OH)₂ nanobristles on various substrates and their applications. *J. Mater. Chem. A* **2016**, *4*, 6919–6925. [[CrossRef](#)]
59. Du, H.M.; Wang, Y.J.; Yuan, H.T.; Jiao, L.F. Facile synthesis and high capacitive performance of 3D hierarchical Ni(OH)₂ microspheres. *Electrochim. Acta* **2016**, *196*, 84–91. [[CrossRef](#)]
60. Ambade, R.B.; Lee, H.; Lee, K.H.; Lee, H.; Veerasubramani, G.K.; Kim, Y.B.; Han, T.H. Ultrafast flashlight sintered mesoporous NiO nanosheets for stable asymmetric supercapacitors. *Chem. Eng. J.* **2022**, *135*, 41. [[CrossRef](#)]
61. Zhou, S.Y.; Wang, S.; Zhou, S.J.; Xu, H.B.; Zhao, J.P.; Wang, J.; Li, Y. An electrochromic supercapacitor based on an MOF derived hierarchical-porous NiO film. *Nanoscale* **2020**, *12*, 8934–8941. [[CrossRef](#)] [[PubMed](#)]
62. Du, H.; Jiao, L.; Cao, K.; Wang, Y.; Yuan, H. Polyol-mediated synthesis of mesoporous alpha-Ni(OH)₂ with enhanced supercapacitance. *ACS Appl. Mater. Interfaces* **2013**, *5*, 6643–6648. [[CrossRef](#)] [[PubMed](#)]
63. Fu, Y.; Song, J.; Zhu, Y.; Cao, C. High-performance supercapacitor electrode based on amorphous mesoporous Ni(OH)₂ nanoboxes. *J. Power Sources* **2014**, *262*, 344–348. [[CrossRef](#)]
64. Li, Z.; Han, J.; Fan, L.; Wang, M.; Tao, S.; Guo, R. The anion exchange strategy towards mesoporous alpha-Ni(OH)₂ nanowires with multinanocavities for high-performance supercapacitors. *Chem. Commun.* **2015**, *51*, 3053–3056. [[CrossRef](#)] [[PubMed](#)]
65. Xie, M.J.; Duan, S.Y.; Shen, Y.; Fang, K.; Wang, Y.Z.; Lin, M.; Guo, X.F. In-situ-grown Mg(OH)₂-derived hybrid α-Ni(OH)₂ for highly stable supercapacitor. *ACS Energy Lett.* **2016**, *1*, 814–819. [[CrossRef](#)]
66. Sun, W.P.; Rui, X.H.; Ulaganathan, M.; Madhavi, S.; Yan, Q.Y. Few-layered Ni(OH)₂ nanosheets for high-performance supercapacitors. *J. Power Sources* **2015**, *295*, 323–328. [[CrossRef](#)]
67. Alhebshi, N.A.; Rakhi, R.B.; Alshareef, H.N. Conformal coating of Ni(OH)₂ nanoflakes on carbon fibers by chemical bath deposition for efficient supercapacitor electrodes. *J. Mater. Chem. A* **2013**, *1*, 14897–14903. [[CrossRef](#)]
68. Li, L.; Tan, L.; Li, G.N.; Zhang, Y.M.; Liu, L.L. Self-templated synthesis of porous Ni(OH)₂ nanocube and its high electrochemical performance for supercapacitor. *Langmuir* **2017**, *33*, 12087–12094. [[CrossRef](#)]
69. Kore, R.M.; Lokhande, B.J. Hierarchical mesoporous network of amorphous a-Ni(OH)₂ for high performance supercapacitor electrode material synthesized from a novel solvent deficient approach. *Electrochim. Acta* **2017**, *245*, 780–790. [[CrossRef](#)]
70. Aguilera, L.; Leyet, Y.; Garcia, R.P.; Hernández, E.P.; Passos, R.R.; Pocrifka, L.A. Cabbage-like α-Ni(OH)₂ with a good long-term cycling stability and high electrochemical performances for supercapacitor applications. *Chem. Phys. Lett.* **2017**, *677*, 75–79. [[CrossRef](#)]
71. Xiong, X.H.; Ding, D.; Chen, D.C.; Waller, G.; Bu, Y.F.; Wang, Z.X.; Liu, M.L. Three-dimensional ultrathin Ni(OH)₂ nanosheets grown on nickel foam for high-performance supercapacitors. *Nano Energy* **2015**, *11*, 154–161. [[CrossRef](#)]
72. Li, L.J.; Xu, J.; Lei, J.L.; Zhang, J.; McLarnon, F.; Wei, Z.D.; Li, N.B.; Pan, F.S. A one-step, cost-effective green method to in situ fabricate Ni(OH)₂ hexagonal platelets on Ni foam as binder-free supercapacitor electrode materials. *J. Mater. Chem. A* **2015**, *3*, 1953–1960. [[CrossRef](#)]
73. Cui, H.T.; Xue, J.Y.; Ren, W.Z.; Wang, M.M. Ultra-high specific capacitance of β-Ni(OH)₂ monolayer nanosheets synthesized by an exfoliation-free sol-gel route. *J. Nanopart. Res.* **2014**, *16*, 2601. [[CrossRef](#)]
74. Naveen, N.; Park, C.; Sohn, K.S.; Pyo, M. Nickel hydroxide nanoplatelets via dendrimer-assisted growth on graphene for high-performance energy-storage applications. *Electrochim. Acta* **2017**, *248*, 313–321. [[CrossRef](#)]
75. Zhang, L.; Wu, T.; Na, H.; Pan, C.; Xu, X.; Huang, G.; Liu, Y.; Liu, Y.; Gao, J. Self-assembly method to fabricate reduced graphene oxide aerogels loaded with nickel hydroxyl nanoparticles and their excellent properties in absorbing and supercapacitors. *Ind. Eng. Chem. Res.* **2016**, *55*, 6553–6562. [[CrossRef](#)]
76. Zhang, H.; Zhang, X.; Zhang, D.; Sun, X.; Lin, H.; Wang, C.; Ma, Y. One-step electrophoretic deposition of reduced graphene oxide and Ni(OH)₂ composite films for controlled syntheses supercapacitor electrodes. *J. Phys. Chem. B* **2013**, *117*, 1616–1627. [[CrossRef](#)] [[PubMed](#)]
77. Sun, Z.; Lu, X. A solid-state reaction route to anchoring Ni(OH)₂ nanoparticles on reduced graphene oxide sheets for supercapacitors. *Ind. Eng. Chem. Res.* **2012**, *51*, 9973–9979. [[CrossRef](#)]
78. Yan, J.; Fan, Z.; Sun, W.; Ning, G.; Wei, T.; Zhang, Q.; Zhang, R.; Zhi, L.; Wei, F. Advanced asymmetric supercapacitors based on Ni(OH)₂/graphene and porous graphene electrodes with high energy density. *Adv. Funct. Mater.* **2012**, *22*, 2632–2841. [[CrossRef](#)]
79. Li, Z.; Zhang, W.; Sun, C.; Feng, Z.; Yang, B. Controlled synthesis of Ni(OH)₂/graphene composites and their transformation to NiO/graphene for energy storage. *Electrochim. Acta* **2016**, *212*, 390–398. [[CrossRef](#)]

80. Xiao, J.; Yang, S. Nanocomposites of Ni(OH)₂/reduced graphene oxides with controllable composition, size, and morphology: Performance variations as pseudocapacitor electrodes. *ChemPlusChem* **2012**, *77*, 807–816. [[CrossRef](#)]
81. Min, S.; Zhao, C.; Zhang, Z.; Chen, G.; Qian, X.; Guo, Z. Synthesis of Ni(OH)₂/RGO pseudocomposite on nickel foam for supercapacitors with superior performance. *J. Mater. Chem. A* **2015**, *3*, 3641–3650. [[CrossRef](#)]
82. Wang, H.; Casalongue, H.S.; Liang, Y.; Dai, H. Ni(OH)₂ nanoplates grown on graphene as advanced electrochemical pseudocapacitor materials. *J. Am. Chem. Soc.* **2010**, *131*, 7472–7477. [[CrossRef](#)] [[PubMed](#)]
83. Yan, J.; Sun, W.; Wei, T.; Zhang, Q.; Fan, Z.J.; Wei, F. Fabrication and electrochemical performances of hierarchical porous Ni(OH)₂ nanoflakes anchored on graphene sheets. *J. Mater. Chem.* **2012**, *22*, 11494–11502. [[CrossRef](#)]
84. Lee, J.W.; Ahn, T.; Soundararajan, D.; Koc, J.M.; Kim, J.D. Non-aqueous approach to the preparation of reduced graphene oxide/ α -Ni(OH)₂ hybrid composites and their high capacitance behavior. *Chem. Commun.* **2011**, *22*, 6305–6307. [[CrossRef](#)] [[PubMed](#)]
85. Fang, D.L.; Chen, Z.D.; Liu, X.; Wu, Z.F.; Zheng, C.H. Homogeneous growth of nano-sized β -Ni(OH)₂ on reduced graphene oxide for high-performance supercapacitors. *Electrochim. Acta* **2012**, *81*, 321–329. [[CrossRef](#)]
86. Wang, R.H.; Jayakumar, A.; Xu, C.; Lee, J.M. Ni(OH)₂ nanoflowers/graphene hydrogels: A new assembly for supercapacitors. *ACS Sustain. Chem. Eng.* **2016**, *4*, 3736–3742. [[CrossRef](#)]
87. Parveen, N.; Ansari, S.A.; Ansari, S.G.; Fouad, H.; Cho, M.H. Intercalated reduced graphene oxide and its content effect on the supercapacitance performance of the three dimensional flower-like β -Ni(OH)₂ architecture. *New J. Chem.* **2017**, *41*, 10467–10475. [[CrossRef](#)]
88. Liu, Y.; Wang, R.; Yan, X. Synergistic effect between ultra-small nickel hydroxide nanoparticles and reduced graphene oxide sheets for the application in highperformance asymmetric supercapacitor. *Sci. Rep.* **2015**, *5*, 11095. [[CrossRef](#)]
89. Zhang, K.; Jia, J.; Tan, L.; Qi, S.P.; Li, B.L.; Chen, J.X.; Li, J.; Lou, Y.B.; Guo, Y.Z. Morphological and electronic modification of NiS₂ for efficient supercapacitors and hydrogen evolution reaction. *J. Power Sources* **2023**, *577*, 233239. [[CrossRef](#)]
90. Liu, J.P.; Pu, Y.; Zhang, Q.Y.; Cheng, Z.Y.; Zheng, Y.; Wang, Y.C.; Liu, W.; Li, S.Y.; Zhang, J.X. Tracking surface ionic movement of Ni₃S₂@CuS electrode materials with high electrochemical performance. *Chem. Eng. J.* **2023**, *461*, 141910. [[CrossRef](#)]
91. Shoeb, M.; Mashkoo, F.; Abdul, H.J.; Anwer, H.; Zhu, S.S.; Zahid, A.M.; Changyoon, J. VARTM-assisted high-performance solid-state structural supercapacitor device based on the synergistic effect of Ni(OH)₂-Co₃S₄ nanocomposite for widened potential window and charge storage mechanism. *Chem. Eng. J.* **2023**, *466*, 143116. [[CrossRef](#)]
92. Azimov, F.; Lee, J.; Park, S.; Hyun, M.J. Fabrication of Assembled FeS₂ Nanosheet and Application for HighPerformance Supercapacitor Electrodes. *ACS Appl. Mater. Interfaces* **2023**, *15*, 26967–26976. [[CrossRef](#)] [[PubMed](#)]
93. Kumar, S.; Mukherjee, A.; Telpande, S.; Mahapatra, A.D.; Kumar, P.; Misra, A. Role of the electrode-edge in optically sensitive three-dimensional carbon foam-MoS₂ based highperformance micro-supercapacitors. *J. Mater. Chem. A* **2023**, *11*, 4963–4976. [[CrossRef](#)]
94. Hu, J.J.; Shi, Y.; Sun, L.; Xie, F.; Gao, K.Y.; Qu, Y.R.; Tan, H.K.; Zhang, Y.H. MOF-derived spherical Ni_xS_y/carbon with B-doping enabling high supercapacitive performance. *J. Mater. Sci. Technol.* **2013**, *153*, 219–227. [[CrossRef](#)]
95. Kushwaha, V.; Gupta, A.; Choudhary, R.B.; Mandal, K.D.; Mondal, R.; Singh, P. Nanocrystalline β -NiS: A redox-mediated electrode in aqueous electrolyte for pseudocapacitor/supercapacitor applications. *Phys. Chem. Chem. Phys.* **2023**, *25*, 555–569. [[CrossRef](#)] [[PubMed](#)]
96. Yang, Y.; Peng, K.; Deng, Y. The synthesis of nickel sulfide deposited with nitrogen-doped carbon quantum dots as advanced electrode materials for supercapacitors. *J. Mater. Sci.* **2022**, *57*, 14052–14064. [[CrossRef](#)]
97. Shi, Y.; Qu, Y.R.; Tan, H.K.; Sun, L.; Sun, C.; Fan, K.F.; Hu, J.J.; Wang, K.; Zhang, Y.H. RGO-loaded double phase Mo-doped NiS for enhanced battery-type energy storage in hybrid supercapacitors. *Electrochim. Acta* **2022**, *426*, 140810. [[CrossRef](#)]
98. Zhang, D.Y.; Gao, S.Y.; Zhang, J.W.; Wang, J.R.; She, W.N.; Wang, K.J.; Xia, X.; Yang, B.; Meng, X.X. Facile solid-phase synthesis of layered NiS/rGO nanocomposite for high-performance hybrid supercapacitor. *J. Power Sources* **2021**, *514*, 230590. [[CrossRef](#)]
99. Que, T.N.; Umesh, T.N.; Chen, J.Y.; Soojin, P.; Sungjune, P. Ceria nanoflowers decorated Co₃O₄ nanosheets electrodes for highly efficient electrochemical supercapacitors. *Appl. Surf. Sci.* **2023**, *613*, 156034.
100. He, Y.; Zhou, W.Q.; Li, D.Q.; Liang, Y.M.; Chao, S.X.; Zhao, X.Q.; Zhang, M.M.; Xu, J.K. Rare Earth Doping Engineering Tailoring Advanced Oxygen-Vacancy Co₃O₄ with Tunable Structures for High-Efficiency Energy Storage. *Small* **2023**, *19*, 2206956. [[CrossRef](#)]
101. Zhang, W.; Zhang, R.J.; Shi, M.P.; Ma, L.N.; Huang, Y.D. Hierarchical polygon Co₃O₄ flakes/N, O-dual doped porous carbon frameworks for flexible hybrid supercapacitors. *Electrochim. Acta* **2022**, *424*, 140631. [[CrossRef](#)]
102. Yang, C.Q.; Li, W.Q.; Liu, X.Q.; Song, X.M.; Li, H.P.; Tan, L.C. Preparation of MoFs-Derived Cobalt Oxide/Carbon Nanotubes Composites for High-Performance Asymmetric Supercapacitor. *Molecules* **2023**, *28*, 3177. [[CrossRef](#)]
103. Merum, D.; Pitcheri, R.; Gonuguntla, V.; Joo, S.W.B. Synthesis and properties of oxygen-deficient cobalt oxide nanocubes for supercapacitor application. *Mater. Lett.* **2023**, *347*, 134585. [[CrossRef](#)]
104. Liu, Q.P.; Zhou, Q.P.; Gao, C.S.; Liu, L.; Ye, H.Y. Excellent electrochemical stability of Co₃O₄ array with carbon hybridization derived from metal-organic framework. *Nanotechnology* **2021**, *32*, 485710. [[CrossRef](#)]
105. Sivakumar, P.; Raj, C.; Justin, J.H.; Park, H.S. 2D/2D nanoarchitecture of Ni/NiCo₂O₄ deposited onto reduced graphene oxide for high-performance hybrid supercapacitor applications. *J. Energy Storage* **2023**, *69*, 107946. [[CrossRef](#)]

106. Babaahmadi, V.; Pourhosseini, S.E.M.; Norouzi, O.; Naderi, H.R. Designing 3D ternary hybrid composites composed of graphene, biochar and manganese dioxide as high-performance supercapacitor electrodes. *Nanomaterials* **2023**, *13*, 1866. [[CrossRef](#)] [[PubMed](#)]
107. Pathak, D.K.; Ghosh, T.; Kumar, R. Improved inclusive performance of bi-stacked NiO nanoflakes coated nano-Co₃O₄ for dual function: An electrochromic-supercapacitor. *J. Energy Storage* **2023**, *67*, 107643. [[CrossRef](#)]
108. Silambarasan, S.; Sivakumar, M.; Kumar, K.R.; Jiang, Z.Q.; Maiyalagan, T. Nickel-doped Co₃O₄ spinel nanospheres embedded in nitrogen-doped carbon composites derived from bimetallic NiCo metal-organic framework as a high-performance asymmetric supercapacitor. *New J. Chem.* **2023**, *47*, 8649–8660. [[CrossRef](#)]
109. Yang, D.D.; Xu, M.; Liang, X.; Wang, J.Y.; Fang, W.Y.; Zhu, C.G.; Wang, F.W. Facile synthesis of Pr-doped Co₃O₄ nanoflakes on the nickel-foam for high performance supercapacitors. *Electrochim. Acta* **2022**, *406*, 139815. [[CrossRef](#)]
110. Zhang, H.; Geng, S.Y.; Ouyang, M.Z.; Mao, M.X.; Xie, F.; Riley, D.J. Using Metal Cation to Control the Microstructure of Cobalt Oxide in Energy Conversion and Storage Applications. *Small* **2022**, *18*, 2106391. [[CrossRef](#)]
111. Cong, Y.; Jiang, T.T.; Dai, Y.M.; Wu, X.F.; Lv, M.Y.; Chen, M.T.; Ye, T.W.; Wu, Q. 3D network structure of Co(OH)₂ nanoflakes/Ag dendrites via a one-step electrodeposition for high-performance supercapacitors. *Mater. Res. Bull.* **2023**, *157*, 112013. [[CrossRef](#)]
112. Liu, Z.Q.; Qiu, Y.L.; Zhang, A.T.; Yang, W.R.; Barrow, C.J.; Razal, J.M.; Li, A.H.; Liu, J.Q. In-situ formation of α -Co(OH)₂ nanosheet arrays on magnesium cobaltate nanowires for hybrid supercapacitors with enhanced electrochemical performance. *Appl. Surf. Sci.* **2021**, *568*, 150856. [[CrossRef](#)]
113. Hao, J.Y.; Yan, J.; Hu, Q.; Bai, Y.C.; Zhou, Y.; Zou, X.F.; Xiang, B. Design of Co(OH)₂ composite electrode with high active surface area by sulfur control and graphene encapsulation strategies. *Appl. Surf. Sci.* **2022**, *596*, 153612. [[CrossRef](#)]
114. Wang, X.X.; Liu, K.H.; Li, J.; Liu, Y.Y.; Wang, M.R.; Cui, H.T. Creation of an extrinsic pseudocapacitive material presenting extraordinary cycling-life with the battery-type material Co(OH)₂ by S²⁻ doping for application in supercapacitors. *Chem. Eng. J.* **2023**, *451*, 138969. [[CrossRef](#)]
115. Zheng, L.X.; Xu, P.H.; Zhao, Y.J.; Peng, J.X.; Yang, P.J.; Shi, X.W.; Zheng, H.J. Unique core-shell Co₂(OH)₂CO₃@MOF nanoarrays with remarkably improved cycling life for high performance pseudocapacitors. *Electrochim. Acta* **2022**, *412*, 140142. [[CrossRef](#)]
116. Li, J.B.; Li, Z.H.; Zhan, F.; Shao, M.F. Phase engineering of cobalt hydroxide toward cation intercalation. *Chem. Sci.* **2021**, *12*, 1756–1761. [[CrossRef](#)] [[PubMed](#)]
117. Xu, L.; Li, L.; Shen, J.; Li, Z.H.; Liu, S.Y. Metal-organic frameworks induced robust layered Co(OH)₂ nanostructures for ultra-high stability hybrid supercapacitor electrodes in aqueous electrolyte. *J. Power Sources* **2020**, *477*, 228974.
118. Gong, W.Z.; Wang, M.J.; An, Y.; Wang, J.L.; Zhou, L.X.; Xia, Y.; Wang, C.J.; Dong, K.; Pan, C.; Zhou, R.F. Rational design and synthesis of hydroxalite-like α -Co(OH)₂ nanoflakes for extrinsic pseudocapacitive electrodes with superb cycling stability. *J. Energy Storage* **2021**, *38*, 102579. [[CrossRef](#)]
119. Gan, Z.W.; Ren, X.H.; Sun, Y.X.; Sun, M.X.; Yan, Y.J.; Cao, B.B.; Shen, W.Z.; Yu, H.J.; Li, Z.J.; Fu, Y.Q. Highly porous nanocomposites of Mn doped cobalt-based hydroxide/sulfide as high-performance electrode materials for hybrid supercapacitors. *J. Energy Storage* **2023**, *69*, 107934. [[CrossRef](#)]
120. Wang, E.T.; Jiang, S.S.; Bu, X.D. One-pot electrochemical assembling of porous cobalt hydroxide/nitrogen-doped porous graphene onto Ni foam as a binder-free electrode for supercapacitor applications. *J. Energy Storage* **2020**, *32*, 101881. [[CrossRef](#)]
121. Salunkhe, A.D.; Pawar, P.S.; Torane, A.P. MOF derived NiCo₂O₄ nanosheets for high performance asymmetric supercapacitor. *J. Electroanal. Chem.* **2023**, *939*, 117475. [[CrossRef](#)]
122. Ghaemi, S.P.; Masoudpanah, S.M.; Alamolhoda, S. CTAB-assisted synthesis of porous cuboid NiCo₂O₄ powders for high-performance supercapacitor. *J. Energy Storage* **2023**, *67*, 107635. [[CrossRef](#)]
123. Pore, O.C.; Fulari, A.V.; Lohar, G.M. Synthesis of NiCo₂O₄ microflowers by facile hydrothermal method: Effect of precursor concentration. *Chem. Phys. Lett.* **2023**, *824*, 140551. [[CrossRef](#)]
124. Zhao, Y.B.; Li, H.; Tang, R.Y.; Wang, X.Y.; Wu, Y.; Shi, Y.; Zhang, Y. Photo-assisted asymmetric supercapacitors based on dual photoelectrodes for enhanced photoelectric energy storage. *J. Mater. Chem. A* **2023**, *11*, 15844–15854. [[CrossRef](#)]
125. Yang, W.D.; Xiang, J.; Wu, F.F. Nanoengineering of ZnCo₂O₄@CoMoO₄ heterogeneous structures for supercapacitor and water splitting applications. *Ceram. Int.* **2022**, *49*, 4422–4434. [[CrossRef](#)]
126. Ma, Q.H.; Cui, F.; Cui, T.Y. Built-in electric field boosted ionic transport kinetics in the heterostructured ZnCo₂O₄/ZnO nanobelts for high-performance supercapacitor. *J. Colloid Interface Sci.* **2023**, *629*, 649–659. [[CrossRef](#)] [[PubMed](#)]
127. Abbas, Q.; Siyal, S.H.; Bocchetta, P. Flower-like Highly Open-Structured Binder-Free Zn-Co-Oxide Nanosheet for High-Performance Supercapacitor Electrodes. *Molecules* **2022**, *27*, 4850. [[CrossRef](#)] [[PubMed](#)]
128. Rajangam, I. Hybrid nanostructures made of porous binary transition metal oxides for high performance asymmetric supercapacitor application. *J. Energy Storage* **2023**, *67*, 107530.
129. Karthik, R.; Sukanya, R.; Chen, S.M.; Hasan, M.; Dhakal, G.; Shafi, P.M.; Shim, J.J. Development of an Amorphous Nickel Boride/Manganese Molybdate Heterostructure as an Efficient Electrode Material for a High-Performance Asymmetric Supercapacitor. *ACS Appl. Mater. Interfaces* **2023**, *15*, 11927–11939. [[CrossRef](#)]
130. Li, P.X.; Qiao, D.W.; Bai, J.K.; Li, X.L. Facile synthesis of petal-like MnMoO₄/Ni(OH)₂ ultrathin nanosheets for high-performance asymmetric supercapacitor. *Mater. Lett.* **2023**, *337*, 134007. [[CrossRef](#)]
131. Nandagopal, T.; Balaji, G.; Vadivel, S. Enhanced electrochemical performance of CoMoO₄ nanorods/reduced graphene oxide (rGO) as asymmetric supercapacitor devices. *J. Energy Storage* **2023**, *68*, 107710. [[CrossRef](#)]

132. Yang, R.; Zhang, Y.; Huang, X.; Yin, H.Q.; Zhang, K.Y.; Qin, A.M.; Chen, S.P. In-situ growth of $\text{KCu}_7\text{S}_4@\text{CoMoO}_4$ core-shell structure on Ni foam for high performance supercapacitor electrode. *J. Alloys Compd.* **2022**, *927*, 166996. [[CrossRef](#)]
133. Liu, L.Y.; Dai, D.F.; Yang, B.; Li, B.; Liu, X.Y. Green preparation of CoMoO_4 nanoparticles through a mechanochemical method for energy storage applications. *New J. Chem.* **2022**, *46*, 23369–23378. [[CrossRef](#)]
134. Zhou, J.H.; Chen, Z.X.; Yang, H.; Liu, M.J.; Gu, B.N.; Chen, C.C.; Lv, H.F.; Zhou, Z.Y.; Chueh, Y.L. Hierarchically Hybrid Porous $\text{Co}_3\text{O}_4@\text{NiMoO}_4/\text{CoMoO}_4$ Heterostructures for High-Performance Electrochemical Energy Storage. *ACS Appl. Mater. Interfaces* **2022**, *14*, 8282–8296.
135. Shen, L.F.; Yu, L.; Yu, X.Y.; Zhang, X.G.; Lou, X.W. Self-templated formation of uniform NiCo_2O_4 hollow spheres with complex interior structures for lithium-ion batteries and supercapacitors. *Angew. Chem. Int. Ed.* **2015**, *54*, 1868–1872. [[CrossRef](#)] [[PubMed](#)]
136. Ji, C.C.; Liu, F.Z.; Xua, L.; Yang, S.C. Urchin-like NiCo_2O_4 hollow microspheres and FeSe_2 micro-snowflakes for flexible solid-state asymmetric supercapacitors. *J. Mater. Chem. A* **2017**, *5*, 5568–5576. [[CrossRef](#)]
137. Li, Q.; Lu, C.X.; Chen, C.M.; Xie, L.J.; Liu, Y.D.; Li, Y.; Kong, Q.Q.; Wang, H. Layered NiCo_2O_4 /reduced graphene oxide composite as an advanced electrode for supercapacitor. *Energy Storage Mater.* **2017**, *8*, 59–67. [[CrossRef](#)]
138. Al-Rubaye, S.; Rajagopalan, R.; Dou, S.X.; Cheng, Z.X. Facile synthesis of a reduced graphene oxide wrapped porous NiCo_2O_4 composite with superior performance as an electrode material for supercapacitors. *J. Mater. Chem. A* **2017**, *5*, 18989–18997. [[CrossRef](#)]
139. Sun, S.M.; Wang, S.; Li, S.D.; Li, Y.N.; Zhang, Y.H.; Chen, J.L.; Zhang, Z.H.; Fang, S.M.; Wang, P.Y. Asymmetric supercapacitors based on a NiCo_2O_4 /three dimensional graphene composite and three dimensional graphene with high energy density. *J. Mater. Chem. A* **2016**, *4*, 18646–18653. [[CrossRef](#)]
140. Ye, Y.; Luo, Y.Z.; Lou, J.T.; Chen, X.L.; Cheng, Y.J.; Xia, J.F.; Li, Y.B.; Guo, K.K. Hollow Spherical $\text{NiCo}_2\text{S}_4@\text{N-CNT}$ Composites with High Energy Density for All-Solid-State Supercapacitors. *ACS Appl. Energy Mater.* **2023**, *6*, 6742–6751. [[CrossRef](#)]
141. Abuali, M.; Arsalani, N.; Ahadzadeh, I. On the effect of polypyrrole on electrochemical performance of micro-sized hollow spheres of NiCo_2S_4 and CuCo_2S_4 nanoparticles. *Electrochim. Acta* **2022**, *427*, 140840. [[CrossRef](#)]
142. Qi, S.H.; Wu, D.X.; Dong, Y.; Liao, J.Q.; Foster, C.W.; Feng, Y.Z.; Liu, C.T.; Ma, J.M. T Cobalt-based electrode materials for sodium-ion batteries. *Chem. Eng.* **2019**, *3*, 166. [[CrossRef](#)]
143. Zhang, H.B.; Lv, Y.; Wu, X.Y.; Guo, J.X.; Jia, D.Z. Electrodeposition synthesis of reduced graphdiyne oxide/ NiCo_2S_4 hierarchical nanosheet arrays for small size and light weight aqueous asymmetry supercapacitors. *J. Alloys Compd.* **2023**, *947*, 169403. [[CrossRef](#)]
144. Peng, T.Q.; Yi, H.; Sun, P.; Jing, Y.T.; Wang, R.J.; Wang, H.W.; Wang, X.F. In situ growth of binder-free CNTs@Ni-Co-S nanosheets core/shell hybrids on Ni mesh for high energy density asymmetric supercapacitors. *J. Mater. Chem. A* **2016**, *4*, 8888–8897. [[CrossRef](#)]
145. Yuan, K.; Gao, T.J.; Yang, Y.; Luo, W.; Li, S.; Zhang, C.Y.; Xu, J.X.; Li, N.; Zhu, Y.R. Template sacrificial controlled synthesis of hierarchical nanoporous carbon@ NiCo_2S_4 microspheres for high-performance hybrid supercapacitors. *Rare Met.* **2023**, *42*, 2643–2657. [[CrossRef](#)]
146. Zhang, Y.F.; Ma, M.Z.; Yang, J.; Sun, C.C.; Su, H.Q.; Huang, W.; Dong, X.C. Shape-controlled synthesis of NiCo_2S_4 and their charge storage characteristics in supercapacitors. *Nanoscale* **2014**, *6*, 9824–9830. [[CrossRef](#)] [[PubMed](#)]
147. Panicker, N.J.; Dutta, J.C.; Sahu, P.P. Confined growth of NiCo_2S_4 on 2D/2D porous carbon self-repairing g- $\text{C}_3\text{N}_4/\text{rGO}$ heterostructure for enhanced performance of asymmetric supercapacitors. *Chem. Eng. J.* **2023**, *463*, 142376. [[CrossRef](#)]
148. Dai, S.G.; Xi, Y.; Hu, C.G.; Yue, X.L.; Cheng, L.; Wang, G. $\text{MnO}_2@\text{KCu}_7\text{S}_4$ NWs hybrid compositions for high-power all-solid-state supercapacitor. *J. Power Sources* **2015**, *274*, 477–482. [[CrossRef](#)]
149. Dai, S.G.; Xi, Y.; Hu, C.G.; Yue, X.L.; Cheng, L.; Wang, G. Different proportions of C/ KCu_7S_4 hybrid structure for high-performance supercapacitors. *J. Power Sources* **2014**, *263*, 175–180. [[CrossRef](#)]
150. Guo, X.L.; Zhang, J.M.; Xu, W.N.; Hu, C.G.; Sun, L.D.; Zhang, Y.X. Growth of Ni/Mn LDH nanosheet arrays on KCu_7S_4 microwires for hybrid supercapacitors with enhanced electrochemical performance. *J. Mater. Chem. A* **2017**, *5*, 20579–20587. [[CrossRef](#)]
151. Dai, S.G.; Xi, Y.; Hu, C.G.; Hu, B.S.; Yue, X.L.; Cheng, L.; Wang, G. C@ KCu_7S_4 microstructure for solid-state supercapacitors. *RSC Adv.* **2014**, *4*, 40542–40545. [[CrossRef](#)]
152. Tang, J.H.; Ge, Y.C.; Shen, J.F.; Ye, M.X. Facile synthesis of CuCo_2S_4 as a novel electrode material for ultrahigh supercapacitor performance. *Chem. Commun.* **2016**, *52*, 1509–1512. [[CrossRef](#)] [[PubMed](#)]
153. Kenesi, A.G.; Ghorbani, M.; Lashkenari, M.S. High electrochemical performance of PANI/CdO nanocomposite based on graphene oxide as a hybrid electrode materials for supercapacitor application. *Int. J. Hydrog. Energy* **2019**, *47*, 38849–38861. [[CrossRef](#)]
154. Ramesh, S.; Karuppasamy, K.; Yadav, H.M.; Lee, Y.J.; Sivasamy, A.; Kathalingam, A.; Kim, H.S.; Kim, J.H.; Kim, H.S. Fabrication of CuCo_2S_4 on composite interface materials made of polypyrrole and nitrogen-doped carbon nanotubes for use in supercapacitors. *J. Energy Storage* **2023**, *67*, 107518. [[CrossRef](#)]
155. Kuo, T.R.; Lin, K.H.; Chen, M.W.; Yougbaré, S.; Lin, L.Y.; Wu, Y.F. Tailing copper cobalt sulfide particle-decorated tube-like structure as efficient active material of battery supercapacitor hybrid. *J. Energy Storage* **2023**, *67*, 107564. [[CrossRef](#)]
156. Yu, X.; Zhang, W.W.; Liu, L.; Fautrelle, Y.; Lu, X.G.; Li, X. High Magnetic Field-Engineered Bunched Zn–Co–S Yolk–Shell Balls Intercalated within S, N Codoped CNT/Graphene Films for Free-Standing Supercapacitors. *ACS Appl. Mater. Interfaces* **2020**, *12*, 33690–33701. [[CrossRef](#)] [[PubMed](#)]

157. Tan, H.; Ge, P.B.; Shao, Y.Q.; Liu, Z.J.; Li, H.H.; Chen, K.F.; Xu, L.H.; Zhuang, J.H.; Chen, Y.X.; Xia, X.J. Zn-Co-S coatings with a rough and porous nano-dendrite structure for high-performance asymmetric supercapacitors without binder. *Electrochim. Acta* **2022**, *429*, 141048. [[CrossRef](#)]
158. Manas, M.; Krishna, C.; Sarbarajan, P.; Adwaita, K.; Malay, C.; Souvik, M.; Wonjae, S.; Sachindranath, D.; Changwoon, N.; Kumar, B.S. Electrodeposited Binder-free Mn-Co-S Nanosheets toward High Specific-Energy Aqueous Asymmetric Supercapacitors. *ACS Appl. Electron. Mater.* **2022**, *4*, 4357–4367.
159. Haider, S.S.; Dad, S.; Zakar, S.; Iqbal, M.Z. Mechanistic scrutinizing the charge storage phenomena of battery-grade Mn-Co-S electrodes. *Mater. Res. Bull.* **2022**, *156*, 111953. [[CrossRef](#)]
160. Xu, J.; Xiang, C.L.; Fang, S.W.; Zhu, L.P.; Xu, F.; Sun, L.X.; Zou, Y.J.; Zhang, J. Template strategy to synthesize porous Mn-Co-S nanospheres electrode for high-performance supercapacitors. *J. Energy Storage* **2021**, *44*, 103267. [[CrossRef](#)]
161. Ramtin, A.; Mohammadi, Z.A.; Davarani, S.S.H. Rational Construction of Core-Shell Ni–Mn–Co–S@Co(OH)₂ Nanoarrays toward High-Performance Hybrid Supercapacitors. *ChemElectroChem* **2020**, *7*, 2816–2825.
162. Moosakhani, S.; Ali, A.S.A.; Mohammadpour, R.; Ge, Y.L.; Hannula, S.P. Solution synthesis of CuSb₂ nanocrystals: A new approach to control shape and size. *J. Alloys Compd.* **2018**, *736*, 190–201. [[CrossRef](#)]
163. Das, A.; Mohapatra, M.; Basu, S. Expeditious synthesis of 3D pyramidal faceted CuSb₂ architectures manifesting unrivalled porous capacitive energy storage. *Mater. Lett.* **2021**, *289*, 129412. [[CrossRef](#)]
164. Javadian, S.; Bayat, E.; Parviz, Z.; Dalir, N.; Gharibi, H. New rationally designed hybrid polypyrrole@SnCoS₄ as an efficient anode for lithium-ion batteries. *New J. Chem.* **2021**, *45*, 11737–11751. [[CrossRef](#)]
165. Zhang, Y.X.; Jin, Y.H.; Song, Y.Y.; Wang, H.; Jia, M.Q. Induced bimetallic sulfide growth with reduced graphene oxide for high-performance sodium storage. *J. Colloid Interface Sci.* **2023**, *642*, 554–564. [[CrossRef](#)] [[PubMed](#)]
166. Guan, B.L.; Qi, S.Y.; Li, Y.; Sun, T.; Liu, Y.G.; Yi, T.F. Towards high-performance anodes: Design and construction of cobalt-based sulfide materials for sodium-ion batteries. *J. Energy Chem.* **2021**, *54*, 680–698. [[CrossRef](#)]
167. Lu, Y.; Zhang, Z.; Liu, X.; Wang, W.; Peng, T.; Guo, P.; Sun, H.; Yan, H.; Luo, Y. NiCo₂S₄/carbon nanotube nanocomposites with a chain-like architecture for enhanced supercapacitor performance. *CrystEngComm* **2016**, *18*, 7696–7706. [[CrossRef](#)]
168. Yu, L.; Zhang, L.; Wu, H.B.; Lou, W. Formation of Ni_xCo_{3–x}S₄ hollow nanoprisms with enhanced pseudocapacitive properties. *Angew. Chem.* **2014**, *126*, 3785–3788. [[CrossRef](#)]
169. Wang, H.; Wang, C.; Qing, C.; Sun, D.M.; Wang, B.X.; Qu, G.; Sun, M.; Tang, Y.W. Construction of carbon-nickel cobalt sulphide hetero-structured arrays on nickel foam for high performance asymmetric supercapacitors. *Electrochim. Acta* **2015**, *174*, 1104–1112. [[CrossRef](#)]
170. Guan, B.Y.; Yu, L.; Wang, X.; Song, S.Y.; Lou, X.W. Formation of onion-like NiCo₂S₄ particles via sequential ion-exchange for hybrid supercapacitors. *Adv. Mater.* **2017**, *29*, 1605051. [[CrossRef](#)]
171. Khumujam, D.D.; Kshetri, T.; Singh, T.I.; Kim, N.H.; Lee, J.H. Hierarchical Integrated Hybrid Structural Electrodes Based on Co-N/C and Mo-doped NiCo-LDH@Co-N/C Anchored on MX/CF for High Energy Density Fiber-Shaped Supercapacitor. *Adv. Funct. Mater.* **2023**, 2302388. [[CrossRef](#)]
172. Hu, H.X.; Li, K.D.; Li, X.S.; Wang, L.Y.; Yang, X.J.; Zhang, Q.X. Facile fabrication of NiCo-LDH on activated rice husk carbon for high-performance all-solid-state asymmetric supercapacitors. *New J. Chem.* **2023**, *47*, 14030–14038. [[CrossRef](#)]
173. Nagaraju, G.; Raju, G.S.; Ko, Y.H.; Yu, J.S. Hierarchical Ni-Co layered double hydroxide nanosheets entrapped on conductive textile fibers: A cost-effective and flexible electrode for high-performance pseudocapacitors. *Nanoscale* **2016**, *8*, 812–825. [[CrossRef](#)] [[PubMed](#)]
174. Yilmaz, G.; Yam, K.M.; Zhang, C.; Fan, H.J.; Ho, G.W. In situ transformation of MOFs into layered double hydroxide embedded metal sulfides for improved electrocatalytic and supercapacitive performance. *Adv. Mater.* **2017**, *29*, 1606814. [[CrossRef](#)] [[PubMed](#)]
175. Bai, X.; Liu, Q.; Lu, Z.T.; Liu, J.Y.; Chen, R.R.; Li, R.M.; Song, D.L.; Jing, X.Y.; Liu, P.L.; Wang, J. Rational design of sandwiched Ni-Co layered double hydroxides hollow nanocages/graphene derived from metal-organic framework for sustainable energy storage. *ACS Sustain. Chem. Eng.* **2017**, *5*, 9923–9934. [[CrossRef](#)]
176. Liu, Y.; Fu, N.Q.; Zhang, G.G.; Xu, M.; Lu, W.; Zhou, L.M.; Huang, H.T. Design of hierarchical Ni-Co@Ni-Co layered double hydroxide core-shell structured nanotube array for high-performance flexible all-solid-state battery-type supercapacitors. *Adv. Funct. Mater.* **2017**, *27*, 1605307. [[CrossRef](#)]
177. Wang, T.; Zhang, S.L.; Yan, X.B.; Lu, M.Q.; Wang, L.Z.; Bell, J.; Wang, H.X. 2-Methylimidazole-derived Ni-Co layered double hydroxide nanosheets as high rate capability and high energy density storage material in hybrid supercapacitors. *ACS Appl. Mater. Interfaces* **2017**, *9*, 15510–15524. [[CrossRef](#)] [[PubMed](#)]
178. Jing, M.J.; Hou, H.S.; Banks, C.E.; Yang, Y.C.; Zhang, Y.; Ji, X.B. Alternating voltage introduced NiCo double hydroxide layered nanoflakes for an asymmetric supercapacitor. *ACS Appl. Mater. Interfaces* **2015**, *7*, 22741–22744. [[CrossRef](#)]
179. Zheng, C.H.; Yao, T.; Xu, T.R.; Wang, H.A.; Huang, P.F.; Yan, Y.; Fang, D.L. Growth of ultrathin Ni-Co-Al layered double hydroxide on reduced graphene oxide and superb supercapacitive performance of the resulting composite. *J. Alloys Compd.* **2016**, *678*, 93–101. [[CrossRef](#)]
180. Ge, X.; Gu, C.D.; Yin, Z.Y.; Wang, X.L.; Tu, J.P.; Li, J. Periodic stacking of 2D charged sheets: Self-assembled superlattice of Ni-Al layered double hydroxide (LDH) and reduced graphene oxide. *Nano Energy* **2016**, *20*, 185–193. [[CrossRef](#)]
181. Li, H.B.; Gao, Y.Q.; Wang, C.X.; Yang, G.W. A simple electrochemical route to access amorphous mixed-metal hydroxides for supercapacitor electrode materials. *Adv. Energy Mater.* **2015**, *5*, 1401767. [[CrossRef](#)]

182. Wang, X.Q.; Li, X.M.; Du, X.; Ma, X.L.; Hao, X.G.; Xue, C.F.; Zhu, H.Y.; Li, S.S. Controllable Synthesis of NiCo LDH nanosheets for fabrication of high-performance supercapacitor electrodes. *Electroanalysis* **2017**, *29*, 1286–1293. [CrossRef]
183. Xu, J.; Ma, C.J.; Cao, J.Y.; Chen, Z.D. Facile synthesis of core-shell nanostructured hollow carbon nanospheres@nickel cobalt double hydroxides as high-performance electrode materials for supercapacitors. *Dalton Trans.* **2017**, *46*, 3276–3283. [CrossRef] [PubMed]
184. Cai, X.Q.; Shen, X.P.; Ma, L.B.; Ji, Z.; Xu, C.; Yuan, A. Solvothermal synthesis of NiCo-layered double hydroxide nanosheets decorated on RGO sheets for high performance supercapacitor. *Chem. Eng. J.* **2015**, *258*, 251–259. [CrossRef]
185. Li, X.C.; Shen, J.J.; Sun, W.; Hong, X.D.; Wang, R.T.; Zhao, X.H.; Yan, X.B. A super-high energy density asymmetric supercapacitor based on 3D core-shell structured NiCo-layered double hydroxide@carbon nanotube and activated polyaniline-derived carbon electrodes with commercial level mass loading. *J. Mater. Chem. A* **2015**, *3*, 13244–13253. [CrossRef]
186. Huang, P.; Cao, C.; Sun, Y.; Yang, S.; Wei, F.; Song, W. One-pot synthesis of sandwich-like reduced graphene oxide@CoNiAl layered double hydroxide with excellent pseudocapacitive properties. *J. Mater. Chem. A* **2015**, *3*, 10858–10863. [CrossRef]
187. Song, Y.; Cai, X.; Xu, X.X.; Liu, X.X. Integration of nickel-cobalt double hydroxide nanosheets and polypyrrole films with functionalized partially exfoliated graphite for asymmetric supercapacitors with improved rate capability. *J. Mater. Chem. A* **2015**, *3*, 14712–14720. [CrossRef]
188. Liu, Z.Q.; Chen, G.F.; Zhou, P.L.; Li, N.; Su, Y.Z. Building layered $Ni_xCo_{2x}(OH)_{6x}$ nanosheets decorated three-dimensional Ni frameworks for electrochemical applications. *J. Power Sources* **2016**, *317*, 1–9. [CrossRef]
189. Pu, J.; Tong, Y.; Wang, S.; Sheng, E.; Wang, Z. Nিকেlecobalt hydroxide nanosheets arrays on Ni foam for pseudocapacitor applications. *J. Power Sources* **2014**, *250*, 250–256. [CrossRef]
190. Huang, L.; Liu, B.C.; Hou, H.J.; Wu, L.S.; Zhu, X.L.; Hu, J.P.; Yang, J.K. Facile preparation of flower-like NiMn layered double hydroxide/reduced graphene oxide microsphere composite for high-performance asymmetric supercapacitors. *J. Alloys Compd.* **2018**, *730*, 71–80. [CrossRef]
191. Chen, D.M.; Chen, H.Y.; Chang, X.; Liu, P.; Zhao, Z.C.; Zhou, J.W.; Xu, G.W.; Lin, H.L.; Han, S. Hierarchical CoMn-layered double hydroxide nanowires on nickel foam as electrode material for high-capacitance supercapacitor. *J. Alloys Compd.* **2017**, *729*, 866–873. [CrossRef]
192. Li, X.Y.; Yu, L.; Wang, G.L.; Wan, G.P.; Peng, X.G.; Wang, K.; Wang, G.Z. Hierarchical NiAl LDH nanotubes constructed via atomic layer deposition assisted method for high performance supercapacitors. *Electrochim. Acta* **2017**, *255*, 15–22. [CrossRef]
193. He, X.Y.; Liu, Q.; Liu, J.Y.; Li, R.M.; Zhang, H.S.; Chen, R.R.; Wang, J. Hierarchical $NiCo_2O_4@NiCoAl$ -layered double hydroxide core/shell nanoforest arrays as advanced electrodes for high-performance asymmetric supercapacitors. *J. Alloys Compd.* **2017**, *724*, 130–138. [CrossRef]
194. Lu, Y.; Jiang, B.; Fang, L.; Ling, F.L.; Wu, F.; Hu, B.S.; Meng, F.M.; Niu, K.Y.; Lin, F.; Zheng, H.M. An investigation of ultrathin nickel-iron layered double hydroxide nanosheets grown on nickel foam for high-performance supercapacitor electrodes. *J. Alloys Compd.* **2017**, *714*, 63–70. [CrossRef]
195. Wu, N.S.; Low, J.X.; Liu, T.; Yu, J.G.; Cao, S.W. Hierarchical hollow cages of Mn-Co layered double hydroxide as supercapacitor electrode materials. *Appl. Surf. Sci.* **2017**, *413*, 35–40. [CrossRef]
196. Zhang, L.; Yao, H.C.; Li, Z.H.; Sun, P.P.; Liu, F.; Dong, C.; Wang, J.S.; Li, Z.J.; Wu, M.W.; Zhang, C.; et al. Synthesis of delaminated layered double hydroxides and their assembly with graphene oxide for supercapacitor application. *J. Alloys Compd.* **2017**, *711*, 31–41. [CrossRef]
197. Li, S.S.; Cheng, P.P.; Luo, J.X.; Zhou, D.; Xu, W.M.; Li, J.W.; Li, R.C.; Yuan, D.S. High-performance flexible asymmetric supercapacitor based on CoAl-LDH and rGO electrodes. *Nano-Micro Lett.* **2017**, *9*, 31. [CrossRef] [PubMed]
198. Zai, J.T.; Liu, Y.Y.; Li, X.M.; Ma, Z.F.; Qi, R.R.; Qian, X.F. 3D Hierarchical Co-Al layered double hydroxides with long term stabilities and high rate performances in supercapacitors. *Nano-Micro Lett.* **2017**, *9*, 21. [CrossRef]
199. Zha, D.S.; Sun, H.H.; Fu, Y.S.; Ouyang, X.P.; Wang, X. Acetate anion-intercalated nickel-cobalt layered double hydroxide nanosheets supported on Ni foam for high-performance supercapacitors with excellent long-term cycling stability. *Electrochim. Acta* **2017**, *236*, 18–27. [CrossRef]
200. Li, M.; Liu, F.; Zhang, X.B.; Cheng, J.P. A comparative study of Ni-Mn layered double hydroxide/carbon composites with different morphologies for supercapacitors. *Phys. Chem. Chem. Phys.* **2016**, *18*, 30068–30078. [CrossRef]
201. Yuan, C.Z.; Gao, B.; Shen, L.F.; Yang, S.D.; Hao, L.; Lu, X.J.; Zhang, F.; Zhang, L.J.; Zhang, X.G. Hierarchically structured carbon-based composites: Design, synthesis and their application in electrochemical capacitors. *Nanoscale* **2011**, *3*, 529–545. [CrossRef] [PubMed]
202. Zhao, B.; Chen, D.C.; Xiong, X.H.; Song, B.; Hu, R.Z.; Zhang, Q.B.; Rainwater, B.H.; Waller, G.H.; Zhen, D.X.; Ding, Y.; et al. A high-energy, long cycle-life hybrid supercapacitor based on graphene composite electrodes. *Energy Storage Mater.* **2017**, *7*, 32–39. [CrossRef]
203. Liu, S.; Lee, S.C.; Patil, U.; Shackery, I.; Kang, S.; Zhang, K.; Park, J.H.; Chung, K.Y.; Jun, S.C. Hierarchical MnCo-layered double hydroxides@Ni(OH)₂ core-shell heterostructures as advanced electrodes for supercapacitors. *J. Mater. Chem. A* **2017**, *5*, 1043–1049. [CrossRef]
204. Kierzek, K.; Frackowiak, E.; Lota, G.; Gryglewicz, G.; Machnikowski, J. Electrochemical capacitors based on highly porous carbons prepared by KOH activation. *Electrochim. Acta* **2004**, *49*, 515–523. [CrossRef]

205. Wang, H.; Liang, Y.; Gong, M.; Li, Y.; Chang, W.; Mefford, T.; Zhou, J.; Wang, J.; Regier, T.; Wie, F.; et al. An ultrafast nickel-iron battery from strongly coupled inorganic nanoparticle/nanocarbon hybrid materials. *Nat. Commun.* **2012**, *3*, 917. [[CrossRef](#)] [[PubMed](#)]
206. Zhang, J.T.; Gong, L.Y.; Sun, K.; Jiang, J.C.; Zhang, X.G. Preparation of activated carbon from waste *Camellia oleifera* shell for supercapacitor application. *J. Solid State Electrochem.* **2012**, *16*, 2179–2186. [[CrossRef](#)]
207. Zhang, B.; Zhao, B.; Wang, J.X.; Qu, C.; Sun, H.B.; Zhang, K.L.; Liu, M.L. High-performance hybrid supercapacitors based on self-supported 3D ultrathin porous quaternary Zn-Ni-Al-Co oxide nanosheets. *Nano Energy* **2016**, *28*, 475–785. [[CrossRef](#)]
208. Liu, S.D.; Lee, S.C.; Patil, U.M.; Ray, C.; Sankar, K.V.; Zhang, K.; Kundu, A.; Kang, S.N.; Park, J.H.; Jun, S.C. Controllable sulfuration engineered NiO nanosheets with enhanced capacitance for high rate supercapacitors. *J. Mater. Chem. A* **2017**, *5*, 4543–4549. [[CrossRef](#)]
209. Zhang, C.Q.; Chen, Q.D.; Zhan, H.B. Supercapacitors based on reduced graphene oxide nanofibers supported Ni(OH)₂ nanoplates with enhanced electrochemical performance. *ACS Appl. Mater. Interfaces* **2016**, *8*, 22977–22987. [[CrossRef](#)]
210. Guan, B.; Li, Y.; Yin, B.Y.; Liu, K.F.; Wang, D.W.; Zhang, H.H.; Cheng, C.J. Synthesis of hierarchical NiS microflowers for high performance asymmetric supercapacitor. *Chem. Eng. J.* **2017**, *308*, 1165–1173. [[CrossRef](#)]
211. Zhao, J.; Guan, B.; Hu, B.; Xu, Z.Y.; Wang, D.W.; Zhang, H.H. Vulcanizing time controlled synthesis of NiS microflowers and its application in asymmetric supercapacitors. *Electrochim. Acta* **2017**, *230*, 428–437. [[CrossRef](#)]
212. Li, T.; Li, H.; Li, L.H.; Liu, L.; Xu, Y.; Ding, H.Y. Large-scale self-assembly of 3D flower-like hierarchical Ni/Co-LDHs microspheres for high-performance flexible asymmetric supercapacitors. *ACS Appl. Mater. Interfaces* **2016**, *8*, 2562–2572. [[CrossRef](#)] [[PubMed](#)]
213. Shang, Y.Y.; Xie, T.; Gai, Y.S.; Su, L.H.; Gong, L.Y.; Lu, H.J.; Dong, F.Y. Self-assembled hierarchical peony-like ZnCo₂O₄ for high-performance asymmetric supercapacitors. *Electrochim. Acta* **2017**, *253*, 281–290. [[CrossRef](#)]
214. Song, D.M.; Zhu, J.K.; Li, J.; Pu, T.; Huang, B.; Zhao, C.L.; Xie, L.; Chen, L.Y. Free-standing two-dimensional mesoporous ZnCo₂O₄ thin sheets consisting of 3D ultrathin nanoflake array frameworks for high performance asymmetric supercapacitor. *Electrochim. Acta* **2017**, *257*, 455–464. [[CrossRef](#)]
215. Yang, J.; Zhang, Y.; Sun, C.C.; Guo, G.L.; Sun, W.P.; Huang, W.; Yan, Q.Y.; Dong, X.C. Controlled synthesis of zinc cobalt sulfide nanostructures in oil phase and their potential applications in electrochemical energy storage. *J. Mater. Chem. A* **2015**, *3*, 11462–11470. [[CrossRef](#)]
216. Liu, S.; Jun, S.C. Hierarchical manganese cobalt sulfide core-shell nanostructures for high-performance asymmetric supercapacitors. *J. Power Sources* **2017**, *342*, 629–637. [[CrossRef](#)]
217. Li, S.F.; Yu, C.; Yang, J.; Zhao, C.T.; Zhang, M.D.; Huang, W.; Liu, Z.B.; Guo, W.; Qiu, J.S. A superhydrophilic “nanoglue” for stabilizing metal hydroxides onto carbon materials for high-energy and ultralong-life asymmetric supercapacitors. *Energy Environ. Sci.* **2017**, *10*, 1958–1965. [[CrossRef](#)]
218. Ye, L.; Zhao, L.J.; Zhang, H.; Zan, P.; Ge, S.; Shi, W.H.; Han, B.; Sun, H.M.; Yang, X.J.; Xu, T.H. Serpent-cactus-like Co-doped Ni(OH)₂/Ni₃S₂ hierarchical structure composed of ultrathin nanosheets for use in efficient asymmetric supercapacitors. *J. Mater. Chem. A* **2017**, *5*, 1603–1613. [[CrossRef](#)]
219. Li, W.; Xin, L.P.; Wu, M.; Long, Y.; Huang, H.T.; Lou, X.J. Facile synthesis of truncated cube-like NiSe₂ single crystals for high-performance asymmetric supercapacitors. *Chem. Eng. J.* **2017**, *330*, 1334–1341.
220. Shi, H. Activated carbons and double layer capacitance. *Electrochim. Acta* **1996**, *41*, 1633–1639. [[CrossRef](#)]
221. Devarajan, J.; Arumugam, P. Nitrogen and phosphorous co-doped carbon nanotubes for high-performance supercapacitors. *Carbon Lett.* **2023**, *23*, 532. [[CrossRef](#)]
222. Huang, X.W.; Huang, J.H.; Yang, J.; Yang, D.; Li, T.T.; Dong, A.G. High-Yield Exfoliation of Large MXene with Flake Sizes over 10 μm Using Edge-Anchored Carbon Nanotubes. *Adv. Funct. Mater.* **2023**, *33*, 2303003. [[CrossRef](#)]
223. Jung, M.Y.; Sivakumar, P.; Park, H.S. Carbon nanotube branch-grown nickel nanoparticles/graphene composites for a high-capacitance electrode. *J. Phys. Energy* **2023**, *5*, 025005. [[CrossRef](#)]
224. Guo, Q.H.; Li, C.W.; Yang, K.H.; Zhou, P.D.; Hua, N.B.; Weng, M.C. Polyaniline/Reduced Graphene Oxide/Carbon Nanotube Composites for Actuation-Based Sensing for Energy Storage. *ACS Appl. Nano Mater.* **2023**, *6*, 4925–4935. [[CrossRef](#)]
225. Han, Y.; Ha, H.; Choi, C.; Yoon, H.; Matteini, P.; Cheong, J.Y.; Hwang, B. Review of Flexible Supercapacitors Using Carbon Nanotube-Based Electrodes. *Appl. Sci.* **2023**, *13*, 3290. [[CrossRef](#)]
226. Mayank, P.; Kiran, M.S. CNT yarn based solid state linear supercapacitor with multi-featured capabilities for wearable and implantable devices. *Energy Storage Mater.* **2023**, *57*, 136–170.
227. Wang, J.G.; Liu, H.Z.; Zhang, X.Y.; Li, X.; Liu, X.R.; Kang, F.Y. Green synthesis of hierarchically porous carbon nanotubes as advanced materials for high-efficient energystorage. *Small* **2018**, *14*, 1703950. [[CrossRef](#)]
228. Baughman, R.H.; Zakhidov, A.A. Carbon nanotubes—the route toward applications. *Science* **2002**, *297*, 787–792. [[CrossRef](#)]
229. Chiu, C.T.; Chen, D.H. One-step hydrothermal synthesis of three-dimensional porous Ni-Co sulfide/reduced graphene oxide composite with optimal incorporation of carbon nanotubes for high performance supercapacitors. *Nanotechnology* **2018**, *29*, 175602. [[CrossRef](#)]
230. Kim, D.K.; Kim, N.D.; Park, S.K.; Seong, K.D.; Hwang, M.; You, N.H.; Piao, Y.Z. Nitrogen doped carbon derived from polyimide/multiwall carbon nanotube composites for high performance flexible all-solid-state supercapacitors. *J. Power Sources* **2018**, *380*, 55–63. [[CrossRef](#)]

231. Jin, L.N.; Shao, F.; Jin, C.; Zhang, J.N.; Liu, P.; Guo, M.X.; Bian, S.W. High-performance textile supercapacitor electrode materials enhanced with three-dimensional carbon nanotubes/graphene conductive network and in situ polymerized polyaniline. *Electrochim. Acta* **2017**, *249*, 387–394. [[CrossRef](#)]
232. Zhou, G.H.; Kim, N.R.; Chun, S.E.; Lee, W.; Um, M.K.; Chou, T.W.; Islam, M.F.; Byun, J.H. Highly porous and easy shapeable poly-dopamine derived graphene-coated single walled carbon nanotube aerogels for stretchable wire-type supercapacitors. *Carbon* **2018**, *130*, 37–144. [[CrossRef](#)]
233. Biswal, M.; Banerjee, A.; Deo, M.; Ogale, S. From dead leaves to high energy density supercapacitors. *Environ. Sci. Technol.* **2013**, *6*, 1249–1259. [[CrossRef](#)]
234. Annamalai, K.; Gao, J.; Liu, L.; Mei, J.; Lau, W.; Tao, Y. Nanoporous graphene/single wall carbon nanohorn heterostructures with enhanced capacitance. *J. Mater. Chem. A* **2015**, *3*, 11740–11744. [[CrossRef](#)]
235. Khaw, L.F.; Koh, W.S.; Yeap, S.P.; Lim, J.K.; Ahmad, A.L.; Toh, P.Y.; Khosravi, V. Shape-controlled synthesis of polyaniline and its synergistic effect with reduced graphene oxide for the fabrication of flexible electrode. *Polym. Eng. Sci.* **2023**, *63*, 2295–2308. [[CrossRef](#)]
236. Zhang, Y.; Zhou, Q.Y.; Ma, W.H.; Wang, C.H.; Wang, X.F.; Chen, J.J.; Yu, T.T.; Fan, S. Nanocellulose/nitrogen and fluorine co-doped graphene composite hydrogels for high-performance supercapacitors. *Nano Res.* **2023**, *23*, 5736. [[CrossRef](#)]
237. Dai, S.G.; Liu, Z.; Zhao, B.; Zeng, J.H.; Hu, H.; Zhang, Q.B.; Chen, D.C.; Qu, C.; Dang, D.; Liu, M.L. A high-performance supercapacitor electrode based on N-doped porous graphene. *J. Power Sources* **2018**, *387*, 43–48. [[CrossRef](#)]
238. Feng, R.M.; Chen, Y.J.; Yang, L.F.; Du, Q.Z.; Zhuo, K.L. Ethyl viologen-functionalized reduced graphene oxide composites for asymmetric ionic liquid-based supercapacitors. *Chem. Eng. J.* **2023**, *468*, 143693. [[CrossRef](#)]
239. Qiu, C.J.; Jiang, L.L.; Gao, Y.G.; Sheng, L.Z. Effects of oxygen-containing functional groups on carbon materials in supercapacitors: A review. *Mater. Des.* **2023**, *230*, 111952. [[CrossRef](#)]
240. Sima, L.; Manila, O.V.; Rajinder, P.; Michael, A.P. Electrolyte-mediated assembly of graphene-based supercapacitors using adsorbed ionic liquid/non-ionic surfactant complexes. *J. Mater. Chem. A* **2023**, *11*, 11222–11234.
241. Qin, Y.; Yuan, J.; Li, J.; Chen, D.C.; Kong, Y.; Chu, F.Q.; Tao, Y.X.; Liu, M.L. Crosslinking graphene oxide into robust 3D porous N-doped graphene. *Adv. Mater.* **2015**, *27*, 5171–5175. [[CrossRef](#)]
242. Wang, K.L.; Xu, M.; Gu, Y.; Gu, Z.G.; Liu, J.; Fan, Q.H. Low-temperature plasma exfoliated n-doped graphene for symmetrical electrode supercapacitors. *Nano Energy* **2017**, *31*, 486–494. [[CrossRef](#)]
243. Sedlovets, D.M. N-Doped Graphene-like Film/Silicon Structures as Micro-Capacitor Electrodes. *Materials* **2023**, *16*, 4007. [[CrossRef](#)]
244. Lee, D.; Banda, H.; Périé, S.; Marcucci, C.; Chenavier, Y.; Dubois, L.; Taberna, P.L.; Simon, P.; Paëpe, G.D.; Duclairoir, F. Revealing Electrolytic Ion Sorption in Layered Graphene Galleries through Low-Temperature Solid-State. *NMR Chem. Mater.* **2023**, *35*, 3841–3848. [[CrossRef](#)]
245. Qiu, Z.P.; Liu, Z.; Lu, X.L.; Zhang, S.; Yan, Y.C.; Chi, C.L.; Chao, H.F.; Wang, G.W.; Gao, P.F.; Chi, W.H.; et al. Dual Molecules Cooperatively Confined In-Between Edge-oxygen-rich Graphene Sheets as Ultrahigh Rate and Stable Electrodes for Supercapacitors. *Small* **2023**, *19*, e2302316. [[CrossRef](#)]
246. Peng, X.Q.; Du, Y.P.; Gu, Z.; Deng, K.; Liu, X.S.; Lv, X.B.; Tian, W.; Ji, J.Y. Rearrangement of GO nanosheets with inner and outer forces under high-speed spin for supercapacitor. *J. Colloid Interface Sci.* **2023**, *644*, 167–176. [[CrossRef](#)]
247. Cung, D.; Nguyen, T.; Mai, V.D.; Vu, V.P.; Kim, S.; Lee, S.H. Integrated solar-rechargeable supercapacitors with a dual-functional-layered electrode. *J. Power Sources* **2023**, *572*, 233086.
248. Pang, J.; Li, J.; Guo, J.H.; Jia, M.J.; Zhang, J.W. Tuning the aggregation structure and surface composition of reduced graphene oxide microspheres for high-rate supercapacitors. *Diam. Relat. Mater.* **2023**, *136*, 109920. [[CrossRef](#)]
249. Li, Z.; Huang, T.Q.; Gao, W.W.; Xu, Z.; Chang, D.; Zhang, C.X.; Gao, C. Hydrothermally activated graphene fiber fabrics for textile electrodes of supercapacitors. *ACS Nano* **2017**, *11*, 11056–11065. [[CrossRef](#)]
250. Liu, Z.; Jiang, L.L.; Sheng, L.Z.; Zhou, Q.H.; Wei, T.; Zhang, B.S.; Fan, Z.J. Oxygen clusters distributed in graphene with “Paddy Land” structure: Ultrahigh capacitance and rate performance for supercapacitors. *Adv. Funct. Mater.* **2018**, *28*, 1705258. [[CrossRef](#)]
251. Hang, W.L.; Xu, C.; Ma, C.Q.; Li, G.X.; Wang, Y.Z.; Zhang, K.Y.; Li, F.; Liu, C.; Cheng, H.M.; Du, Y.W.; et al. Nitrogen-superdoped 3D graphene networks for high-performance supercapacitors. *Adv. Mater.* **2017**, *29*, 1701677.
252. Zhang, W.Y.; Liu, H.L.; Kang, H.W.; Zhang, S.R.; Yang, B.C.; Li, Z.K. 2-aminoanthraquinone anchored on N-doped reduced graphene oxide for symmetric supercapacitor with boosting energy density. *Electrochim. Acta* **2023**, *448*, 142194. [[CrossRef](#)]
253. Liang, J.Y.; Wang, Z.; Huang, L.T.; Zou, P.; Liu, X.L.; Ni, Q.; Wang, X.Y.; Wang, W.J.; Tao, R.M. Facile and Tunable Synthesis of Nitrogen-Doped Graphene with Different Microstructures for High-Performance Supercapacitors. *ACS Mater. Lett.* **2023**, *5*, 944–954. [[CrossRef](#)]
254. Song, B.; Zhao, J.X.; Wang, M.J.; Mullaveya, J.; Zhua, Y.T.; Geng, Z.S.; Chen, D.C.; Ding, Y.; Moon, K.; Liu, M.L.; et al. Systematic study on structural and electronic properties of diamine/triamine functionalized graphene networks for supercapacitor application. *Nano Energy* **2017**, *31*, 183–193. [[CrossRef](#)]
255. Zhang, S.; Sui, L.N.; Dong, H.Z.; He, W.B.; Dong, L.F.; Yu, L.Y. High-Performance Supercapacitor of Graphene Quantum Dots with Uniform Sizes. *ACS Appl. Mater. Interfaces* **2018**, *10*, 15. [[CrossRef](#)] [[PubMed](#)]

256. Shao, Y.L.; El-Kady, M.F.; Lin, C.W.; Zhu, G.Z.; Marsh, K.L.; Hwang, J.Y.; Zhang, Q.H.; Li, Y.G.; Wang, H.Z.; Kaner, R.B. 3D freeze-casting of cellular graphene films for ultrahigh power-density supercapacitors. *Adv. Mater.* **2016**, *28*, 6719–6726. [[CrossRef](#)] [[PubMed](#)]
257. Li, L.Y.; Song, B.; Maurer, L.; Lin, Z.Y.; Lian, G.; Tuan, C.C.; Moon, K.S.; Wong, C.P. Molecular engineering of aromatic amine spacers for high-performance graphene-based supercapacitors. *Nano Energy* **2016**, *21*, 276–294. [[CrossRef](#)]
258. Lu, Y.; Zhang, F.; Zhang, T.; Leng, K.; Zhang, L.; Yang, X.; Ma, Y.; Huang, Y.; Zhang, M.; Chen, Y. Synthesis and supercapacitor performance studies of N-dope graphene materials using o-phenylenediamine as the double-N precursor. *Carbon* **2013**, *63*, 508–516. [[CrossRef](#)]
259. Zhang, S.; Sui, L.; Kang, H.Q.; Dong, H.Z.; Dong, L.F.; Yu, L.Y. High performance of N-doped graphene with bubble-like textures for supercapacitors. *Small* **2018**, *14*, 1702570. [[CrossRef](#)]
260. Zhao, Y.F.; Huang, S.F.; Xia, M.R.; Rehman, S.; Mu, S.C.; Kou, Z.K.; Zhang, Z.; Chen, Z.Y.; Gao, F.M.; Hou, Y.L. N-P-O co-doped high performance 3D graphene prepared through red phosphorous-assisted “cutting-thin” technique: A universal synthesis and multifunctional applications. *Nano Energy* **2016**, *28*, 346–355. [[CrossRef](#)]
261. Zhao, C.M.; Zheng, W.T. A review for aqueous electrochemical supercapacitors. *Front. Energy Res.* **2015**, *3*, 23. [[CrossRef](#)]
262. Amaral, M.M.; Venâncio, R.; Peterlevitz, A.C.; Zanin, H. Recent advances on quasi-solid-state electrolytes for supercapacitors. *J. Energy Chem.* **2021**, *11*, 11. [[CrossRef](#)]
263. Xu, T.; Liu, K.; Sheng, N.; Zhang, M.H.; Liu, W.; Liu, H.Y.; Dai, L.; Zhang, X.Y.; Si, C.L.; Du, H.H.; et al. Biopolymer-based hydrogel electrolytes for advanced energy storage/conversion devices: Properties, applications, and perspectives. *Energy Storage Mater.* **2022**, *3*, 13. [[CrossRef](#)]
264. Qu, J.Q.; Bai, Y.C.; Li, X.M.; Song, K.L.; Zhang, S.; Wang, X.X.; Wang, X.C.; Dai, S.G. Rational design of NiSe₂@rGO nanocomposites for advanced hybrid supercapacitors. *J. Mater. Res. Technol.* **2021**, *15*, 6155–6161. [[CrossRef](#)]
265. Zhao, J.; Li, Z.J.; Yuan, X.C.; Yang, Z.; Zhang, M.; Meng, A.; Li, Q.D. A high-energy density asymmetric supercapacitor based on Fe₂O₃ nanoneedle arrays and NiCo₂O₄/Ni(OH)₂ hybrid nanosheet arrays grown on SiC nanowire networks as free-standing advanced electrodes. *Adv. Energy Mater.* **2018**, *8*, 1702787. [[CrossRef](#)]
266. Zhang, Q.B.; Liu, Z.C.; Zhao, B.; Cheng, Y.; Zhang, L.; Wu, H.H.; Wang, M.S.; Dai, S.G.; Zhang, K.L.; Ding, D.; et al. Design and understanding of dendritic mixed-metal hydroxide nanosheets@N-doped carbon nanotube array electrode for highperformance asymmetric supercapacitors. *Energy Storage Mater.* **2018**, *16*, 632–645. [[CrossRef](#)]
267. Choudhary, N.; Li, C.; Moore, J.L.; Nagaiah, N.; Zhai, L.; Jung, Y.; Thomas, J.Y. Asymmetric Supercapacitor Electrodes and Devices. *Adv. Mater.* **2017**, *29*, 1605336. [[CrossRef](#)]
268. Chang, X.W.; Liu, T.T.; Li, W.L.; Gao, R.X.; Lei, H.; Ren, Z.Y. Porous prussian blue analogs derived nickel-iron bimetallic phosphide nanocubes on conductive hollow mesoporous carbon nanospheres for stable and flexible high-performance supercapacitor electrode. *J. Colloid Interface Sci.* **2023**, *650*, 728–741. [[CrossRef](#)]
269. Ji, P.Y.; Li, Q.Y.; Zhang, X.M.; Hu, Y.W.; Han, X.Y.; Zhang, D.Z.; Hu, C.G.; Xi, Y. Achieving Continuous Self-Powered Energy Conversion-Storage-Supply Integrated System Based on Carbon Felt. *Adv. Sci.* **2023**, *10*, 2207033.
270. Kim, S.I.; Kang, J.H.; Kim, S.W.; Jang, J.H. A new approach to high-performance flexible supercapacitors: Mesoporous three-dimensional Ni-electrodes. *Nano Energy* **2017**, *39*, 639–646. [[CrossRef](#)]
271. Zhang, C.Y.; Cai, X.Y.; Qian, Y.; Jiang, H.F.; Zhou, L.J.; Li, B.S.; Lai, L.F.; Shen, Z.X.; Huang, W. Electrochemically synthesis of nickel cobalt sulfide for high-performance flexible asymmetric supercapacitors. *Adv. Sci.* **2018**, *5*, 1700375. [[CrossRef](#)] [[PubMed](#)]
272. Huang, J.; Wei, J.C.; Xiao, Y.B.; Xu, Y.Z.; Xiao, Y.J.; Wang, Y.; Tan, L.C.; Yuan, K.; Chen, Y.W. When Al-doped cobalt sulfide nanosheets meet nickel nanotube arrays: A highly efficient and stable cathode for asymmetric supercapacitors. *ACS Nano* **2018**, *12*, 3030–3041. [[CrossRef](#)] [[PubMed](#)]
273. Lee, S.; Hwang, J.; Kim, D.; Ahn, H. Oxygen incorporated in 1T/2H hybrid MoS₂ nanoflowers prepared from molybdenum blue solution for asymmetric supercapacitor applications. *Chem. Eng. J.* **2021**, *419*, 129701. [[CrossRef](#)]
274. Mohammad, M.A.; Hamideh, M.S.; Hamidreza, N.; Fatemeh, F.; Fariba, S. Fabrication of a high-performance hybrid supercapacitor using a modified graphene aerogel/cerium oxide nanoparticle composite. *J. Energy Storage* **2019**, *26*, 100998.
275. Nagaraju, G.; Sekhar, S.C.; Bharat, L.K.; Yu, J.S. Wearable fabrics with self-branched bimetallic layered double hydroxide coaxial nanostructures for hybrid supercapacitors. *ACS Nano* **2017**, *11*, 10860–10874. [[CrossRef](#)]
276. Lee, D.G.; Choi, H.; Park, Y.; Kim, M.C.; Park, J.B.; Lee, S.; Cho, Y.Y.; Ahn, W.; Jang, A.R.; Sohn, J.I.; et al. Utilizing hybrid faradaic mechanism via catalytic and surface interactions for high-performance flexible energy storage system. *J. Energy Chem.* **2023**, *83*, 541–548. [[CrossRef](#)]
277. Dai, S.G.; Liu, J.L.; Wang, C.S.; Wang, X.; Xi, Y.; Wei, D.P.; Hu, C. Hierarchical porous nanostructures of manganese(III) oxyhydroxide for all-solid-state flexible supercapacitors. *Energy Technol.* **2016**, *4*, 1450–1454. [[CrossRef](#)]
278. Kareri, T.; Hossain, M.S.; Ram, M.K.; Takshi, A. A flexible fiber-shaped hybrid cell with a photoactive gel electrolyte for concurrent solar energy harvesting and charge storage. *Energy Res.* **2022**, *46*, 17084–17095. [[CrossRef](#)]
279. Jiang, Z.M.; Sheng, L.Z.; Lin, Y.Q.; Zhang, S.; Zhang, L.H.; Wei, T.; Zhou, J.L.; Liu, C.Q.; Jiang, H.; Zhou, Q.; et al. Weldable and flexible graphene ribbon@Ni fibers with ultrahigh length capacitance for all-solid-state supercapacitors. *Chem. Eng. J.* **2021**, *426*, 131361. [[CrossRef](#)]

280. Sun, J.; Zhang, Q.C.; Wang, X.N.; Zhao, J.X.; Guo, J.B.; Zhou, Z.Y.; Zhang, J.; Man, P.; Sun, J.; Li, Q.W.; et al. Constructing hierarchical dandelion-like molybdenum-nickel-cobalt ternary oxide nanowire arrays on carbon nanotube fiber for highperformance wearable fiber-shaped asymmetric supercapacitors. *J. Mater. Chem. A* **2017**, *5*, 21153–21160. [[CrossRef](#)]
281. Jin, H.Y.; Zhou, L.M.; Mak, C.L.; Huang, H.T.; Tang, W.M.; Chan, H.L. High-performance fiber-shaped supercapacitors using carbon fiber thread (CFT)@polyaniline and functionalized CFT electrodes for wearable/stretchable electronics. *Nano Energy* **2015**, *11*, 662–670. [[CrossRef](#)]
282. Liu, W.W.; Feng, K.; Zhang, Y.N.; Yu, T.W.; Han, L.; Lui, G.; Lia, M.; Chiu, G.; Fung, P.; Yu, A.P. Hair-based flexible knittable supercapacitor with wide operating voltage and ultra-high rate capability. *Nano Energy* **2017**, *34*, 491–499. [[CrossRef](#)]
283. Senthilkumar, S.T.; Kim, J.; Wang, Y.; Huang, H.T.; Kim, Y.S. Flexible and wearable fiber shaped high voltage supercapacitors based on copper hexacyanoferrate and porous carbon coated carbon fiber electrodes. *J. Mater. Chem. A* **2016**, *4*, 493440. [[CrossRef](#)]
284. Dai, S.G.; Guo, H.Y.; Wang, M.J.; Liu, J.L.; Wang, G.; Hu, C.G.; Xi, Y. A Flexible micro-supercapacitor based on a pen ink-carbon fiber thread. *J. Mater. Chem. A* **2014**, *2*, 19665–19669. [[CrossRef](#)]
285. Lee, J.; Shin, M.K.; Kim, S.H.; Cho, H.U.; Spinks, G.M.; Wallace, G.G.; Lima, M.D.; Lepro, X.; Kozlov, M.; Baughman, R.H.; et al. Ultrafast charge and discharge biscrolled yarn supercapacitors for textiles and microdevices. *Nat. Commun.* **2013**, *4*, 1970. [[CrossRef](#)]
286. Kou, L.; Huang, T.; Zheng, B.; Han, Y.; Zhao, X.; Gopalsamy, K.; Sun, H.; Gao, C. Coaxial wet-spun yarn supercapacitors for high-energy density and safe wearable electronics. *Nat. Commun.* **2014**, *5*, 3754. [[CrossRef](#)] [[PubMed](#)]
287. Zhang, Q.C.; Xu, W.W.; Sun, J.; Pan, Z.H.; Zhao, J.X.; Wang, X.N.; Zhang, J.; Man, P.; Guo, J.B.; Zhou, Z.Y.; et al. Constructing ultrahigh-capacity zinc-nickel-cobalt oxide@Ni(OH)₂ core-shell nanowire arrays for high-performance coaxial fiber shaped asymmetric supercapacitors. *Nano Lett.* **2017**, *17*, 7552–7560. [[CrossRef](#)]
288. Li, Z.H.; Shaon, M.F.; Zhou, L.; Zhang, R.K.; Zhang, C.; Han, J.B.; Wein, M.; Evans, D.G.; Duan, X. A flexible all-solid-state micro-supercapacitor based on hierarchical CuO@layered double hydroxide core-shell nanoarrays. *Nano Energy* **2016**, *20*, 294–304. [[CrossRef](#)]
289. Nagaraju, G.; Sekhar, S.C.; Yu, J.S. Utilizing waste cable wires for high-performance fiber-based hybrid supercapacitors: An effective approach to electronic-waste management. *Adv. Energy Mater.* **2018**, *8*, 1702201. [[CrossRef](#)]
290. Gao, L.B.; Surjad, J.U.; Cao, K.; Zhang, H.T.; Li, P.F.; Xu, S.; Jiang, C.C.; Song, J.; Sun, D.; Lu, Y. Flexible fiber-shaped supercapacitor based on nickel-cobalt double hydroxide and pen ink electrodes on metallized carbon fiber. *ACS Appl. Mater. Interfaces* **2017**, *9*, 5409–5418. [[CrossRef](#)]
291. Varakin, I.; Stepanov, A.; Menukhov, V. Capacitor with a Double Electrical Layer. U.S. Patent 5,986,876, 14 August 1995.
292. Brezesinski, T.; Wang, J.; Tolbert, S.H.; Dunn, B. Li-O₂ and Li-S batteries with high energy storage. *Nat. Mater.* **2010**, *9*, 146–151. [[CrossRef](#)] [[PubMed](#)]
293. Dubal, D.P.; Ayyad, O.; Ruiz, V.; Romero, P.G. Hybrid energy storage: The merging of battery and supercapacitor chemistries. *Chem. Soc. Rev.* **2015**, *44*, 1777–1790. [[CrossRef](#)] [[PubMed](#)]

Disclaimer/Publisher's Note: The statements, opinions and data contained in all publications are solely those of the individual author(s) and contributor(s) and not of MDPI and/or the editor(s). MDPI and/or the editor(s) disclaim responsibility for any injury to people or property resulting from any ideas, methods, instructions or products referred to in the content.